T.R.
GEBZE TECHNICAL UNIVERSITY
GRADUATE SCHOOL OF NATURAL AND APPLIED SCIENCES

SYNTHESIS AND CHARACTERIZATION OF β-CYCLODEXTRIN INCORPORATED NANOCOMPOSITE HYDROGELS AND INVESTIGATION OF CONTROLLED RELEASE BEHAVIOR

MELTEM KASAPOĞLU ÇALIK

A THESIS SUBMITTED FOR THE DEGREE OF
DOCTOR OF PHILOSOPHY
DEPARTMENT OF CHEMICAL ENGINEERING

GEBZE
2019

T.R.

GEBZE TECHNICAL UNIVERSITY

GRADUATE SCHOOL OF NATURAL AND APPLIED SCIENCES

SYNTHESIS AND CHARACTERIZATION OF β-CYCLODEXTRIN INCORPORATED NANOCOMPOSITE HYDROGELS AND INVESTIGATION OF CONTROLLED RELEASE BEHAVIOR

MELTEM KASAPOĞLU ÇALIK

A THESIS SUBMITTED FOR THE DEGREE OF DOCTOR OF PHILOSOPHY

DEPARTMENT OF CHEMICAL ENGINEERING

THESIS SUPERVISOR

PROF. DR. MURAT ÖZDEMİR

GEBZE

2019

T.C.
GEBZE TEKNİK ÜNİVERİSTESİ
FEN BİLİMLERİ ENSTİTÜSÜ

β-SİKLODEKSTRİN DAHİL EDİLMİŞ NANOKOMPOZİT HİDROJELLERİN SENTEZİ, KARAKTERİZAYONU VE KONTROLLÜ SALIM DAVRANIŞININ İNCELENMESİ

MELTEM KASAPOĞLU ÇALIK
DOKTORA TEZİ
KİMYA MÜHENDİSLİĞİ ANABİLİM DALI

DANIŞMANI
PROF. DR. MURAT ÖZDEMİR

GEBZE
2019

GEBZE TEKNİK ÜNİVERSİTESİ	**DOKTORA JÜRİ ONAY FORMU**

GTÜ Fen Bilimleri Enstitüsü Yönetim Kurulu'nun 03/01/2019 tarih ve 2019/02 sayılı kararıyla oluşturulan jüri tarafından 16/01/2019 tarihinde tez savunma sınavı yapılan Meltem KASAPOĞLU ÇALIK'ın tez çalışması Kimya Mühendisliği Anabilim Dalında DOKTORA tezi olarak kabul edilmiştir.

JÜRİ

ÜYE
(TEZ DANIŞMANI) : Prof. Dr. Murat ÖZDEMİR

ÜYE : Doç. Dr. Rezan DEMİR-ÇAKAN

ÜYE : Prof. Dr. İbrahim DOYMAZ

ÜYE : Prof. Dr. Alp Er KONUKMAN

ÜYE : Prof. Dr. Hasan SADIKOĞLU

ONAY

Gebze Teknik Üniversitesi Fen Bilimleri Enstitüsü Yönetim Kurulu'nun
......./......./....... tarih ve ..../....... sayılı kararı.

SUMMARY

Poly(N-isopropylacrylamide) and sodium alginate-based nanocomposite and conventional hydrogels were synthesized via free radical solution polymerization in which nanoclay was used as the cross-linker for poly(N-isopropylacrylamide) and sodium alginate-based nanocomposite hydrogels while N,N′-methylenebis(acrylamide) was used as the cross-linker in the conventional hydrogels. Prepared hydrogels were characterized by Fourier Transform Infrared (FT-IR) spectroscopy, scanning electron microscopy (SEM), differential scanning calorimetry (DSC) and X-ray diffraction (XRD). The hydrogels revealed a highly porous structure in which pore sizes decreased, and number of pores increased with increasing nanoclay content in the hydrogels. Swelling studies were conducted in the pH range of 1.2-10.0 and in the temperature range of 5-37 °C. The prepared hydrogels showed pH and temperature responsive behavior. The nanocomposite hydrogels showed higher dependency on pH, temperature and hydrogel composition than the conventional hydrogels. Inclusion complex of curcumin with β-cyclodextrin (Cur-β-CD) was prepared using co-precipitation method. Stoichiometric ratio between curcumin and β-cyclodextrin was found to be 1:2 with an association constant of $3.80 \times 10^{8}\ \mathrm{M}^{-2}$ using Benesi-Hildebrand method. Inclusion complex formation was confirmed by FT-IR and DSC analyses. Water solubility of curcumin increased from 0.00122 to 0.721 mg ml^{-1} with the inclusion complex formation. Release of the inclusion complex from the prepared nanocomposite and conventional hydrogels were investigated in simulated gastrointestinal conditions. Cumulative release was dependent on the hydrogel composition and pH. At pH = 1.2, hydrogels showed the lowest release ratio while at pH = 6.8 highest swelling ratios were attained. Nanocomposite hydrogels were found to have potential as drug carriers for the targeted delivery of antiproliferative drug of curcumin in gastrointestinal tract of humans to increase solubility and bioavailability of curcumin.

Key Words: Hydrogel, Sodium Alginate, Poly(N-isopropylacrylamide), Swelling, β-Cyclodextrin, Curcumin.

ÖZET

Poli(N-izopropilakrilamid ve sodium aljinat içeren nanokompozit ve geleneksel hidrojeller serbest radikal çözelti polimerizasyonu yöntemi ile üretilmiş olup, poli(N-izopropilakrilamid ve sodium aljinat içeren nanokompozit hidrojellerde nanokil, geleneksel hidrojellerde ise N,N'-metilenbis(akrilamid) çapraz bağlayıcı olarak kullanıldı. Sentezlenen hidrojeller Fourier dönüşümlü kızılötesi (FT-IR) spektroskopisi, taramalı elektron mikroskopu (SEM), diferansiyel taramalı kalorimetre (DSC) ve X-ışını kırınım (XRD) cihazı ile karakterize edildi. Nanokompozit hidrojellerin yüksek oranda gözenekli yapıya sahip olduğu ve içerdikleri nanokil miktarı arttıkça, gözenek sayısının artarken, gözenek çapının küçüldüğü gözlendi. Hidrojellerin şişme davranışları pH 1.2-10 ile 5-37 °C sıcaklık aralığında incelendi. Hazırlanan hidrojeller, pH ve sıcaklığa duyarlı davranış gösterdi. Nanokompozit hidrojellerin geleneksel hidrojellerden pH, sıcaklık ve hidrojel kompozisyonu değişimine daha duyarlı olduğu görüldü. Birlikte çöktürme yöntemi kullanılarak kurkumin molekülünün β-siklodekstrin ile inkluzyon kompleksi (Cur-β-CD) hazırlandı. Benesi-Hildebrand metodundan yararlanılarak kurkumin ve β-siklodekstrin arasındaki stokiyometrik oranın 1:2 olduğu ve kararlılık sabitinin $3.80 \times 10^{8}\ \mathrm{M}^{-2}$ olduğu belirlendi. İnkluzyon kompleks oluşumu FT-IR ve DSC analizleri ile doğrulandı. İnkluzyon kompleksi oluşumu sonucunda kurkumin molekülünün sudaki çözünürlüğünün 0.00122 mg ml^{-1} değerinden 0.721 mg ml^{-1} değerine yükseldiği tespit edildi. İnkluzyon kompleksinin, hazırlanan nanokompozit ve geleneksel hidrojellerden salınması simüle edilerek mide-bağırsak koşullarında incelendi. Kümülatif salım değerlerinin hidrojel kompozisyonu ve salınım yapılan ortamın pH değerine bağlı olarak değiştiği görüldü. En düşük şişme pH = 1.2 değerinde gözlenirken, en yüksek şişme pH = 6.8 değerinde gerçekleşti. Nanokompozit hidrojellerin, insan mide bağırsak sisteminde antiproliferat bir ilaç olan kurkuminin sudaki çözünürlüğünü ve biyoyararlılığını arttıracak potansiyel ilaç taşıyıcı sistemler olabileceği görüldü.

Anahtar Kelimeler: Hidrojel, Sodyum Aljinat, Poli(N-izopropilakrilamid), Şişme, β-siklodekstrin, Kurkumin

ACKNOWLEDGEMENTS

First of all, I would like to express my sincere thanks to my advisor Prof. Dr. Murat Özdemir for his valuable guidance, advice and encouragement throughout this work. It was a pleasure for me to study under his supervision.

I am also thankful to all my committee members Prof. Dr. Hasan Sadıkoğlu, Prof. Dr. Alp Er Konukman, Prof. Dr. İbrahim Doymaz and Assoc. Prof. Dr. Rezan Demir-Çakan, for their help, support and comments.

I would like to thank all members of the Chemical Engineering Department for their encouragement and assistance throughout this study.

This dissertation would not have been possible without my caring and loving parents, my mother Fatma Kasapoğlu, my father Yüksel Kasapoğlu, my sister Erçe Su Kasapoğlu and my husband Oğuzhan Çalık, who have always motivated me during difficult times and always believed in me. It is very difficult for me to express my gratitude and sincere love for them. All my work is dedicated to them to whom I owe everything.

Lastly, I am particularly grateful to The Scientific and Technological Research Council of Turkey (TUBITAK) for granting Ph.D. scholarship (BIDEB 2211-C).

TABLE of CONTENTS

LIST of ABBREVIATIONS and ACRONYMS

Abbreviations and Acronyms		**Explanations**
A	:	Absorbance of the curcumin solution in the presence and β-CD
A_0	:	Absorbance of the curcumin solution in the absence of β-CD
A_∞	:	Expected absorbance
C	:	Curcumin concentration
C_0	:	Initial concentration of complex solution before loading study
C_1	:	Concentration of complex solution after loading study
Cur_E	:	Calculated amount of curcumin in inclusion complex
Cur_T	:	Amount of curcumin used to prepare the inclusion complex
IC_T	:	Total amount of inclusion complex obtained
K_n	:	Association constant
l	:	Width of the UV cuvette
M_∞	:	Total amount of loaded complex in the hydrogels
m_{Cur}	:	Initially added weight of curcumin
m_{IC}	:	Weight of obtained inclusion complex
M_t	:	Amount of released complex at time t
$m_{\beta\text{-}CD}$	:	Initially added weight of β-CD
T_g	:	Glass transition temperature
W_d	:	Weight of dried hydrogel
Ws	:	Weight of swollen hydrogel
W_t	:	Weight of the hydrogel at time t during swelling
ε	:	Molar absorption coefficient
θ	:	Angle of diffraction
λ	:	Wavelength
AA	:	Acrylic acid
BIS	:	N,N’-methylenebis(acrylamide)
$CaCl_2$	:	Calcium Chloride
CD	:	Cyclodextrin
CL	:	Complex Loading
Cur-β-CD	:	Curcumin-β-Cyclodextrin inclusion complex

DMA	:	N, N-dimethylaminoethyl Methacrylate
EE	:	Entrapment Efficiency
ESR	:	Equilibrium Swelling Ratio
FT-IR	:	Fourier Transform Infrared
GMA	:	Glycidyl Methacrylate
GRAS	:	Generally Recognized as Safe
HA	:	Hyaluronic Acid
HCl	:	Hydrochloric Acid
IPN	:	Interpenetrating Polymer Network
KH_2PO_4	:	Potassium Dihydrogen Phosphate
KPS	:	Potassium Peroxodisulfate
LCST	:	Lower Critical Solution Temperature
MAA	:	Methacrylic Acid
NaAlg	:	Sodium Alginate
NaCl	:	Sodium Chloride
NaOH	:	Sodium Hydroxide
NMR	:	Nuclear Magnetic Resonance
PAA	:	Poly(acrylic acid)
PCL	:	Poly(caprolactone)
PCLA	:	Poly(ε-caprolactone-co-lactide)
PEG	:	Poly(ethylene glycol)
PEI	:	Polyethylenimine
PHEMA	:	Poly(2-hydroxyethyl methacrylate)
PMAA	:	Poly(methacrylic acid)
PNIPA	:	Poly(N-isopropylacrylamide)
PVA	:	Poly(vinyl alcohol)
SEM	:	Scanning Electron Microscope
SR	:	Swelling Ratio
TEMED	:	N,N,N′,N′-tetramethylethylene diamine
XRD	:	X-Ray Diffraction
β-CD	:	β-Cyclodextrin

LIST of FIGURES

LIST of TABLES

1. INTRODUCTION

Hydrogels are cross-linked hydrophilic polymer networks able to absorb aqueous solutions to a high degree without dissolving [1]. They have been used in many fields such as bioengineering, biotechnology, agriculture, food industry and pharmacy [2]. Hydrogels have unique advantages in drug delivery when they are synthesized as environmentally responsive in which especially pH and temperature responsive hydrogels have been taking great attention because pH and temperature are two important factors affecting the release of active agents inside the human body.

Poly(N-isopropylacrylamide) (PNIPA) is one of the most widely studied temperature sensitive polymer which has a phase transition temperature at around 32 °C. Based on its temperature sensitive property, PNIPA has been used in controlled drug delivery [3], enzyme immobilization [4] and tissue engineering [5]. The PNIPA hydrogels are usually cross-linked by some chemical organic cross-linkers to form conventional hydrogels. These conventional hydrogels have some limitations such as weak mechanical properties, brittleness and slow response rates. Haraguchi et al. reported that mechanical properties, thermal stability, and swelling and deswelling behavior of hydrogels can be improved by using nanoclays [6], [7]. Polymer-clay nanocomposite hydrogels exhibited remarkably improved mechanical and thermal properties, and improved release rates when compared with the conventional hydrogels [8], [9]. Another advantage of using nanoclay is that it acts as an inorganic cross-linker, and overcomes the use of organic cross-linkers such as N,N'-methylenebis(acrylamide) (BIS) which is toxic when inhaled, swallowed or ingested and classified as a hazardous material according to Directives 67/548/EEC and 1999/45/EC. To overcome the toxic effects and health risks of BIS, a nanocomposite hydrogel consisting of PNIPA and Laponite was developed where the hydrogel was prepared by in situ free radical redox polymerization without using any organic cross-linker [10]. The clay sheets acted as multifunctional cross-linkers for the polymer. The nanocomposite hydrogels exhibited extraordinary mechanical properties with high mechanical strength, high degrees of swelling and rapid shrinking capacity [8], [10]-[12]. These nanocomposite hydrogels could be used as smart delivery devices in several applications including drug delivery and delivery of active agents (antimicrobials, antioxidants, nutraceuticals, etc.) in intelligent food packaging.

Bentonite nanoclay is a highly pure aluminosilicate mineral which has a sheet type structure with high aspect ratio, large specific surface area and high cation exchange capacity. The nanoclay consists of about 1 nm thick layers surface substituted with metal cations and stacked in about 10 nm sized multilayer stacks. The stacks can be dispersed in a polymer matrix to form polymer-clay nanocomposite. Bentonite nanoclay because of its low cost and unique properties is a preferred inorganic cross-linker over the other nanoclays such as Laponite and kaolinite. The high price of Laponite limits its use as an inorganic cross-linker in industrial applications.

Conventional polymeric drug delivery systems release the drug immediately without having any control on the release rate [13]. Controlling the drug release using a responsive polymer system with a known release profile is necessary to avoid large fluctuations in release rates and obtain effective delivery. The aim of a controlled drug release system is to transfer the drug molecules to the target at a specific rate to maintain a predetermined concentration of drug in the release medium for a predetermined period of time. Hydrogels with controlled release properties improve therapeutic effectiveness of the drugs and reduce their side-effects [14]. The swelling ability of hydrogels allows them to absorb and release high quantities of drugs [15]. The release rate of the drug is directly associated with the swelling behavior of the hydrogel [16]. Hydrogels that are able to trigger the drug release by changing external properties, like pH or temperature, are classified as smart hydrogels [17]. The oral route is the most convenient and comfortable way of administering drugs but the main challenge in an oral drug delivery is to prevent the drug release in the acidic stomach environment [18], [19]. In addition, the carrier should be resistant to the body temperature and pH changes during the gastrointestinal transit time from the mouth to the colon to keep the bioactivity of the drug [20]. Therefore, a smart hydrogel system with resistance to acidic medium is necessary for a successful oral delivery.

Sodium alginate (NaAlg) is a naturally derived, non-toxic, water soluble and biocompatible polysaccharide. It can be extracted from marine algae or produced by bacteria. Alginates comprised of two different kinds of monomers having carboxylic groups, L-mannuronic and L-guluronic acids. These monomers can form several possible arrangements of chain segments which generate alginates with different gelation properties. Alginates form mechanically stable pH responsive hydrogel networks in presence of divalent cations such as Ca^{2+}, Mg^{2+} and Ba^{2+}. The interaction between the functional groups of alginate and divalent cations results in the formation of cross-links according to the “egg-box” model [21]. The cross-linked structure of alginate has been used to produce drug delivery systems to release various drugs, proteins and active agents from the matrix [22]. Extensive number of studies also confirmed that the NaAlg based hydrogels are extremely superior in superabsorbent, non-toxic character, sustained and targeted delivery of drugs [23]-[25].

Curcumin is a hydrophobic natural polyphenol derived from the rhizomes of the Curcuma Longa. It is an important natural colorant which is used in food and pharmaceutical preparations [26]. Curcumin has been reported to have various pharmaceutical functions including antimicrobial, antioxidant, anti-inflammatory, antitumor and anticarcinogenic activities [27], [28]. Curcumin is considered as “Generally Recognized as Safe” (GRAS) by the United States (US) Food and Drug Administration (FDA) even when ingested at relatively high levels [29]. Despite these advantages, curcumin exhibits very low solubility in aqueous solutions, limiting its pharmaceutical use. Therefore, solubility of curcumin in aqueous environments needs to be improved to use the curcumin in pharmaceutical applications.

Several studies showed that encapsulation of curcumin in different carriers such as starch [30], gelatin [31], yeast cell [32], liposome [33] and cyclodextrins (CDs) [34] is an effective way of improving its solubility in aqueous solutions and thus, increasing its bioavailability. Among them, CDs were found to be the best carriers in increasing the solubility of curcumin in aqueous environments and improving its anti-inflammatory and antiangiogenic activity [35]. CDs have the ability to form inclusion complexes with hydrophobic guest compounds which enter into the hydrophobic cavity of CDs (host) only by physical forces without any covalent bonding [36]. They protect the guest compound from the aqueous environment while the hydrophilic outer surface provides the solubilizing effect [35]. Incorporation of compounds with CDs not only increase the aqueous solubility but also enhance the stability of flavors to oxygen, heat and light [37]. The most widely used CD is β-cyclodextrin (β-CD) whose cavity size is suitable for common drugs with molecular weights between 200 and 800 g mol^{-1}, and it has been on the GRAS list since 1998 [37], [38].

1.1. Hypothesis

A pH and temperature responsive oral delivery hydrogel system can be prepared to protect curcumin from deteriorating effects of acidic gastric medium and release it to the intestinal medium in a controlled manner.

1.2. Objectives

The objectives of this study are to:

i) Synthesize a series of pH/temperature sensitive nanocomposite and conventional hydrogel networks made of PNIPA chains crosslinked with nanoclay and conventional cross-linker,

ii) Determine physicochemical, thermal and structural properties of the prepared hydrogels,

iii) Investigate swelling behavior of prepared hydrogels at different pH and temperature media,

iv) Synthesize of inclusion complex of curcumin with β-CD using co-precipitation method,

v) Determine thermal and structural properties of prepared curcumin-β-cyclodextrin inclusion complex,

vi) Investigate swelling and inclusion complex release behavior of the prepared hydrogels under the conditions of simulating pH, temperature and time likely to be encountered during transit in the gastrointestinal tract.

2. METHODOLOGY

Figure 2.1 shows schematic diagram of the methods described in this study.

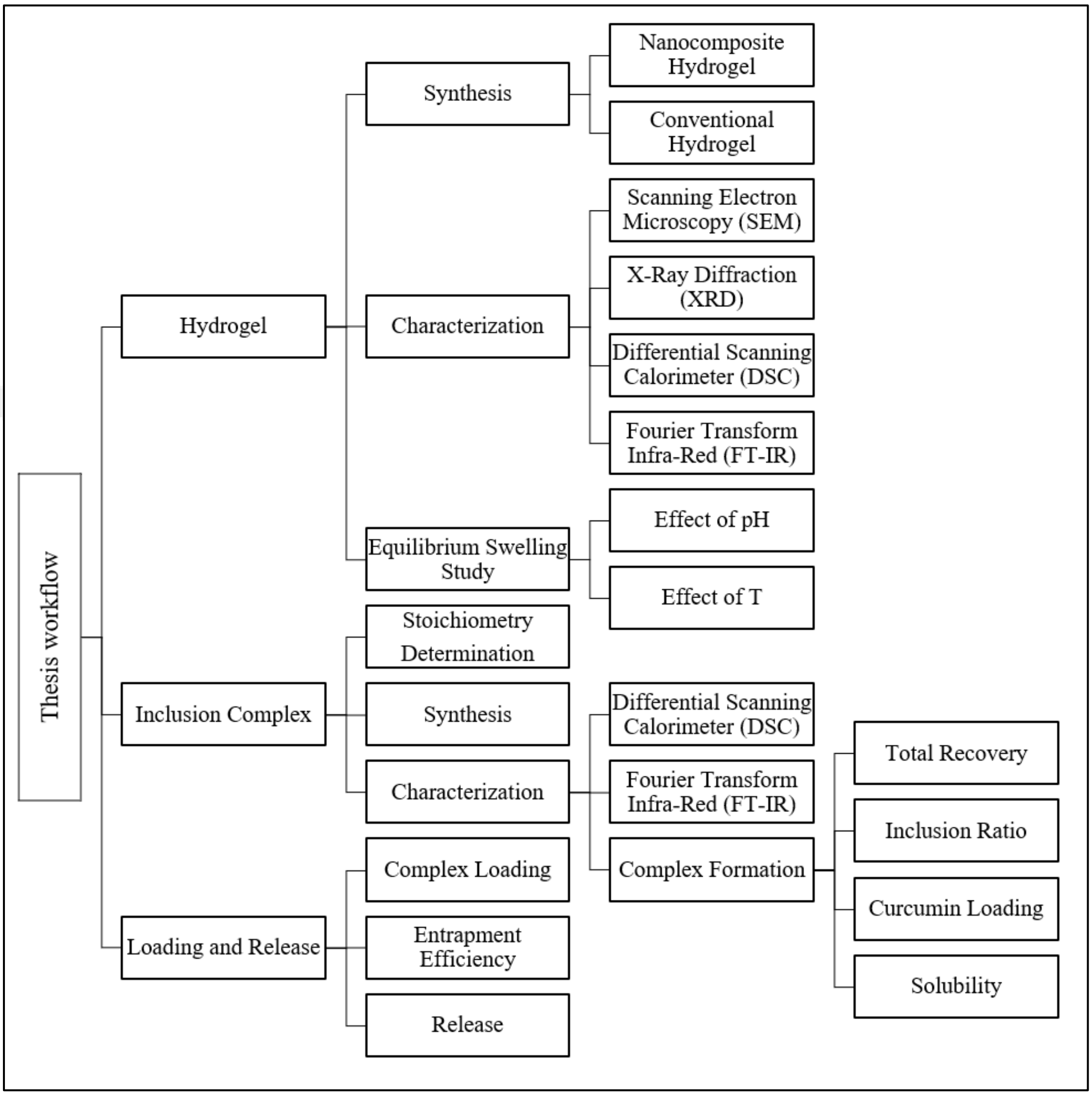

Figure 2.1: The schematic diagram of the methods described in this study.

3. SYNTHESIS, CHARACTERIZATION and SWELLING BEHAVIOR of pH/TEMPERATURE RESPONSIVE NANOCOMPOSITE HYDROGELS

Over the past a few decades, hydrogels have received great attention due to their ability to swell without dissolving in aqueous solutions. Hydrogels absorb water through hydrophilic functional groups attached to the polymer backbone while they resist to dissolution through the cross-links between the network chains [39]. The cross-linking density mainly determines the degree of swelling of the hydrogels [40]. By changing the cross-linking density, hydrogels having different water absorption capacity can be synthesized. The ability of hydrogels to exhibit both solid-like and liquid-like properties have application in a wide variety of fields. Ferfera-Harrar and Dairi prepared chitosan-graft polyacrylamide/gelatin hydrogels for wastewater purification [41]; Rakhshaei and Namazi synthesized carboxymethyl cellulose based nanocomposite hydrogel film as drug carrier for wound healing and dressing applications [42]; Capuano et al. showed that knee implants can be coated with antibiotic drug loaded hydrogel in order to be used in prosthetic applications [43]; Thombare et al. synthesized guar gum and acrylic acid based hydrogels which can be used as soil conditioners and water conserving agent in agricultural sector [44] and Treenate and Monvisade prepared a hydroxyethylacryl chitosan/sodium alginate hydrogel for paracetamol release to be use used in drug delivery systems [45].

One of the most remarkable research areas of hydrogels over the past few decades have been their environmental sensitivity. Hydrogels undergo shape and volume changes from their collapsed and swollen states in response to environmental changes such as pH, temperature, light and electric and magnetic fields [46]. When received an external signal, the environmentally sensitive hydrogels make conformational and chemical changes which result variations in the physical properties such as solubility of the hydrogel [47]. Collapse of the hydrogel chains by the volume transition was first observed by Tanaka et al. who demonstrated that small changes in the external conditions could produce remarkable changes in the state of a gel [48]. Among all of the responsive hydrogels, pH and temperature responsive hydrogels have attracted the most attention because of both pH and temperature are important environmental factors, and they can be easily controlled and applicable *in vivo* and *in vitro* studies [49].

The interpenetrating polymer network (IPN) technology is a combination of two polymers where at least one of the polymers is cross-linked in the presence of another [50]. In semi-IPN systems, there are no chemical bonds between components and, each polymer network can be sensitive independently to the different external stimuli, such as pH and temperature [51], [52]. The interpenetration of two networks may lead to higher mechanical strength, and improved pH and temperature responsive swelling/deswelling behavior compared with conventional PNIPA hydrogels [51], [53]. The semi-IPN hydrogels with non-toxic synthetic polymers can be a promising alternative in a wide range of applications because of their high sensitivity to external stimuli, good biocompatibility and biodegradability. In recent years, particular interest has been focused to the semi-IPN hydrogels. Ganguly et al. synthesized sodium alginate and poly(methacrylic acid) based semi-IPN hydrogels and observed that the drug release and pH oscillatory features were improved [23]. Wen et al. prepared biopolymer IPN hydrogels composed of gelatin and sodium alginate. The authors reported that the tensile and compressive strength of the hydrogels were significantly improved by the formation of IPN structure [24]. Kulkarni et al. synthesized IPN hydrogel membranes of NaAlg and poly(vinyl alcohol) (PVA) and observed that the drug release properties were greatly improved with the formation of IPN structure. They reported that the IPN hydrogels extended drug release up to 24 h, while NaAlg and PVA membranes discharged the drug quickly [25].

Hydrogels that are able to respond reversibly more than one external stimulus are known as multi-responsive. Dhara et al. prepared a series of interpenetrating polymer network of poly(N-isopropylacrylamide) (PNIPA) with anionic poly(acrylic acid) (PAA) and cationic poly((3-(methacryloylamino)propyl)trimethylammonium chloride) (PMAPTAC) polymers. The swelling behavior of the prepared hydrogels was monitored as a function of pH and temperature and it was observed that the degree of swelling was dependent on the pH and temperature of the medium [54]. Liu et al. copolymerized acrylic acid (AA) and N, N-dimethylaminoethyl methacrylate (DMA) with PNIPA to obtain pH-induced thermosensitive functionality [55]. Brazel and Peppas prepared pH and temperature responsive poly(N-isopropylacrylamide-co-methacrylic acid) hydrogels and determined the swelling characteristics of the hydrogels [56]. Diez-Pena et al. also prepared pH and temperature responsive hydrogels based on PNIPA and poly(methacrylic acid) (PMAA) and studied their swelling behavior as a function of pH and temperature [57]. However, all the multi sensitive hydrogels described above are based on chemically cross-linked hydrogels prepared using organic cross-linkers such as BIS, tri(propyleneglycol) diacrylate, ethyleneglycol dimethylacrylate and tetraethyleneglycol dimethylacrylate, respectively. The organic cross-linkers are toxic and the conventional hydrogels that prepared by using this kind of cross-linker are often brittle and have limited swelling capacity due to its rigid structure. These disadvantages in terms of mechanical properties of conventional hydrogels limited their potential applications [58].

Recently, it was reported that a novel polymer-clay nanocomposite hydrogel was synthesized without using any organic cross-linker [10]. Haraguchi and Takehisa prepared a stable nanocomposite hydrogel by using inorganic laponite clay as multifunctional cross-linker in the polymer structure. The polymer chains are attached to the surface of clay sheets through ionic interactions. It was also indicated that the polymer chains in nanocomposite hydrogels are long and flexible which makes them adopting flexible random conformations. The authors indicated that polymer/clay network could only be formed by free-radicals solution polymerization which was initiated the redox system close to the surface of clay. They observed that the many properties such as swelling ratio, optical transparency, mechanical modulus were improved by incorporation of clay particles into the polymer structure.

Xiang et al. who prepared poly(2-hydroxyethyl methacrylate-co-poly(ethylene glycol) methyl ether methacrylate-co-methacrylic acid) (poly(HEMA–PEGMA–MAA)) hydrogel cross-linked by attapulgite clay reported that these nanocomposite hydrogel had much higher equilibrium swelling ratio, much faster response rate to pH and significantly improved mechanical properties [59]. Shen et al. was also reported similar results who prepared PNIPA based hydrogels cross-linked by laponite clay [60]. Haraguchi and Takada who prepared PNIPA based nanocomposite hydrogel cross-linked by laponite reported nanocomposite hydrogels can withstand better than the conventional ones the sliding friction under conditions of high loading [61]. In brief, the nanocomposite hydrogels were found more favorable for practical applications when compared to the conventional hydrogels because the hydrogel properties such as mechanical, thermal, optical, electrical responsiveness and frictional were improved.

In the study implemented by Zhang et al. the swelling behavior of polyacrylamide superabsorbent nanocomposites with five different clays including vermiculite, montmorillonite (bentonite), mica, kaolin and attapulgite was evaluated [62]. The effects of clay type and content on equilibrium swelling ration of the composites were investigated. Results showed that the type of clay affected the swelling rate differently and bentonite composites displayed the highest swelling rate. When compared to others its low cost and superior characteristics such as high water absorption, extensive swelling in water and higher cation exchange capacity, bentonite as inorganic layered nanoclay has unique advantages over the other clays.

3.1. Materials and Methods for Hydrogel Synthesis and Characterization

Potassium peroxodisulfate ($K_2S_2O_8$) (>99%, w/w) was purchased from Merck (Darmstadt, Germany). N-isopropylacrylamide (NIPA) (> 98%, w/w) was purchased from ABCR (Karlsruhe, Germany). NaAlg was kindly provided by GMT food (Istanbul, Turkey). N,N′-methylenebis(acrylamide) (BIS) (99%, v/v), N,N,N′,N′-tetramethylethylene diamine (TEMED) (99%, v/v), calcium chloride ($CaCl_2$) (>99.9%, w/w), sodium chloride (NaCl) (>99%, w/w), hydrochloric acid (HCl) (37%, v/v), sodium hydroxide (NaOH) (>97%, w/w), potassium dihydrogen phosphate (KH_2PO_4) (>98%, w/w) and Nanomer® PGV (bentonite nanoclay > 98% montmorillonite) were purchased from Sigma-Aldrich (St. Louis, MO, USA). The Nanomer® PGV is a product of Nanocor Inc. (Arlington Heights, IL, USA). It has a thickness of 1 nm, specific gravity = 2.6, cation exchange capacity = 145 meq 100 g^{-1} and individual sheets have aspect ratios (L/W) varying from 150 to 200. All reagents were analytical grade and used as received. All solutions used in the experiments were prepared with deionized water.

3.1.1. Hydrogel Synthesis

Nanocomposite hydrogels of various compositions were synthesized by free radical solution polymerization of NIPA monomer by using potassium peroxodisulfate (KPS) as the initiator and TEMED as the accelerator at room temperature according to the previously described method by Kasapoglu-Calik and Ozdemir with minor modifications [49]. Briefly, TEMED (40 μl), deionized water (10 ml) and nanoclay (20, 30 and 40% by weight with respect to NIPA) were stirred with a magnetic stirrer (IKA® RCT Basic, Staufen, Germany) at 23 °C for 18 h. The NIPA monomer (1 g) and NaAlg (20, 30 and 40% by weight with respect to NIPA) were added to the dispersion. The dispersion was stirred in an iced-water bath for 1 h until a homogeneous dispersion was obtained. The dispersion was degassed with nitrogen for 15 min to remove dissolved oxygen. Finally, 500 μL KPS (0.06 g in 1 ml H_2O) was added to the dispersion to initiate polymerization. The free radical polymerization was carried out in a water bath at 23 ºC for 48 h to allow complete polymerization/cross-linking of NIPA with nanoclay. The conventional hydrogels cross-linked with BIS (2 and 4% by weight with respect to NIPA) instead of nanoclay were also synthesized under the same conditions as the control.

After polymerization was completed, the prepared hydrogels were cut into discs with a thickness of 4 mm and diameter of 10 mm, and then immersed in an aqueous $CaCl_2$ solution (0.03 g ml^{-1}) for 15 min to form cross-linked NaAlg network followed by immersing the discs in deionized water for 4 days to remove unreacted constituents by changing the water daily. Finally, the hydrogel discs were dried in a freeze-dryer (Virtis Ultra Super XL, New York, USA) under vacuum at −35 °C for overnight. The compositions of prepared nanocomposite and conventional hydrogels are given in Table 3.1. Hydrogels with various NIPA and NaAlg ratios were labeled as NIPA/NaAlg-*m*C and NIPA/NaAlg-*n*B where the letters *m* and *n* correspond to the weight percent of nanoclay and BIS with respect to NIPA monomer, respectively.

Table 3.1: Compositions of Prepared Nanocomposite and Conventional Hydrogels.

Hydrogel Code	NIPA (g)	NaAlg (g)	Nanoclay (g)	BIS (g)
83/17-20C	1	0.2	0.2	-
83/17-30C	1	0.2	0.3	-
83/17-40C	1	0.2	0.4	-
77/23-20C	1	0.3	0.2	-
71/29-20C	1	0.4	0.2	-
83/17-2B	1	0.2	-	0.04
83/17-4B	1	0.2	-	0.08
77/23-2B	1	0.3	-	0.04
77/23-4B	1	0.3	-	0.08
71/29-2B	1	0.4	-	0.04
71/29-4B	1	0.4	-	0.08

3.1.2. SEM Analysis

The freeze-dried samples were fractured and coated with a thin layer of gold prior to analysis. The structure and morphology of the hydrogels were analyzed by a SEM (Philips XL30 FEG, Oregon, USA) an operating at a voltage of 2 kV.

3.1.3. Thermal Analysis

The lower critical solution temperature (LCST) and the glass transition temperature (T_g) of the prepared hydrogels were measured using a DSC (Perkin Elmer, Jade DSC, Shelton, CT, USA). The LCST determination of the swollen hydrogels was performed from 20 to 45 °C at a heating rate of 3 °C/min under nitrogen with a flow rate of 25 ml/min to avoid sample degradation in aluminum pans. Deionized water was used as the reference in DSC analysis. The LCST was the onset point of the endothermal peak, which was determined by intersecting point of two tangent lines from the baseline and slope of the endothermic peak.

For the determination of glass transition temperatures (T_g) of the freeze-dried hydrogels, approximately 5 mg of dried samples was scanned at a heating rate of 15°C/min under nitrogen with a flow rate of 25 ml/min to prevent oxidation. The first scan was done from 50 to 150 °C to remove all residual moisture and erase any thermal history. The T_g values were determined from the second scan performed from 30 to 300 °C.

3.1.4. FT-IR Analysis

FT-IR analysis of PNIPA, NaAlg, nanoclay, nanocomposite and conventional hydrogels were performed by a FT-IR spectrometer (Perkin Elmer Spectrum 100, Shelton, CT, USA) with a 4 cm^{-1} resolution in the wavenumber range of $650-4000$ cm^{-1}.

3.1.5. XRD Analysis

XRD patterns of dried and milled hydrogel samples were determined with an X-ray diffractometer (Rigaku D-max 2200PC, Tokyo, Japan) equipped with an X-ray source of Cu K_α radiation with wavelength, $\lambda = 0.15418$. Data were collected from 2θ of 5° to 70° (θ being the angle of diffraction) with a scanning rate of 1.2°/min. The voltage and current of the X-ray tubes were 40 kV and 40 mA, respectively.

3.1.6. Hydrogel Swelling Behavior

Swelling behavior of prepared nanocomposite and conventional hydrogels was investigated in buffer solutions with pH values of 1.2, 3.0, 5.0, 6.8, 8.0 and 10.0 to study of pH sensitivity of the hydrogels and temperatures at 5, 15, 25 and 37 °C to determine the temperature dependence of swelling degree. The concentrations of buffer solutions were 0.1 M and the temperature and pH values of buffer solutions were checked with a pH meter (Mettler-Toledo, SevenEasy model S20, Schwerzenbach, Switzerland). First, the dried hydrogels were weighed and immersed in 50 ml of buffer solution at determined pH and temperature value. Then the swelling experiments were carried out in a shaking water bath (Termal H11960, Istanbul, Turkey) at a rotational speed of 50 rpm. The hydrogels were removed from the buffer solutions periodically, blotted with a filter paper to remove excess water and weighed. The swelling ratio (SR) and equilibrium swelling ratio (ESR) values were calculated using Equation (3.1) and Equation (3.2), respectively.

$$SR = \frac{W_t - W_d}{W_d} \tag{3.1}$$

$$\mathrm{ESR} = \frac{W_s - W_d}{W_d} \tag{3.2}$$

where W_t is the weight of the hydrogel at time t during swelling, W_s is the weight of the swollen hydrogel and W_d is the weight of the dried hydrogel. The graphs were constructed by plotting the SR against time (t).

3.2. Results and Discussion for Hydrogel Synthesis and Characterization

3.2.1. Structure and Morphology of the Hydrogels

The prepared nanocomposite and conventional hydrogels with different nanoclay and BIS contents, were synthesized without any precipitation and phase separation. The hydrogels did not dissolve when they were put into an excess of distilled water for a week at room temperature, but they swelled and kept their original shapes. This result showed that all prepared hydrogels have cross-linked network structure. It was also confirmed that NIPA and nanoclay formed network structure without using any organic cross-linker. This result is consistent with the results obtained by Haraguchi and Takehisa and Ma et al. [10], [63]. As suggested by Haraguchi and Takehisa, the initiator molecule KPS strongly interacts with nanoclay sheets through ionic interactions and the KPS molecules were closely associated on the nanoclay surface in aqueous suspension [10]. Radical formation was initiated followed by the propagation reaction, and thus the PNIPA chains were attached to the nanoclay sheets forming a cross-linked network structure. A mixture of the aqueous solution of nanoclay and NaAlg was prepared without PNIPA with the same procedure used in the preparation of nanocomposite hydrogels to prove that the nanoclay was cross-linked with the PNIPA and not the NaAlg. When the prepared material was immersed in an excess of water, NaAlg dissolved and a turbid solution was formed. This showed that NaAlg was not cross-linked by the nanoclay when there is no NIPA monomer in the hydrogel.

The structure and morphological characteristics of freeze-dried nanocomposite and conventional hydrogels were examined by SEM. Figure 3.1 shows the SEM micrographs of the prepared hydrogels. The SEM micrographs of all prepared hydrogels revealed porous, sponge-like structure. The porous structure indicates the formation of cross-linking between the polymer chains [49]. It was observed that the internal structure of the hydrogels depends on the hydrogel composition. The effect of cross-linker change on structure of the prepared hydrogels with the same amount of NaAlg is given from Figure 3.1a through 3.1e. It was observed that the number of pores increased, and the pore size decreased with the increasing the cross-linker content.

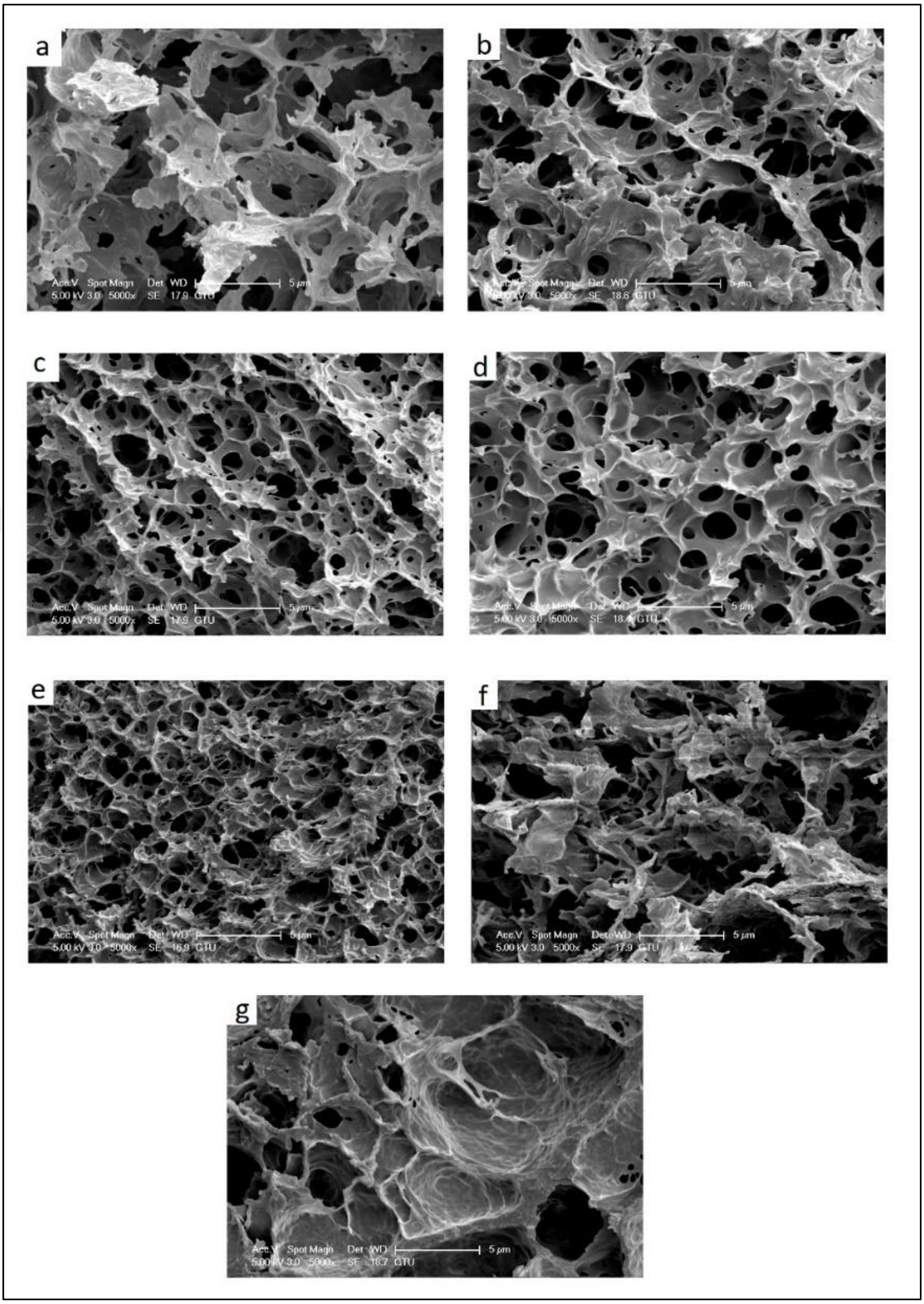

Figure 3.1: SEM micrographs of nanocomposite and conventional hydrogels: (a) 83/17-20C, (b) 83/17-30C, (c) 83/17-40C, (d) 83/17-2B, (e) 83/17-4B, (f) 77/23-20C and (g) 71/29-20C. Scale bar is 5 μm. Magnification: 5000x.

The average pore sizes of nanocomposite hydrogels were found to be 6, 3, and 1.5 μm for 83/17-20C, 83/17-30C and 83/17-40C, while average pore sizes of conventional hydrogels were 3 and 1 μm for 83/17-2B, 83/17-4B, respectively. It can be concluded from the results that the higher cross-linker content caused to form more cross-linking points and thus decreased the spaces between the polymer chains. These results are in agreement with the results reported by Haraguchi et al. who indicated that the clay content had a large effect on the characteristic properties of PNIPA based nanocomposite hydrogels and that the main result of increasing the clay content was an increase in the cross-link density [8]. Lee and Fu reported also similar results for PNIPA based nanocomposite hydrogels which number of pores increased and pore sizes decreased with the increased amount of cross-linker [64]. Conventional hydrogels were found to have more porous network structure than the nanocomposite hydrogels due to higher cross-linking density when BIS is used as the cross-linker (Figure 3.1a through 3.1d). The effect of NaAlg change on structure of the prepared hydrogels with the same amount of cross-linker is given in Figure 3.1a, f and g. The nanocomposite hydrogels with the same amount of nanoclay have been observed to have same pore sizes, regardless of the amount of NaAlg they contain. This result showed that pore sizes of prepared hydrogels were not affected by NaAlg content. This is because NaAlg does not participate the cross-linking reaction which may affect the pore size of the hydrogel network.

3.2.2. Thermal Analysis

The LCST values of prepared nanocomposite and conventional hydrogels are shown in Figures 3.2 and 3.3. The temperature at the onset point of the DSC endotherm is referred to as the LCST of the hydrogel [65]. The main mechanism for the phase transition involves the change of the hydration-dehydration behavior in PNIPA chains in hydrogels. LCST is the point where the hydrophobic interactions of the $-CH(CH_3)_2$ groups of PNIPA predominate the hydrophilic nature of the amide groups on the pendant groups in PNIPA chains, forcing water out of the hydrogels, then the network structure collapses. This cause to a smaller heat capacity. When the temperature is below LCST, the PNIPA based hydrogels show water-swollen property due to the hydrogen bond interactions between water and hydrophilic amide groups of the polymer. At temperature above LCST, thermal dissociation of hydrating water molecules from the polymer chains makes the intrinsic affinity of PNIPA polymer chains enhanced [66], [67]. The prepared nanocomposite hydrogels exhibited similar LCST values around 32.8 °C, while conventional hydrogels exhibited LCST values around 33.8 °C. Schild et al. observed similar LCST value of pure PNIPA hydrogel at 32 °C [68]. It was also observed that the LCST value was not dependent on the NaAlg and cross-linker amount. The water solubility of hydrogel is associated with hydrophilic-hydrophobic balance between the hydrogen bonds and the hydrophobic moieties of the polymer. These results indicated that the PNIPA polymer network retains its own property because of no chemical bond formed between NaAlg and PNIPA network which may change the hydrophilic-hydrophobic balance between the hydrogen bonds of PNIPA [69]. These results are consistent with the findings found by Zhang et al., Shi et al. and Ma et al. who reported that these hydrogels can be considered as semi-IPN systems [63], [70], [71]. Moreover, the LCST of conventional hydrogels was found to be approximately 1 °C higher than the nanocomposite hydrogels due to the formation of denser structures of PNIPA network when cross-linked with BIS as confirmed by SEM.

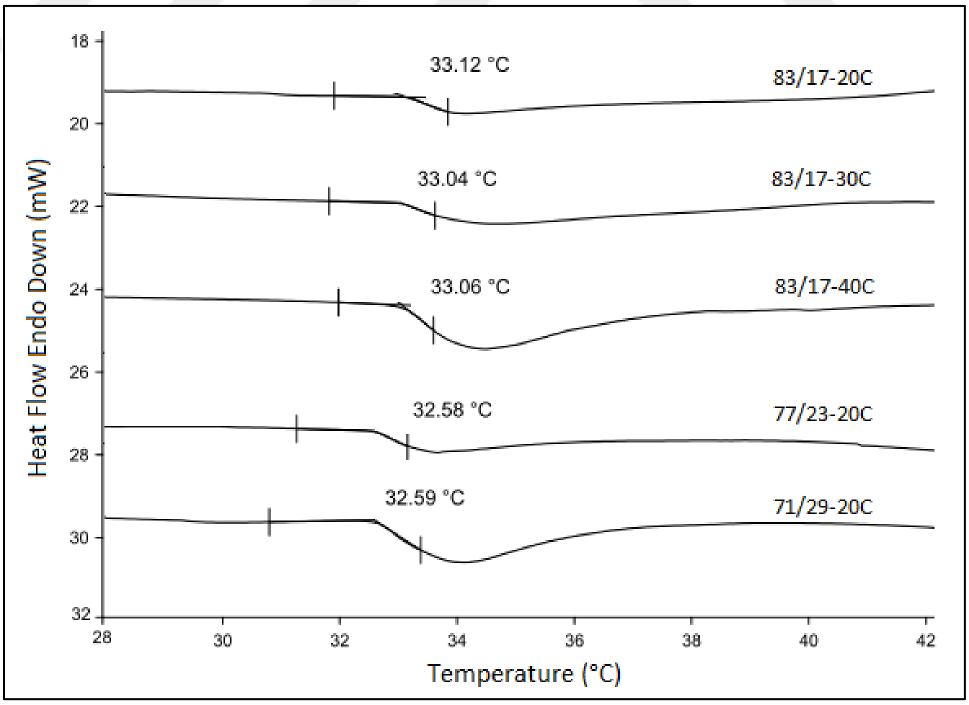

Figure 3.2: DSC thermograms of swollen nanocomposite hydrogels.

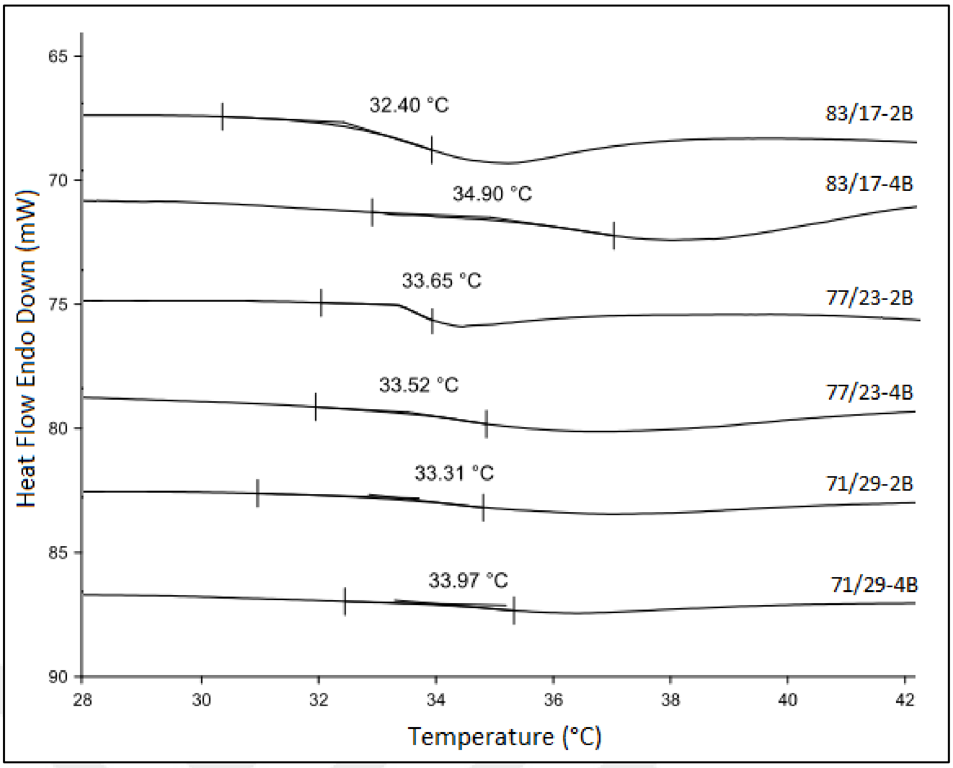

Figure 3.3: DSC thermograms of swollen conventional hydrogels.

The T_g values of prepared nanocomposite and conventional hydrogels are presented in Figures 3.4 and 3.5, respectively. The effect of different nanoclay contents on the T_g of 83/17-20C, 83/17-30C and 83/17-40C nanocomposite hydrogels with the same amount of NaAlg is given in Figure 3.4. The nanocomposite hydrogels with the same NaAlg content have been observed almost the same T_g (about 137 °C), irrespective of the amount of nanoclay, close to the linear PNIPA (135 °C). The effect of different BIS contents on the T_g of conventional hydrogels with the same amount of NaAlg is given in Figure 3.5. Contrary to the nanocomposite hydrogels, the T_g value in conventional hydrogels increased from about 156 to 176 °C with increasing BIS content from 2 to 4%. The T_g is an indication of polymer chain mobility and flexibility. It increases as the chain mobility is restricted [72]. It can be concluded from the results that the molecular motion of PNIPA chains in conventional hydrogels was restricted by cross-linking, while the PNIPA chains in the nanocomposite hydrogel network are still sufficiently long and flexible, similar to those in linear PNIPA. The results are consistent with the findings reported by Haraguchi and Takehisa who reported the T_g of the PNIPA based conventional hydrogels increased with increasing BIS content while the T_g of nanocomposite hydrogels did not affected by nanoclay content [10].

Haraguchi et al. was also observed the similar results for poly(N,N-dimethylacrylamide) based nanocomposite and conventional hydrogels [6].

The effect of different NaAlg contents on the T_g were also investigated. The T_g values of prepared nanocomposite and conventional hydrogels with the same nanoclay content decreased as the NaAlg content increased. This can be interpreted that additional NaAlg might act as plasticizer, hence lowering the T_g. The T_g values of prepared nanocomposite hydrogels with the same nanoclay content decreased from 139.42 to 134.59 °C as the NaAlg content increased from 20 to 40%. The T_g values of prepared conventional hydrogels with the same nanoclay content decreased from 156.39 to 141.44 °C as the NaAlg content increased from 20 to 40%. This can be interpreted that additional NaAlg increases the flexibility by acting as a plasticizer in the hydrogel matrix, hence lowering the T_g [49].

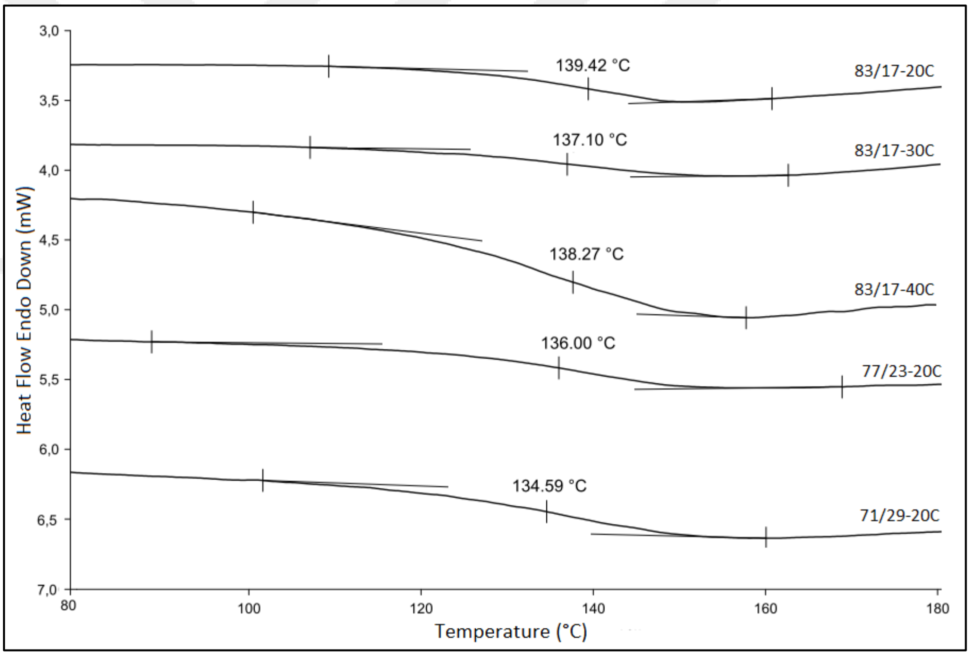

Figure 3.4: DSC thermograms of dried nanocomposite hydrogels.

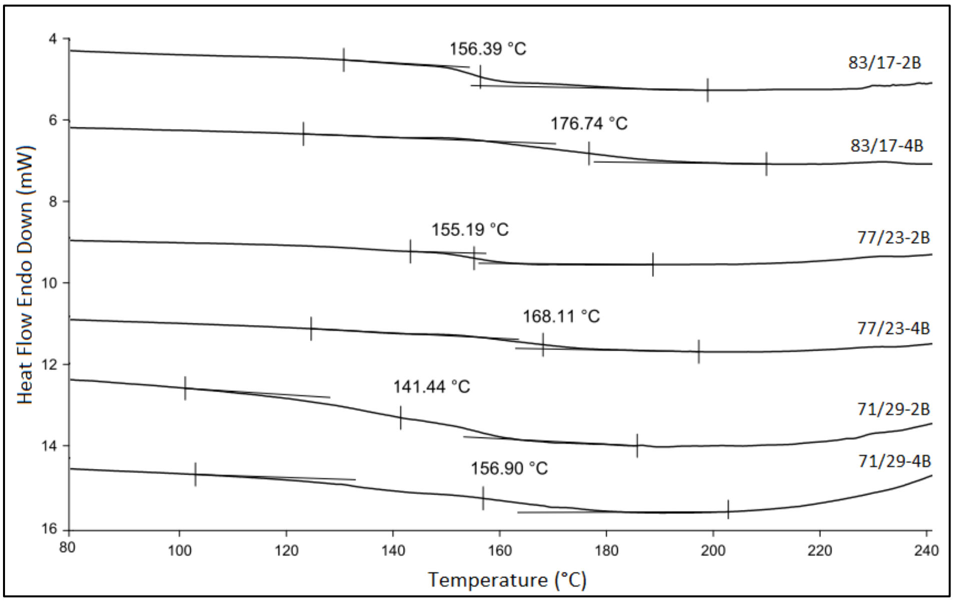

Figure 3.5: DSC thermograms of dried conventional hydrogels.

3.2.3. FT-IR Analysis

FT-IR spectroscopy was used for characterizing the molecular structure of prepared nanocomposite and conventional hydrogels. The FT-IR absorption spectra of nanoclay, NaAlg, PNIPA and prepared nanocomposite and conventional hydrogels are shown in Figure 3.6. The spectrum of nanoclay (Figure 3.6a) showed a characteristic peak at 3615 cm^{-1} corresponding to the –OH stretching vibrations of lattice hydroxyl groups. The broad absorption band at 3400 cm^{-1} was assigned to the –OH stretching vibrations of free H_2O. The HO–H bending vibrations of water appeared at 1633 cm^{-1} [73], [74]. The peak at 1425 cm^{-1} corresponded to the –OH bending of hydrated water [73]. The peak at 1110 cm^{-1} and the intensive absorption band at 1000 cm^{-1} were attributed to the Si–O–Si and Si–O stretching vibrations, respectively [75], [76]. The weak peaks at 910 and 840 and 780 cm^{-1} were attributed to the Al–O–H, Al–Mg–OH and Si–O–Al stretching vibrations, respectively [76], [77]. The spectrum of NaAlg (Figure 3.6b) showed characteristic absorption band at 3275 cm^{-1} corresponding to the stretching vibrations of –OH groups [78]. The peak at 2928 cm^{-1} corresponds to the vibration of –CH stretching. The peaks at 1594 and 1408 cm^{-1} are attributed to the asymmetric and symmetric stretching vibrations of COO^- groups, respectively. The band at 1298 cm^{-1} is the skeletal vibration of NaAlg [79]. The broad band around 1028 cm^{-1} is attributed to C–O–C stretching of saccharide structure [78]. The FT-IR spectra of PNIPA (Figure 3.6c) showed a broad band at 3286 cm^{-1} which is attributed to the N–H stretching vibration [69]. The peaks at 2972 and 2921 cm^{-1} were assigned to the C–H stretching vibrations. The typical amide peaks observed at 1630 and 1540 cm^{-1} corresponded to the C=O stretching of amide I group and N–H bending and C–H stretching vibrations of amide II group, respectively [69], [80]. The peak at 1460 cm^{-1} and a double band at 1387 and 1368 cm^{-1} corresponded to the C–H bending vibrations of isopropyl group ($-CH(CH_3)_2$) [81].

In the FT-IR spectrum of nanocomposite hydrogel (Figure 3.6d), the characteristic absorptions of bands of PNIPA (2972, 2921, 1540 and 1460 cm^{-1}) and NaAlg (1408 cm^{-1}) were maintained. The successful cross-linking of PNIPA/NaAlg based nanocomposite hydrogels by using nanoclay was confirmed by the presence of nanoclay peaks (3615, 1633 and 1000 cm^{-1}) in the spectrum of nanocomposite hydrogel. The FT-IR spectrum of conventional hydrogel (Figure 3.6e) also showed characteristic absorption bands present in PNIPA (2972 and 2921 cm^{-1}) and NaAlg (1408 and 1298 cm^{-1}) indicating the presence of these substances in the conventional hydrogel network. The peak at 1171 cm^{-1} which attributed to C–N stretching vibration of amide group in PNIPA hydrogel disappeared in the spectrum of conventional hydrogel due to the organic cross-linking of PNIPA with BIS. Common peaks were seen in the spectrum of both nanocomposite and conventional hydrogels. The broad band which range from 1590 to 1610 cm^{-1} was due to the overlapping of amide I and amide II peaks of PNIPA and carboxyl groups of NaAlg. The bands of between 2870 and 3000 cm^{-1} and 840 and 760 cm^{-1} which corresponds to the C–H stretching vibrations of PNIPA and NaAlg, respectively. The peak at 1408 cm^{-1} deceased apparently in the spectrum of both nanocomposite and conventional hydrogel, which indicated that the COO^- groups on NaAlg cross-linked by Ca^{2+} ions in the hydrogel matrix. The results from FT-IR spectroscopy showed that PNIPA and NaAlg successfully formed nanocomposite and conventional hydrogel networks.

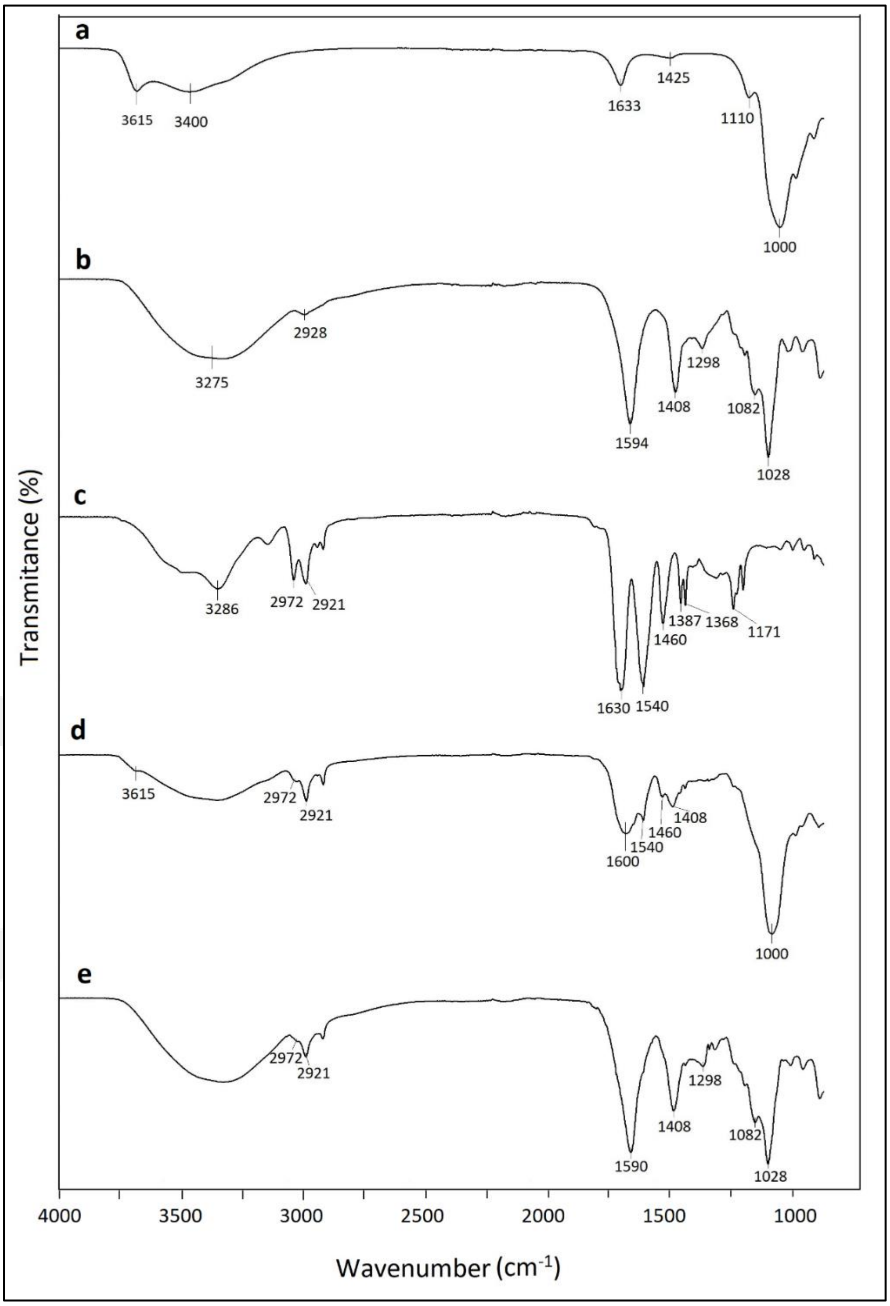

Figure 3.6: The FT-IR absorption spectra of (a) nanoclay, (b) NaAlg, (c) PNIPA and prepared (d) nanocomposite and (e) conventional hydrogels.

3.2.4. XRD Analysis

The XRD is an effective method for the investigation of the interaction among nanoclay and polymer matrix. The XRD patterns of nanoclay, freeze-dried nanocomposite hydrogels and conventional hydrogels are shown in Figure 3.7. The basal spacing value was calculated by Bragg's Law ($n\lambda = 2d\sin\theta$). The nanoclay pattern displayed diffraction a peak at 2θ angle of 5.98º corresponded to a nanoclay interlayer spacing value of 1.48 (Figure 3.7a). In the case of nanocomposite hydrogels (Figure 3.7b), the strength of the reflections tended to be weaker compared with nanoclay itself [49]. In other words, the position of the diffraction peaks corresponding to nanoclay and nanocomposite hydrogels did not change, but the strength of the peaks became weaker when the nanoclay is incorporated into the hydrogel structure. If the polymer chains were intercalated between the nanoclay sheets, the XRD peaks for the nanocomposite hydrogels would be shifted to a lower angle. If the nanoclay sheets were completely exfoliated in the hydrogel network, there would be no distinct diffraction peak. Based on these XRD results, it could be suggested that some of the nanoclay sheets are exfoliated in the structure whereas some of exist as clay tactoids in the polymeric matrix [82]. The XRD pattern of conventional hydrogels did not show any diffraction peak due to the non-crystalline structure of conventional hydrogels (Figure 3.7c).

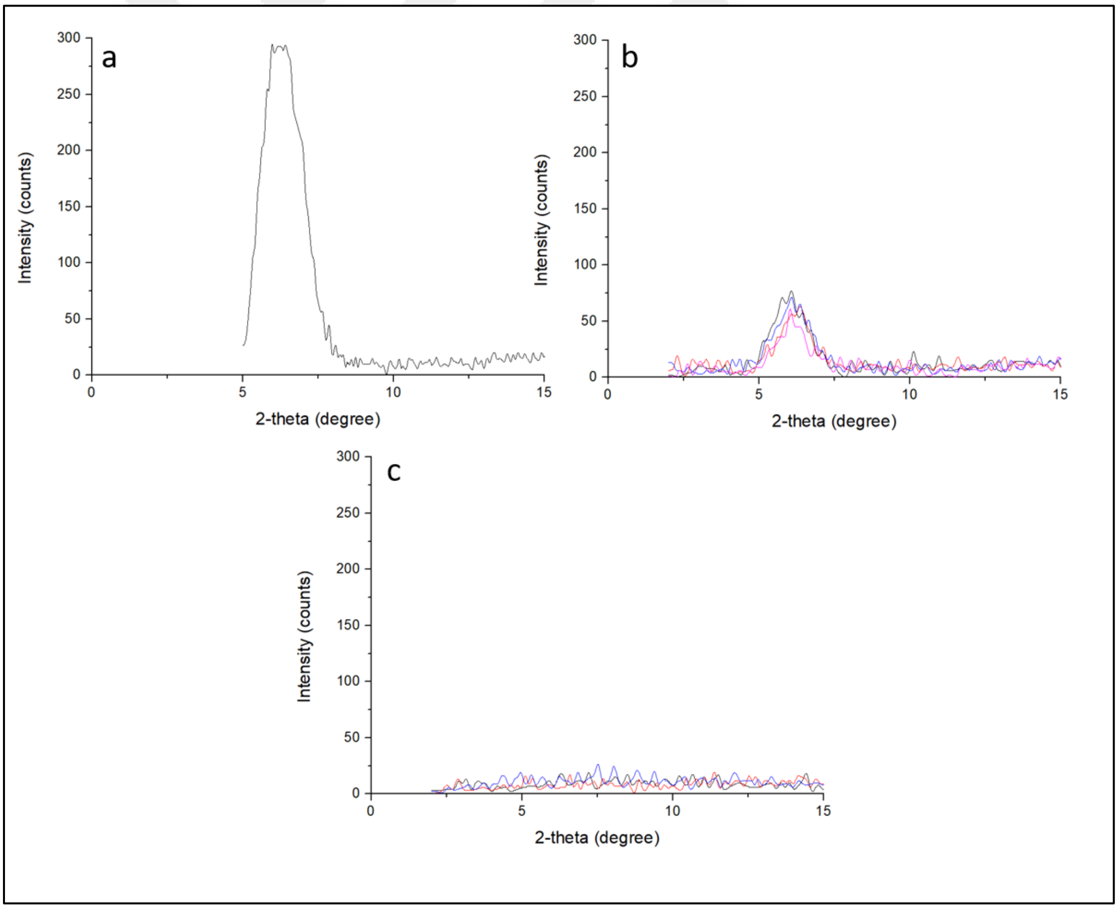

Figure 3.7: XRD profiles for (a) nanoclay, (b) nanocomposite hydrogels and (c) conventional hydrogels.

3.2.5. Effect of pH on Equilibrium Swelling

The effect of pH on ESR of the prepared nanocomposite and conventional hydrogels was determined in buffer solutions in the pH range from 1.2 to 10.0 (Figure 3.8). The ESR of all prepared nanocomposite hydrogels increased with increasing the pH from 1.2 to 6.8 at the temperature of 5 °C (Figure 3.8a). NaAlg is a kind of polyelectrolyte, which has carboxylic groups in its molecular chain [69]. At low pH values (below the $pK_a \cong 4.6$ of the carboxylic groups), the $–COO^-$ groups in NaAlg are protonated to form –COOH groups, and the hydrogen bonds between the –COOH groups in alginate and –CONH groups in PNIPA are formed. Hydrogen bonds lead to polymer-polymer interactions predominating over the polymer-water interactions which result in a decrease of swelling ratios [83]. Cao et al. indicated that alginate molecules form hydrophilic-hydrophobic aggregates in aqueous solutions depending pH of the medium [84]. The aggregation of NaAlg decreased the mobility of the hydrogel network as well as the water uptake. When the pH is above the pK_a value of the carboxylic groups of NaAlg, the carboxylic groups become ionized and the electrostatic repulsions among the molecular chains is predominated which leads to the network to expand. This increases the diffusion of water molecules into the hydrogel until the maximum swelling ratio is attained around pH of 6.8 [63], [70]. At pH $\cong$ 6.8, most of the –COOH groups were converted to $–COO^-$ groups, and this resulted in higher anion-anion repulsions and higher swelling ratio. At temperatures higher than 5 °C, the maximum ESR values obtained at pH = 8 (Figure 3.8b through 3.8d). The PNIPA chains swelled rapidly due to its hydrophilic characteristics at the low temperature values. Thus, the hydrogel reached the maximum swelling value at lower pH value. Highly expanded network of PNIPA hinders the further expansion of hydrogel by absorption of additional water. Above pH of 8.0, a screening effect of counter ions, such as Na^+, shielded the $–COO^-$ groups and prevented anion-anion repulsions, resulting in limited water diffusion into the nanocomposite hydrogels. As a result, a significant decrease in ESR observed. At pH = 10.0, all prepared nanocomposite hydrogels revealed second minimum ESR value. Ma et al. found similar results for carboxymethylcellulose/PNIPA/clay nanocomposite hydrogels where maximum swelling ratio was attained at pH = 5.9 because both alginate and carboxymethylcellulose have carboxylic groups [85]. Pourjavadi et al. also reported that alginate-g-poly(sodium acrylate)/kaolin nanocomposite hydrogels reached maximum swelling ratio at pH = 8 [86].

The effect of different nanoclay contents on ESR of 83/17-20C, 83/17-30C and 83/17-40C nanocomposite hydrogels with the same amount of NaAlg were also shown in Figure 3.8 in buffer solutions with pH values of 1.2, 3.0, 5.0, 6.8, 8.0 and 10.0 and temperatures at 5, 15, 25 and 37 °C. It was observed that the ESR value of nanocomposite hydrogels decreased with increasing the nanoclay content regardless of pH and temperature. In all cases, maximum ESR values were obtained for the 83/17-20C hydrogel while the minimum ESR value took place for the 83/17-40C hydrogel. When the amount of nanoclay in the hydrogel was increased, the polymer chains in the hydrogel were restricted by large number of cross-links, resulting in a polymer network with less ESR value [8], [59]. In other words, increasing the nanoclay content caused to decrease the cross-linking distance between polymer chains, resulting in the formation of denser polymeric network with less water swelling as confirmed by SEM images. Similar results were also reported by Li et al. who found that the equilibrium swelling ratio of PNIPA and poly(acrylamide) based nanocomposite hydrogels decreased as the nanoclay content in the hydrogel was increased [66]. Mahdavinia et al. observed a similar swelling behavior for poly(acrylamide)/carrageenan/ montmorillonite hydrogels. They reported that high clay concentration increased the extent of cross-linking of the polymer network, resulting in less swelling [87]. Ma et al. also found that the equilibrium swelling ratios of carboxymethylcellulose/PNIPA/laponite hydrogels decreased as the clay content increased from 20% to 60% at pH = 1.2 and 7.4 [63]. The effect of different NaAlg contents on ESR of 83/17-20C, 77/23-20C and 71/29-20C nanocomposite hydrogels with the same amount of nanoclay in buffer solutions with pH values of 1.2, 3.0, 5.0, 6.8, 8.0 and 10.0 and temperatures at 5, 15, 25 and 37 °C are given in Figure 3.8. The ESR of the nanocomposite hydrogels decreased as the NaAlg content increased from 20 to 40%. Maximum ESR value was obtained for the 83/17-20C hydrogel which has the lowest amount of NaAlg. When the amount of NaAlg in the hydrogel increases, the available free network space decreases, which preventing the movement of the chains and thus resulting in lower ESR.

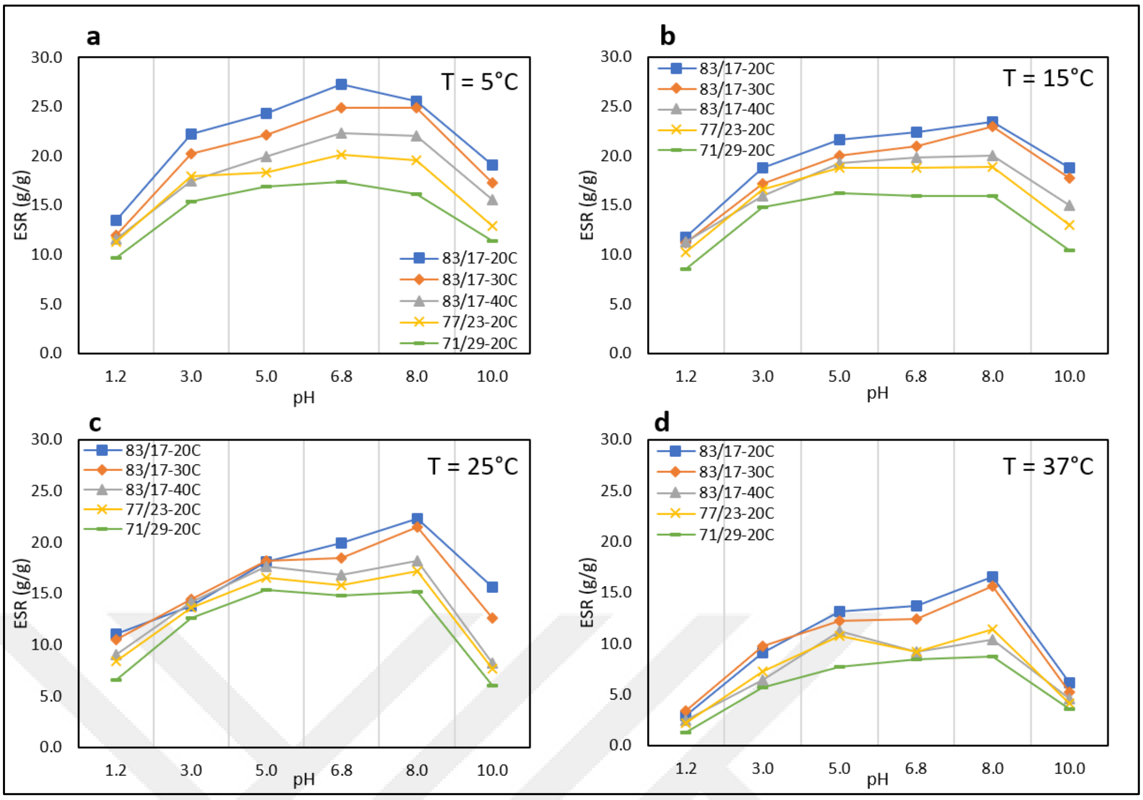

Figure 3.8: The ESR of nanocomposite hydrogels as a function of pH at (a) 5 °C, (b) 15 °C, (c) 25 °C and (d) 37°C.

Conventional hydrogels showed similar pH dependency as the nanocomposite hydrogels because of containing the same amounts of NaAlg (Figure 3.9). At 5 °C, the ESR value of the conventional hydrogels also increased with increasing the pH from 1.2 to 6.8. The maximum ESR was obtained at pH = 6.8. At the temperatures above 5 °C, the maximum ESR was obtained at pH = 8.0. At pH = 10.0, the ESR decreased for the same reasons formerly described. The effect of different NaAlg contents on ESR of the prepared conventional hydrogels with the same amount of BIS can be shown in Figure 3.9. It was observed that the ESR value decreased with the increase in the amount of NaAlg from 20 to 40%. The similar decrease was observed with the increase in the amount of BIS content from 2 to 4% when the amount of NaAlg kept constant. Although the conventional hydrogels showed similar swelling behavior on pH change of the medium, they showed less dependency on amount of NaAlg and cross-linker change and have lower ESR values than the nanocomposite hydrogels (Figure 3.9). This can be explained by the fact that the cross-linking with the BIS caused to form rigid structures of conventional hydrogels which limits the ESR [6]. Haraguchi and Takehisa (2002) indicated that the polymer chains between the cross-linking points in hydrogels cross-linked by nanoclay were long and flexible than the hydrogels cross-linked by BIS [10]. Therefore, it is reasonable to conclude that the nanocomposite hydrogels which cross-linked by nanoclay have lower cross-linking density which caused them to have higher ESR values than conventional hydrogels.

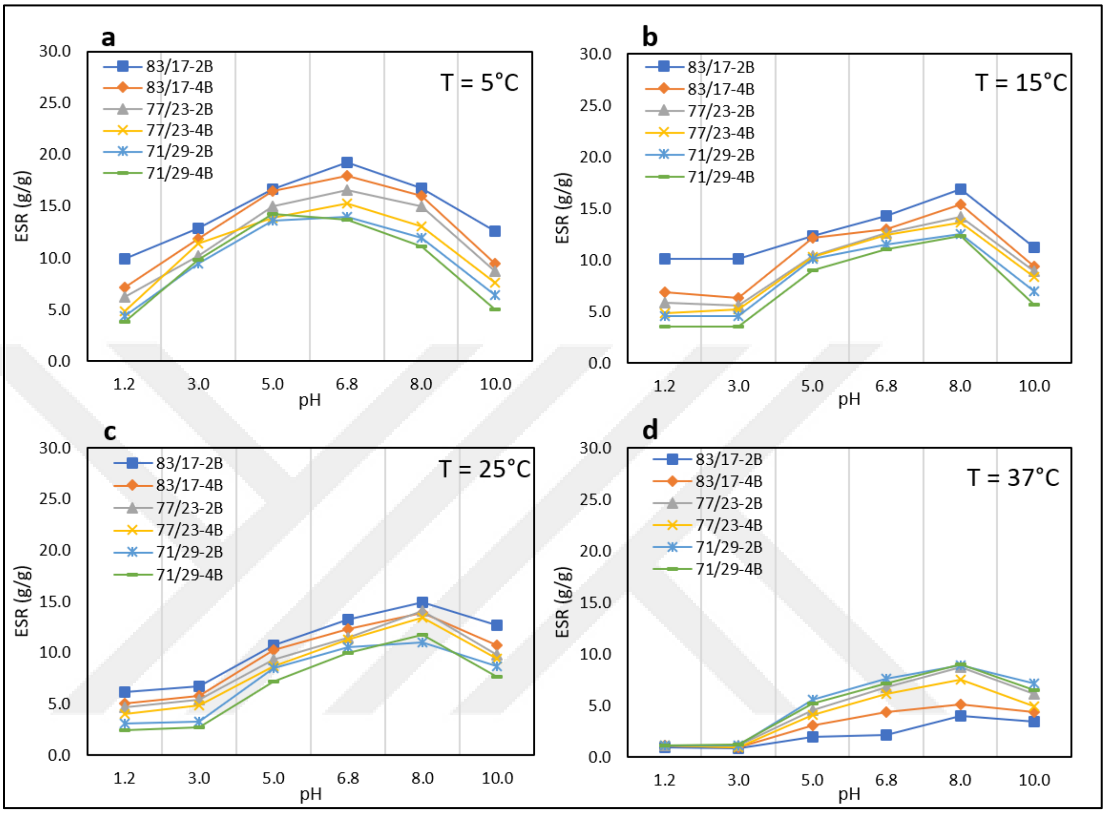

Figure 3.9: The ESR of conventional hydrogels as a function of pH at (a) 5 °C, (b) 15 °C, (c) 25 °C and (d) 37°C.

3.2.6. Effect of Temperature on Equilibrium Swelling

The effect of temperature on ESR of the prepared nanocomposite and conventional hydrogels was determined in the temperature range from 5 to 37 °C (Figure 3.10). All prepared nanocomposite hydrogels showed thermal responsivity due to the temperature sensitive behavior of PNIPA. It was observed that the ESR of all prepared nanocomposite hydrogels decreased as the temperature increases above to the LCST. At the temperature below the LCST, the hydrogel network was relaxed and highly swollen state. As the temperature was increased above to the LCST, the hydrophobic interactions among the hydrophobic –NH and C=O groups of PNIPA became dominant, then the phase transition occurred, finally the hydrogel collapsed.

At the temperatures below the LCST, the ESR of the nanocomposite hydrogels decreases with the increase of the nanoclay content (Figure 3.10a). For example, at 5, 15 and 25 °C, the 83/17-20C hydrogel has the highest ESR while the 83/17-40C has the lowest. Increase of nanoclay content in hydrogels resulted in less amount of water absorption into the hydrogels by increasing the cross-linking density in the hydrogel network. Li et al. reported similar results for PNIPA based nanocomposite hydrogels which ESR was decreased with the increased amount of nanoclay [66]. Similarly, the ESR of the nanocomposite hydrogels decreased with increase of the NaAlg content. When compared the nanocomposite hydrogels containing the same amount of nanoclay, the highest ESR was obtained at the 83/17-20C hydrogel while the lowest ESR was attained at 71/29-20C hydrogel. The increase of NaAlg content decreased the mobility of the hydrogel network as well as the water uptake, resulting in lowering the temperature sensitivity of the hydrogel. At 37 °C (above LCST), the ESR of all nanocomposite hydrogels decreased sharply, which is ascribed to the hydrophilic/hydrophobic balances of PNIPA formerly explained. As comparison, the temperature dependence of conventional hydrogels was also investigated (Figure 3.11). The conventional hydrogels exhibited lower ESR than nanocomposites. This result is consistent with the findings of Li et al. who prepared PNIPA based nanocomposite and conventional hydrogels and observed that the swelling ratio of nanocomposite hydrogels were much larger than those of conventional hydrogels [88]. The low ESR of conventional hydrogels was due to the restrictions of mobility of polymer chains by the high number of cross-links with BIS, even at commonly used moderate cross-linker concentrations [89]. The conventional hydrogels also showed poor thermal responsivity than those of nanocomposites due to the same reason. Almost no thermal sensitivity was observed in conventional hydrogels containing a higher amount of NaAlg, such as 71/29 and 77/23.

The conventional hydrogels showed a quite different swelling behavior than the nanocomposite hydrogels. At the temperatures of 5, 15, 25 °C, the ESR was decreased with increasing NaAlg content, whereas at 37 °C, the ESR was increased with increasing the NaAlg content, contrary to the nanocomposite hydrogels (Figure 3.11). Haraguchi et al. also reported PNIPA based nanocomposite and conventional hydrogels exhibit opposite swelling behaviors with respect to the cross-linker content [89]. These results showed that higher amounts of BIS should be used as cross-linker to achieve higher release values for the conventional hydrogels.

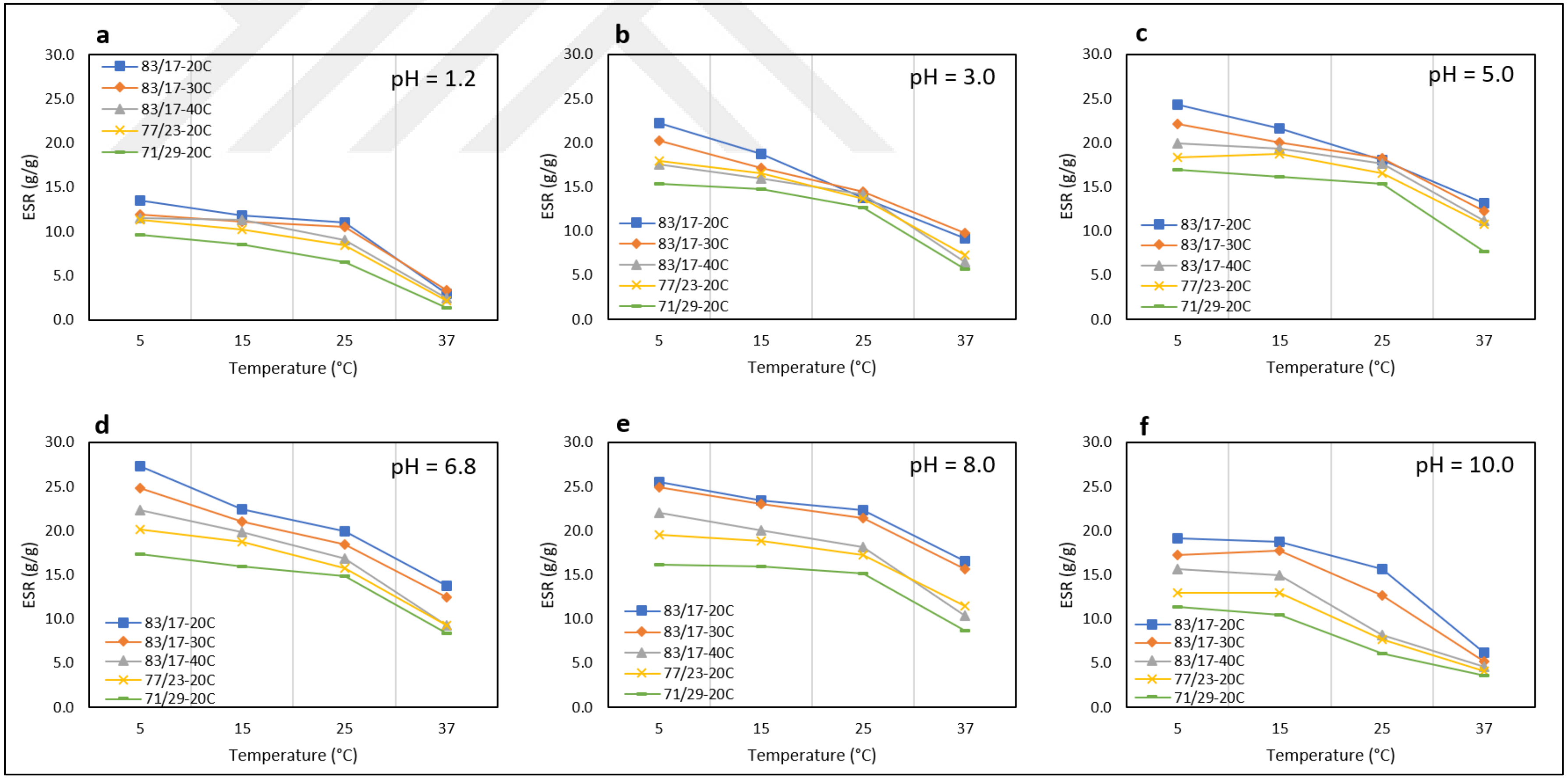

Figure 3.10: The ESR of nanocomposite hydrogels as a function of temperature in the pH of (a) 1.2, (b) 3.0, (c) 5.0, (d) 6.8, (e) 8.0 and (f) 10.0.

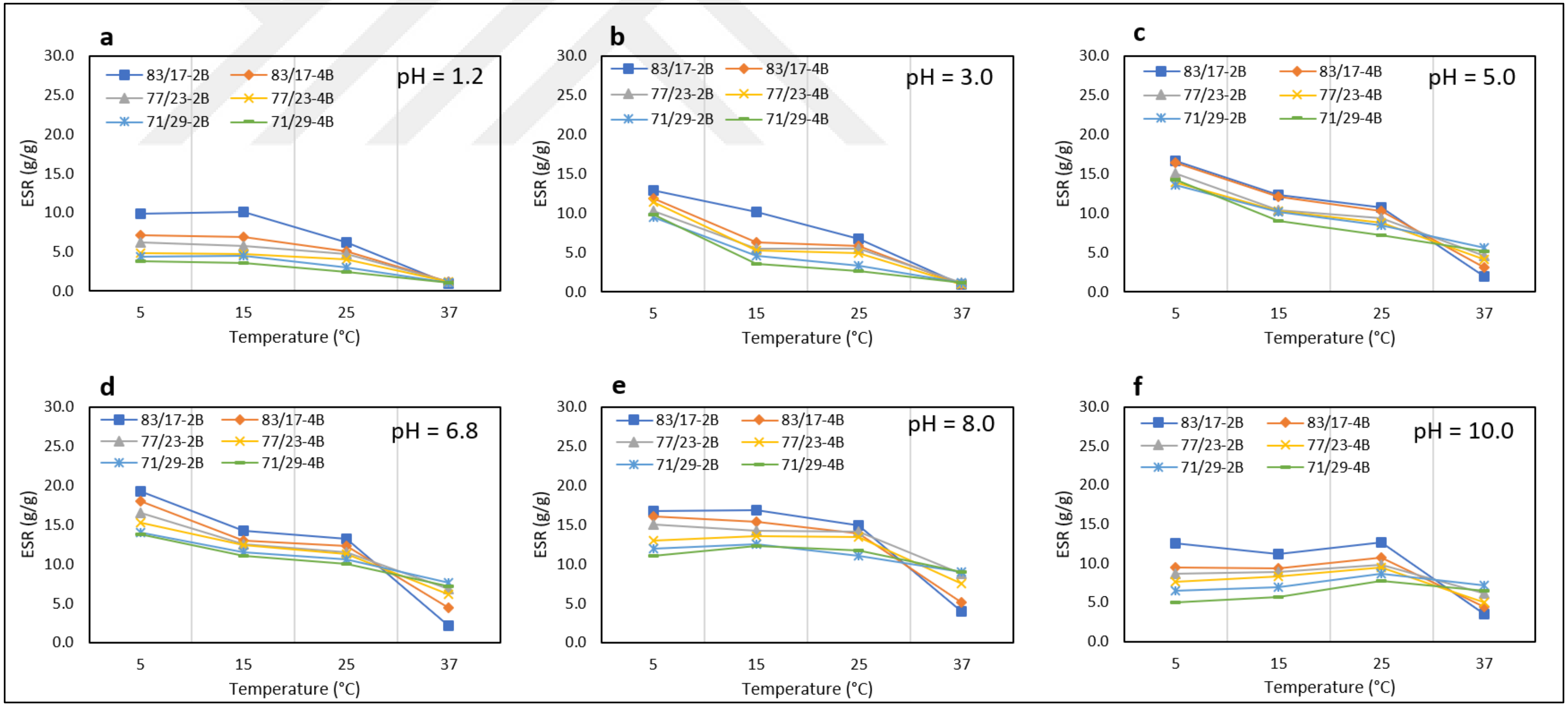

Figure 3.11: The ESR of nanocomposite hydrogels as a function of temperature in the pH of (a) 1.2, (b) 3.0, (c) 5.0, (d) 6.8, (e) 8.0 and (f) 10.0.

4. SYNTHESIS and CHARACTERIZATION of CURCUMIN-β-CYCLODEXTRIN INCLUSION COMPLEX

Curcumin (1,7-bis (4-hydroxy-3-methoxyphenyl)-1,6-heptadiene-3,5-dione) is a phytochemical that gives yellow color to turmeric which derived from the rhizome of Curcuma longa (Figure 4.1). It has been used in traditional medicine for many centuries in India and China. In recent years, curcumin has gained widespread popularity as a multipurpose drug due to its antioxidant [90], anti-inflammatory [91], antimicrobial [92] and antiproliferative [27] properties. It also found effective in treatment of various types of cancers, including multiple myeloma [93], head and neck squamous cell carcinoma [94], prostate [95] and breast cancer [96]. Moreover, it is considered as safe when administered at high doses [29]. However, its extremely low aqueous solubility, low oral bioavailability and intolerance to acidic or basic conditions prevents its therapeutic efficiencies [32], [97]. Although it has remarkable medicinal effects, the curcumin has not been approved as a therapeutic drug for biomedical applications [98]. There is a need for delivery systems to improve the aqueous solubility and bioavailability of curcumin.

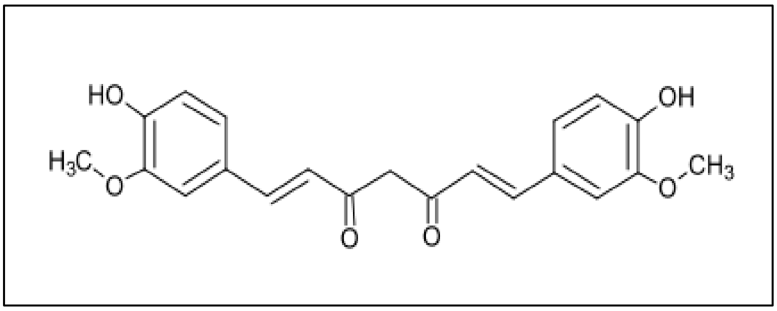

Figure 4.1: Chemical structure of curcumin.

To overcome these limitations, different formulations developed by several researchers. Merrel et al. investigated the feasibility and potential of poly(caprolactone) (PCL) nanofibres as a delivery vehicle for curcumin for wound healing applications [99]. It was observed that the curcumin-loaded nanofibres exhibited antioxidant properties. Wang et al. improved the aqueous solubility and stability of curcumin against light, heat and pH by preparing microcapsules using starch and gelatin as wall material [30]. Guo et al. construct curcumin/gelatin microspheres/collagen cellulose nanocrystals (Cur/GMs/coll-CNCs) scaffolds to obtain long and sustained release of curcumin [31]. The prepared curcumin based scaffolds exhibited remarkable antibacterial and anti-inflammatory activity on rat full-thickness burn infection model. Paramera et al. encapsulated curcumin in Saccharomyces cerevisiae yeast microcapsules. The heat stability and thermally induced release properties of curcumin were improved by the encapsulation. It was observed that the curcumin was significantly protected against oxidative degradation [32]. Hasan et al. reported an approach of encapsulation curcumin by nanoliposome to achieve an improved bioavailability of a poorly absorbed hydrophobic compound [33].

Harada et al. prepared γ-CD-curcumin complex to suppress the decomposition of curcumin in the aqueous environment at physiological conditions for the first time. The authors observed the significantly improved aqueous solubility of curcumin [100]. Hegge et al. investigated the effect of different combinations of cyclodextrins on curcumin release towards hydrophilic membranes. They reported that the inclusion complex of curcumin with hydroxypropyl-β-CD is the best choice with respect to curcumin solubility [101]. Jahed et al. investigated the solubility improvement of curcumin through inclusion complexation β-CD. It was shown that the curcumin solubility increased linearly with increasing β-CD concentration in the inclusion complex [34]. Among these investigations, CD formulations were found to improve aqueous solubility higher than 100-fold and eliminate the limitations of therapeutic properties [102].

CD’s are cyclic oligosaccharides consisting of several units of α-glucopyranose linked by α-1,4 glucoside bonds. The most common CDs are α-, β-, and γ-CD that are formed 6, 7, and 8 glucose units, respectively, which defines the width of the cavity and flexibility of the compound [103]. CD’s are formed by the enzymatic reaction of starch and all types are non-toxic and stable when heated up to 100 °C [32], [104]. The inner cavity of the CD molecules is hydrophobic whereas the outer surface is hydrophilic due to the –OH groups located in the rims of the truncated cone (Figure 4.2a). The hydrophilic outer surface permits aqueous miscibility of the CD molecule while the inner cavity allows hydrophobic molecules to be entrapped and form inclusion complexes. Among all of CD types, β-CD is the most widely used because its cavity size fits the common hydrophobic drugs with the molecular weights between 200-800 g mol^{-1} (Figure 4.2b) [26], [105].

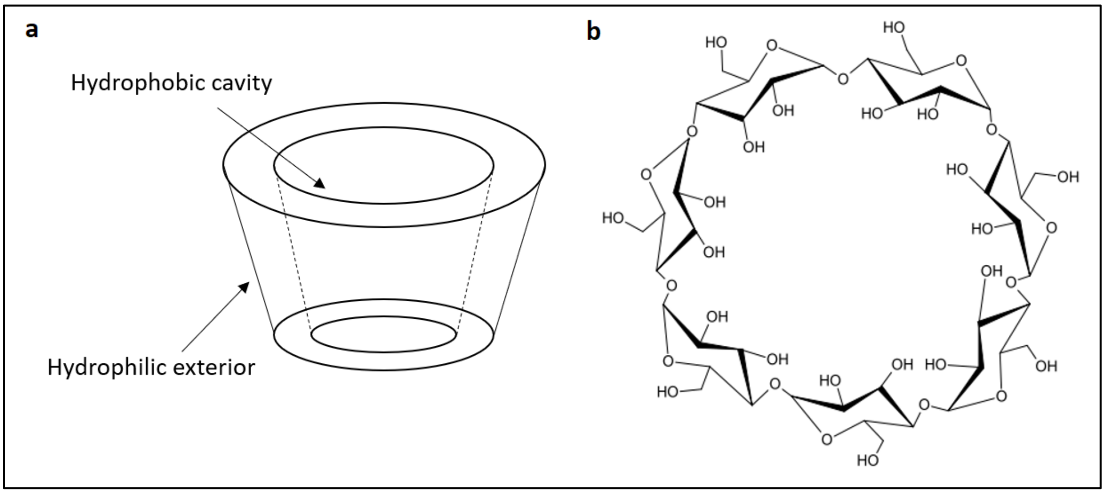

Figure 4.2: (a) The truncated cone shape of CDs and (b) chemical structure of β-cyclodextrin.

It has been shown in several studies that the β-CD inclusion complexes improve some properties of the guest molecules such as solubility, bioavailability and stability. Furthermore, the β-CD act as efficient drug carrier providing sustained release [103]. Medronho et al. formed an inclusion complex of β-CD and the polyphenol rosmarinic acid and reported that the antioxidant activity and storage stability remarkably improved with the complexation [106]. Wang et al. prepared β-CD/soybean lecithin inclusion complex and observed that the thermal stability of soybean lecithin in inclusion complex was significantly improved compared with free soybean lecithin [107]. Wang et al. investigated the physicochemical and release characteristics of inclusion complexes of garlic oil in β-CD [108]. Patro et al. investigated the effect of curcumin-CD complexation on its solubility and bioavailability. The authors observed significant enhancement on solubility and bioavailability of curcumin-CD inclusion complexes [109].

There are several methods to prepare β-CD inclusion complexes such as co-precipitation [105], kneading [38], freeze-drying [110], spray-drying [111], solvent evaporation [27], gas-liquid method [112], ultrasonic method [113], sealed heating method [114] and supercritical fluid technology [115]. The co-precipitation method has attracted more attention by researchers due to the advantages of being simple, easy observation of complex formation, and determination of guest disappearing [116], [117]. Marcolino et al. showed that in the co-precipitation method, a better interaction occurred between bixin and β-CD molecules when compared with the kneading method, and the highest aqueous solubility of curcumin was achieved with the co-precipitation method [105]. Paramera et al. noted that the interaction of curcumin with organic solvents restricted the total inclusion of curcumin to β-CD cavity in the kneading and co-evaporation methods and reported that the co-precipitation method was the most effective method for the inclusion of curcumin in β-CD [32]. Mangolim et al. also reported that the curcumin-β-CD inclusion complex obtained with the co-precipitation method had higher complexation efficiency (inclusion ratio) than the freeze-drying and solvent evaporation methods [26].

The stoichiometric ratio is an important parameter of inclusion complex formation. It was observed by researchers that curcumin forms inclusion complexes with β-CD in a 1:1 and 2:1 stoichiometric ratios [34], [103]. Tonnesen et al. assumed 1:1 complex formation and determined association constant only for 1:1 molar ratio [97]. In the contrary, Tang et al. indicated that, curcumin is too large to be included entirely into one β-CD cavity according to its molecular dimension [118]. They suggested 2:1 inclusion where each of benzene rings of curcumin was included into one β-CD cavity with the driving of van der Waals interactions, hydrophobic interactions and hydrogen bonding. Recently, Jahed et. al. have published a report on this subject, and concluded that a 1:2 complex is formed, based on Roesy Nuclear Magnetic Resonance (Roesy NMR) experiments and molecular modelling [34]. To clarify this contradiction, in the present study the stoichiometric ratio of the inclusion determined by using the Benesi-Hildebrand method [119].

4.1. Materials and Methods for Inclusion Complex

Curcumin (1,7-Bis(4-hydroxy-3-methoxyphenyl)-1,6-heptadiene-3,5-dione) (100%, w/w) and methanol (99.9%, v/v) were purchased from Merck (Darmstadt, Germany). β-cyclodextrin (β-CD) (100%, w/w) was obtained from Applichem GmbH (Darmstadt, Germany).

4.1.1. Determination of Stoichiometric Ratio and Association Constant of Inclusion

For the determination of the stoichiometric ratio and association constant of inclusion, the modified Benesi-Hildebrand method was used [103]. The mixed solutions of curcumin and β-CD with different concentrations were prepared. The curcumin concentration was kept constant at 3.0×10^{-5} M while the β-CD concentration varied from 3.0×10^{-5} to 15.0×10^{-5} M. The absorbance of curcumin was measured at 425 nm by a UV-visible spectrophotometer (Perkin Elmer Lambda 35, Shelton, CT, USA). Experimental data were fitted to Equation (4.1) by assuming stoichiometric ratio (1:n, Cur:β-CD) of 1:1 and 1:2.

$$\frac{1}{A_1 - A_0} = \frac{1}{(A_\infty - A_0)K_n[CD]^n} + \frac{1}{A_\infty - A_0} \tag{4.1}$$

where A_1 and A_0 are the observed absorbances of the curcumin solution in the presence and the absence of β-CD, respectively. A_∞ is the expected absorbance when all the curcumin molecules have made a complex. $[CD]$ is the concentration of β-CD (M). The association constant (K_n) was calculated from the double-reciprocal plot.

4.1.2. Preparation of Curcumin-β-Cyclodextrin (Cur-β-CD) Inclusion Complex

The inclusion complex of Cur-β-CD with a stoichiometric ratio of 1:2 was prepared by co-precipitation method described by Marcolino et al. with minor modification. An aqueous solution of β-CD with a concentration of 0.06 mol L^{-1} was stirred at 60 °C for 1 h [105]. Curcumin was dissolved in minimum volume of methanol added dropwise to the β-CD solution. The mixture was refluxed with vigorous stirring at 70 °C for 4 h. The solution was then stirred for an additional 1 h at 70 °C without reflux to remove methanol followed by cooling the solution to room temperature. After stirring at ambient temperature for 8 h, the solution was stored overnight at 4 °C and filtered through a sintered glass filter (Schott P5, Duryea, PA, USA). The final product was dried in a vacuum oven (Binder VD 23, Tuttingen, Germany) at 50 °C and stored at 4 °C until further use. The total recovery was calculated according to Equation (4.2).

$$Total\ recovery\ (\%) = \frac{m_{IC}}{m_{Cur} + m_{\beta-CD}} \times 100 \tag{4.2}$$

where m_{IC} is the weight of obtained inclusion complex (mg), m_{Cur} and $m_{\beta-CD}$ are the initially added weights of curcumin (mg) and β-CD (mg), respectively.

A physical mixture of curcumin and β-CD was prepared as the control. Curcumin and β-CD with the same stoichiometric ratio (1:2) as the inclusion complex were mixed together with a marble mortar and pestle for 5 min until a homogeneous mixture was formed.

4.1.3. Determination of Curcumin Content in the Inclusion Complex

Curcumin content in the inclusion complex was determined using the method described by Wang et al. with minor modification [108]. Curcumin solutions in anhydrous methanol with the concentrations of 1.0, 2.0, 3.0, 4.0, 5.0, 6.0 7.0 and 10.0 μg mL^{-1} were prepared. Absorbance values were measured with a UV-visible spectrophotometer (Perkin Elmer Lambda 35, Shelton, CT, USA) at 425 nm. The calibration curve of curcumin was prepared by plotting absorbance values of curcumin solutions against curcumin concentration. To determine the curcumin concentration in the inclusion complex, 20 mg of the inclusion complex and 30 ml of methanol were mixed in a conical flask, and the mixture was ultrasonically agitated in an ultrasonic bath (Bandelin Sonorex RK 31 H, Berlin, Germany) operated at a frequency of 35 kHz for 10 min. The resulting solution was centrifuged at 2500 rpm for 20 min with a centrifuge (Ortoalresa Digicen 21, Madrid, Spain). The amount of curcumin was quantified spectrophotometrically by measuring the absorbance at 425 nm. The curcumin inclusion ratio (%) and curcumin loading (%) were calculated by using Equation (4.3) and Equation (4.4), respectively.

$$Inclusion\ ratio\ (\%) = \frac{Cur_E}{Cur_T} \times 100 \tag{4.3}$$

$$Curcumin\ loading\ (\%) = \frac{Cur_E}{IC_T} \times 100 \tag{4.4}$$

where Cur_E is the calculated amount of curcumin in inclusion complex (mg), Cur_T *is* the amount of curcumin initially used to prepare the inclusion complex (mg) and IC_T is the total amount of inclusion complex obtained (mg).

4.1.4. Assessment of Aqueous Solubilities of Curcumin and Cur-β-CD Inclusion Complex

Molar absorption coefficients of curcumin were calculated to determine aqueous solubilities of curcumin and inclusion complex. First, a stock solution of curcumin (3.0×10^{-3} mol L^{-1}) in methanol/water solution (1:1, v/v) was prepared. Then, different solutions containing various concentrations (2.0, 4.0, 6.0 8.0, 10.0 and 12.0 μg mL^{-1}) of curcumin were prepared by diluting the stock solution with methanol/water solution. Absorbance values of the prepared solutions were measured spectrophotometrically at 425 nm. The molar absorption coefficient of curcumin in methanol/water solution was calculated by the Beer-Lambert law according to the Equation (4.5).

$$A = \varepsilon \cdot l \cdot C \tag{4.5}$$

where A is the measured absorbance, ε is the molar absorption coefficient (L mol^{-1} cm^{-1}), l is the width of the UV cuvette (cm) and C is the curcumin concentration (mol L^{-1}).

The solubilities of curcumin and inclusion complex were determined by adding excess amounts of curcumin and inclusion complex separately to the 10 ml of water. The flasks were sealed and shaken with a shaking water bath (Termal H11960, Istanbul, Turkey) at a rotational speed of 50 rpm at ambient temperature for 48 h. The samples were filtered using a 0.45 μm PVDF syringe filter (Millipore, Milan, Italy). One ml of the filtrate was mixed with an equal volume of methanol, and the mixture was analyzed spectrophotometrically at 425 nm. The dissolved curcumin concentration was calculated using the Beer-Lambert law.

4.1.5. Characterization of Cur-β-CD Inclusion Complex

Thermal analysis of curcumin, β-CD, Cur-β-CD complex, and the physical mixture of curcumin and β-CD were performed by using a DSC (Perkin Elmer, Jade DSC, Shelton, CT, USA). Approximately 10 mg of each sample was sealed into aluminum pans. Samples were scanned at a heating rate of 10 °C min^{-1} under nitrogen with a flow rate of 25 ml min^{-1} to prevent oxidation. The first scan was done from 50 to 150 °C to remove all residual moisture and erase any thermal history. The thermal properties were determined from the second scan performed from −20 to 350 °C.

FT-IR analysis of curcumin, β-CD, Cur-β-CD complex, and the physical mixture of curcumin and β-CD were performed by a FT-IR spectrometer (Perkin Elmer Spectrum 100, Shelton, CT, USA) with a 4 cm^{-1} resolution in the wavenumber range of 650–4000 cm^{-1}.

4.2. Results and Discussion for Inclusion Complex

4.2.1. Stoichiometric Ratio and Association Constant of Inclusion

The modified Benesi-Hildebrand method has been used extensively to determine the stoichiometry and the association constants of the inclusion complexes [119], [120]. In this context, the modified Benesi-Hildebrand method was used to determine stoichiometry and association constants by constructing the Benesi-Hildebrand plots for Cur-β-CD inclusion complexes in which 1:1 and 1:2 (Cur:β-CD) stoichiometric ratios were assumed (Figure 4.3). There was not a linear relationship between $1/(A_1 - A_0)$ and $1/[CD]^1$ (Figure 4.3a) which indicates that the stoichiometric ratio of 1:1 was not appropriate suggesting the presence of higher order inclusion complex formation. The best linear fit for the Cur-β-CD inclusion was obtained when $1/(A_1 - A_0)$ was plotted against $1/[CD]^2$ (Figure 4.3b), suggesting the formation of 1:2 inclusion complex ($R^2 = 0.9991$). The stoichiometric ratio of 1:2 of the inclusion complex between curcumin and β-CD was also determined by Jahed et al. who characterized the inclusion complex by NMR spectroscopy and molecular modeling, and they observed that two aromatic rings of curcumin interact with two β-CD molecules through hydrogen bonds [34]. Chalumot et al. also found that the 1:2 stoichiometric ratio some aromatic compounds and β-CD using the modified Benesi-Hildebrand method [121]. During the inclusion complex formation, water molecules inside the β-CD cavity were released and curcumin molecules entered to the β-CD cavity, causing the formation of apolar-apolar interactions [122]. The probable structure of Cur-β-CD inclusion complex with stoichiometric ratio of 1:2 can be shown in Figure 4.4.

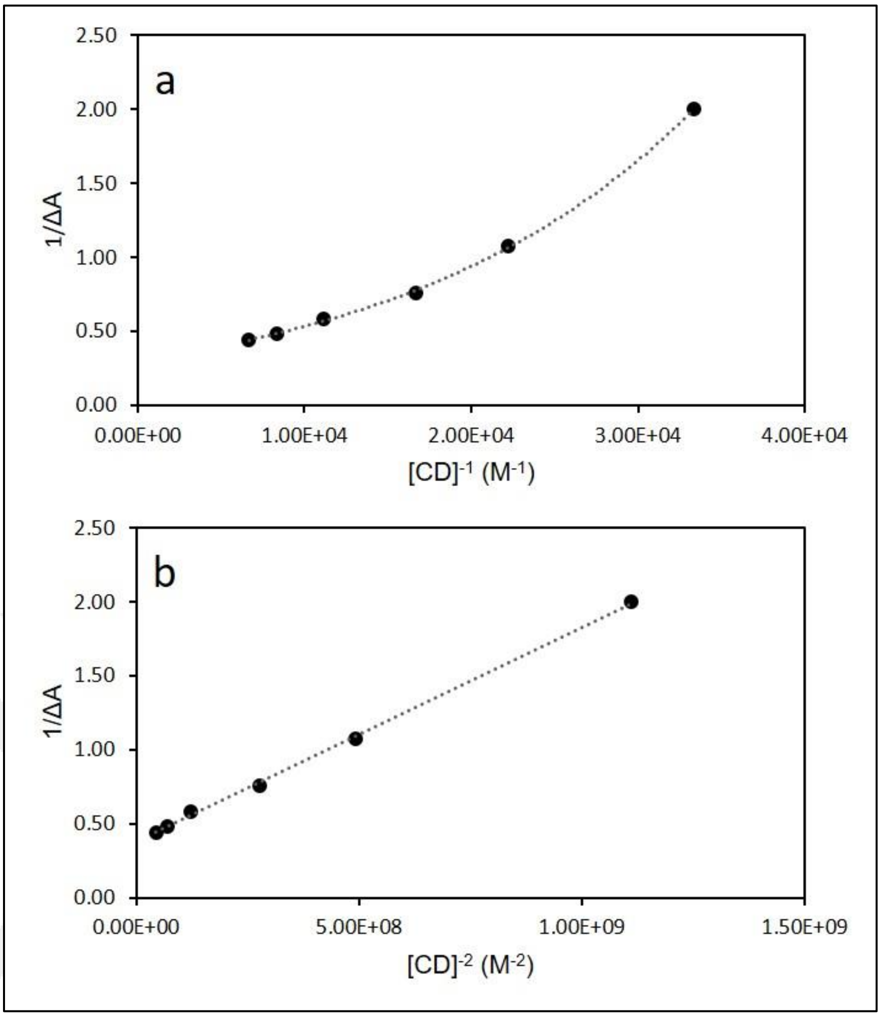

Figure 4.3: Benesi-Hildebrand plots for Cur-β-CD inclusion complexes.

The determination of stoichiometric ratio of the inclusion is strongly correlated with the estimation of the association constant. The association constant controls the formation of the inclusion complex and represents a quantitative measure of the host-guest interaction [123]. Higher association constant refers to a stronger relationship between the host and the guest molecules. The association constant (K_2) in this study for the 1:2 stoichiometric ratio between curcumin and β-CD was found to be $3.80 \times 10^8\ \mathrm{M}^{-2}$. Higher value of K_2 indicates a higher association between the host and the guest molecule [124].

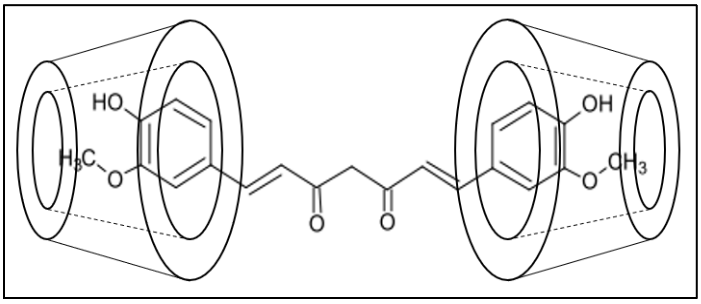

Figure 4.4: Probable structure of 1:2 Cur-β-CD inclusion complex.

4.2.2. Total Recovery, Inclusion Ratio and Curcumin Loading of the Cur-β-CD Inclusion Complex

The total recovery of curcumin in this study was found to be 77.8% which is in the range of total recovery values for β-CD and curcumin inclusion complexes (between 73 and 83%) prepared by Yallapu et al. [27]. The inclusion ratio of the prepared Cur-β-CD inclusion complex was 60.9%. Mangolim et al. prepared an inclusion complex of curcumin and β-CD with the co-precipitation method using ethanol as the solvent and found an inclusion ratio of 74% [26]. Paramera et al. also used co-precipitation method and prepared an inclusion complex of curcumin and β-CD in presence of 50% methanol and obtained lower inclusion ratio [32]. The differences in the inclusion ratios could be attributed to the type and concentration of the solvent used in the co-precipitation method. Wang et al. complexed garlic oil with β-CD with the co-precipitation method and obtained an inclusion ratio of 90.3% [108]. Tao et al. prepared thyme oil and thymol inclusion complexes with β-CD using freeze-drying and kneading methods and obtained values between 71.3 and 82.6% [38]. The inclusion ratio obtained in the present study is relatively low compared with the inclusion ratios obtained for thymol and garlic oil inclusion complexes with β-CD. This is due to the larger molecular dimension of curcumin than the thyme oil, thymol and garlic oil, and the inclusion complexation method used. Hedges et al. indicated that the shape of the guest molecule is an important factor for complexation [125]. Larger guest molecules such as curcumin can complex with more than one molecule of cyclodextrin and this lowers the value of inclusion ratio. The type of the inclusion complexation method used was found to affect the inclusion ratio by different researchers [26], [32].

The curcumin loading in the present study was found to be 10.9% for the Cur-β-CD inclusion complex prepared. This finding is considerably higher than the result reported by Paramera et al. who found a curcumin loading value of 2.7% [32]. Higher curcumin loading values obtained in this study could be attributed to the concentration of methanol (99.9% v/v) used in the co-precipitation compared to the study of Paramera et al.who used 50% v/v methanol [32].

4.2.3. Aqueous Solubility of Curcumin and Cur-β-CD Inclusion Complex

Molar absorption coefficient (ε) of curcumin in methanol/water solution was determined to be 45.3×10^3 $\mathrm{L\,mol^{-1}cm^{-1}}$ by the Beer-Lambert law. The aqueous solubility of pure curcumin and the Cur-β-CD inclusion complex was found to be 0.00122 and 0.721 $\mathrm{mg\,ml^{-1}}$, respectively. The increase in solubility of curcumin after complexation was 590-fold compared to the solubility of pure curcumin. Yadav et al. reported aqueous solubility of pure curcumin as 0.003 $\mathrm{mg\,ml^{-1}}$ and the aqueous solubility of Cur-β-CD inclusion complex as 0.609 $\mathrm{mg\,ml^{-1}}$ [35]. The solubility of curcumin after complexation using kneading method increased by only 202-fold. Higher solubility value for the curcumin inclusion complex obtained in the present study is due to the better compatibility of β-CD with curcumin in co-precipitation method.

4.2.4. Characterization of Cur-β-CD Inclusion Complex

DSC is a very useful tool in the investigation of thermal properties of inclusion complexes. It provides invaluable information about the physicochemical state of the drug inside the cyclodextrin complexes [35]. Figure 4.5 shows the DSC thermograms of curcumin, β-CD, the physical mixture of curcumin and β-CD, and Cur-β-CD inclusion complex. Curcumin showed the endothermic peak of its melting point at 176 °C (Figure 4.5a). The DSC thermogram of β-CD (Figure 4.5b) showed two endothermic peaks at 94 °C and 326 °C corresponding to dehydration of water from its cavity and its melting point, respectively. The physical mixture of curcumin and β-CD had the same endothermic peaks identical to pure curcumin and β-CD (Figure 4.5c). This indicates that no inclusion between curcumin and β-CD has occurred by simple mixing. In the DSC thermogram of Cur-β-CD inclusion complex. (Figure 4.5d), characteristic melting peak of curcumin at 176 °C disappeared, indicating that all the curcumin molecules incorporated into the β-CD cavity by replacing the water molecules and formed an inclusion complex. Similar results were also found by Yallapu et al., Paramera et al. and Mohan et al. [27], [32], [110].

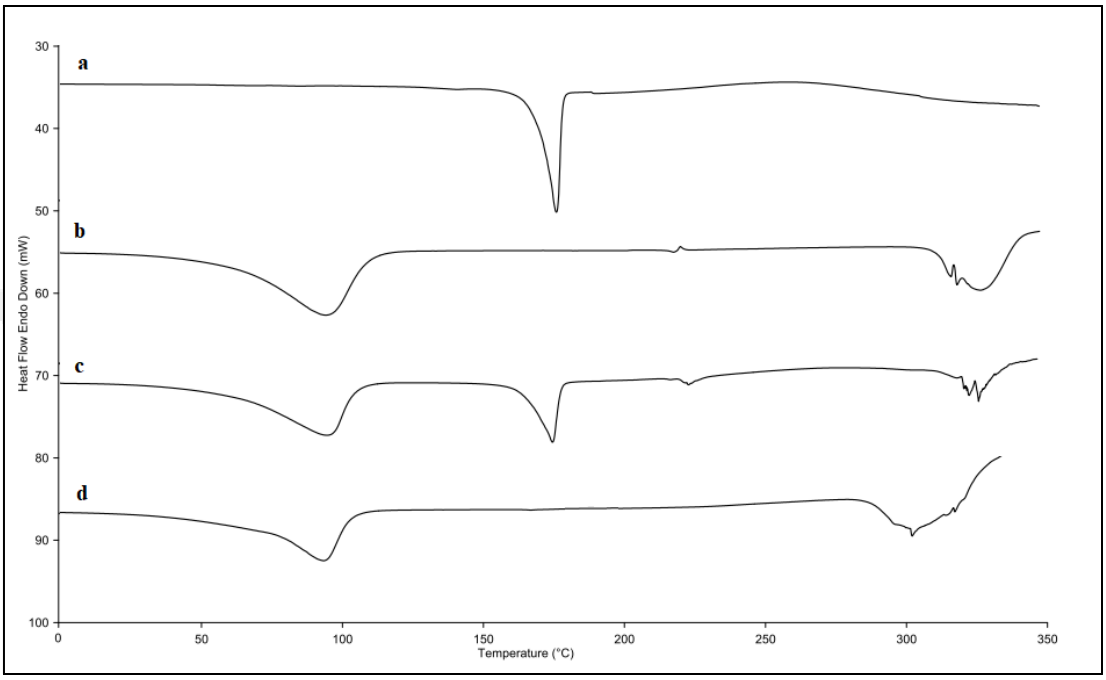

Figure 4.5: DSC curves of (a) curcumin, (b) β-CD, (c) physical mixture of curcumin and β-CD, and (d) Cur-β-CD inclusion complex.

FT-IR spectroscopy is a useful technique used to confirm the formation of an inclusion complex. The FT-IR spectra of curcumin, β-CD, the physical mixture of curcumin and β-CD, and Cur-β-CD complex are shown in Figure 4.6. The spectrum of curcumin (Figure 4.6a) showed a characteristic peak at 3510 cm^{-1} corresponding to the phenolic O−H stretching vibration. The peaks at 1626 and 1506 cm^{-1} corresponded to mixed stretching and bending vibrations of C=C and C=O. The peaks at 1602, 1427 and 1273 cm^{-1} were attributed to the stretching vibration of benzene ring skeleton, olefinic C−H plane bending vibration and aromatic C−O stretching vibrations, respectively. The peaks at 1152 and 808 cm^{-1} were assigned to aromatic C−H bending vibrations while the peak at 1023 cm^{-1} corresponded to the C−O−C vibrations. In addition, C=O peak was obtained at 962 cm^{-1} and cis vibration of aromatic ring was observed at 714 cm^{-1} [27], [110], [126].

The spectrum of β-CD (Figure 4.6b) showed characteristic bands at 3308 and 2925 cm^{-1} attributed to O−H and C−H stretching vibrations, respectively. The peak at 1643 cm^{-1} corresponded to H−O−H deformation of water present in cyclodextrin. The band at 1418 cm^{-1} was assigned to in plane bending of CH_3 groups. C−H overtone stretching vibrations and C−O−C vibrations were observed at 1153 cm^{-1} [27], [110].

The spectrum of physical mixture (Figure 4.6c) was basically the combination of β-CD and curcumin spectra, which showed identical peaks corresponding to both β-CD and curcumin. This indicates that inclusion complex between curcumin and β-CD has not formed by simply mixing the components. It is clear that the spectrum of Cur-β-CD inclusion complex (Figure 4.6d) is different from the spectrum of physical mixture. For instance, the peak at 3510 cm^{-1} assigned to the OH stretching of phenol groups in the physical mixture of curcumin and β-CD (Figure 4.6c) disappeared in the spectrum of Cur-β-CD inclusion complex. This phenomenon is attributed to the inclusion of aromatic rings of curcumin into the β-CD cavity which can be accepted as a good evidence of complex formation. Compared to the spectrum of curcumin, some characteristic peaks of curcumin shifted in the spectrum of Cur-β-CD inclusion complex (Figure 4.6d). Another evidence in which the Cur-β-CD inclusion complex has formed is that the peak at 1506 cm^{-1} due to the C=O stretching and C=C bending vibrations shifted to 1510 cm^{-1} in the spectrum of Cur-β-CD complex [26]. In addition, the intensities of the peaks at 1626 and 1602 cm^{-1} corresponding to the C=C stretching vibrations considerably weakened in the spectrum of Cur-β-CD inclusion complex. The peak at 1273 cm^{-1} (aromatic C−O stretching) shifted to 1281 cm^{-1} and the peak at 782 cm^{-1} (plane bending vibration of phenolic C=C−H) shifted to 779 cm^{-1}. The peak intensity of the $O{-}CH_3$ vibration due to the benzene ring of curcumin molecule at 1115 cm^{-1} almost disappeared in the spectrum of Cur-β-CD inclusion complex. Our results are consistent with the findings of Mangolim et al. and Tang et al. [26], [118].

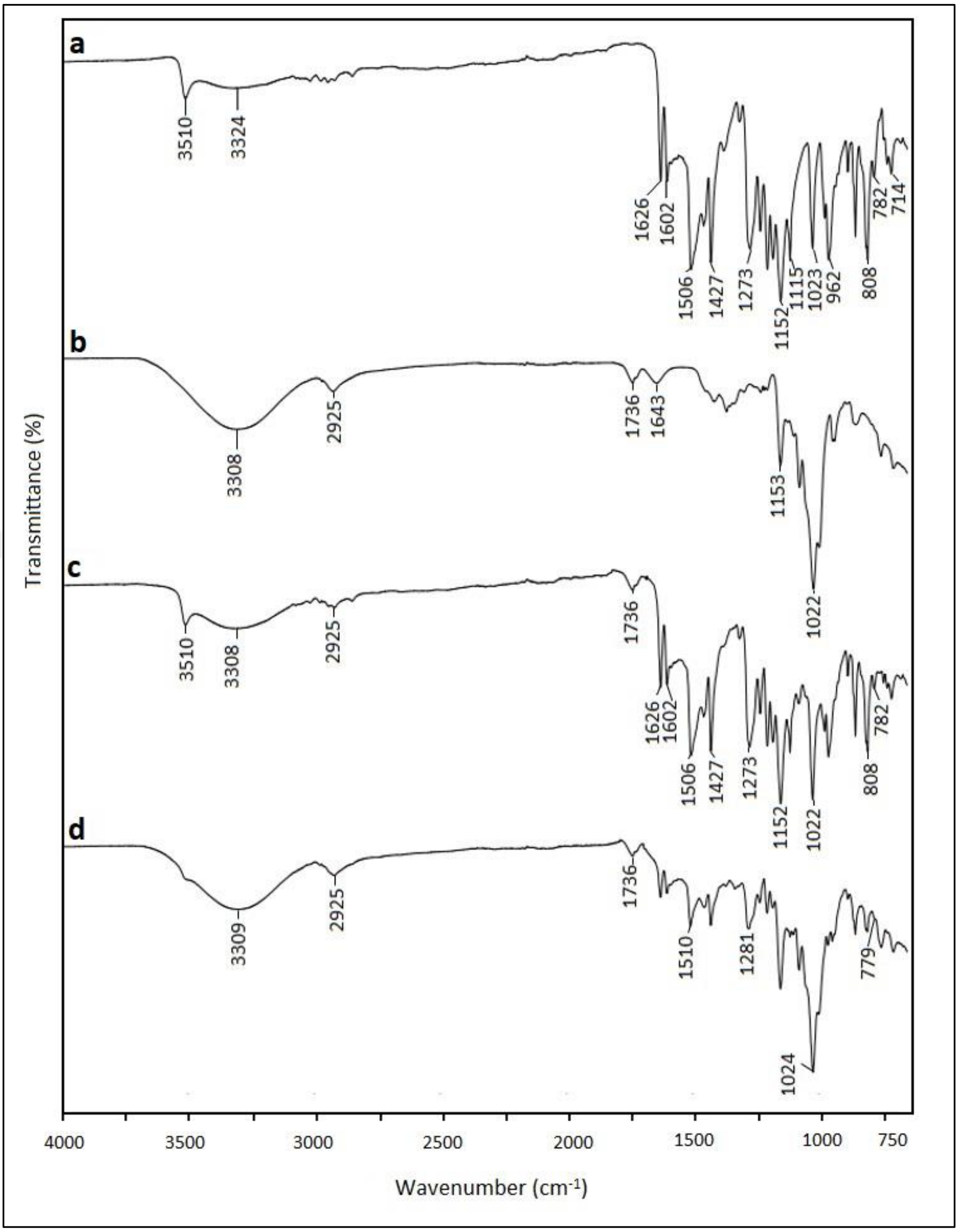

Figure 4.6: FT-IR spectra of (a) curcumin, (b) β-CD, (c) physical mixture of curcumin and β-CD, and (d) Cur-β-CD inclusion complex.

5. CONTROLLED RELEASE of CURCUMIN-β-CYCLODEXTRIN INCLUSION COMPLEX from NANOCOMPOSITE HYDROGELS

In recent years, considerable efforts have been made to provide colon specific delivery of small or large molecular weight drugs and active agents [127]. Several drug delivery systems such as microsphere [128], polyelectrolyte complex [129], liposome [130] and lipid based carriers [131] have been used as drug delivery systems. The design of a drug delivery system is depending on the physicochemical and pharmacokinetic properties of the drugs. Conventional drug delivery systems are limited to provide fast release of a drug with little or no control over the release rate. The release of the drug should be controlled to reach and maintain effective drug plasma concentration [132].

Hydrogels have attracted interest in drug release studies. In comparison to the other synthetic biomaterials, hydrogels as swelling networks have the ability of load and release drug molecules for oral, nasal, rectal and parenteral routes of administration [132]. The water inside the swollen hydrogel structure allows diffusion of drug molecules while the cross-linked network structure hold water together [39]. In hydrogel drug delivery systems, the drug diffusion is achieved by the swelling of hydrogel matrix rather than traditional Fickian diffusion [133]. The drug release amount is affected directly by hydrogel swelling. Bilia et al. prepared pH responsive poly(acrylic acid)/poly(ethylene oxide) hydrogel granules and studied the drug release behavior of prepared hydrogels in simulated gastric and intestinal fluid mediums. The authors observed that the release was limited to an initial burst in the simulated gastric fluid. When the gastric fluid changed to intestinal fluid, the release rate increased to maximum value [134]. Zhang et al. prepared a novel type temperature responsive PNIPA based hydrogel system for release of 5-fluorouracil. The 5-fluorouracil was loaded into the PNIPA hydrogel, then the drug incorporated PNIPA hydrogel was enveloped in the dialysis bag to form a novel type drug delivery system with controlled release [135]. Hua et al. prepared pH responsive sodium alginate/poly(vinyl alcohol) hydrogel beads as drug delivery carrier for release of diclofenac sodium [136].

In drug delivery applications, the oral route was found the most convenient way for the safe delivery of drugs to improve therapeutic effects [1]. Oral route administration with a controlled delivery system should prevent the deteriorating effects of acidic pH of stomach of gastrointestinal transit from mouth to cecum. Therefore, it is essential to develop an oral delivery system that releases the drug at the intestine while it is resistant to the acidic gastric medium. Dual responsive hydrogel systems which are sensitive to two different external stimuli are new advantageous approach in the drug delivery systems that meet the requirements [137]. The dual responsive systems are prepared by combination of at least two polymer or monomer that are responsive to one or more stimuli. Among all the dual responsive systems, the pH and temperature responsive hydrogels attracted the most attention because both stimuli are important parameter for human body, are applicable and controlled easily *in vitro* and *in vivo* conditions [137].

Shim et al. prepared a pH and temperature responsive block copolymer composed of poly(ε-caprolactone-co-lactide) (PCLA) and (poly(ethylene glycol)) (PEG) and evaluated its sol-to-gel transition behavior upon pH and temperature. The prepared copolymer was found applicable for injectable drugs [138]. Gao et al. prepared xylan based pH and temperature sensitive hydrogels as the intestinal targeted oral acetylsalicylic acid carriers. The hydrogels were synthesized by the cross-linking copolymerization of xylan with NIPA and acrylic acid monomers. The researchers obtained the cumulative drug release percentage up to 90.12% [14]. Shi et al. prepared a series of pH and temperature hydrogel beads, composed of calcium alginate and PNIPA for the controlled release of indomethacin. Different drug release values were obtained by changing the pH and temperature of the release medium which indicated the prepared hydrogels have the potential to be used as effective pH/temperature sustainable delivery system [71].

Despite their promising drug release properties, hydrogels are limited in terms of loading of hydrophobic drugs due to their hydrophilic nature. Recently, many hydrogels covalently bonded with CDs to increase the loading of hydrophobic drugs by copolymerizing CD-containing vinyl monomer with water soluble monomers. Zawko et al. copolymerized hyaluronic acid (HA) with β-CD to improve the hydrophobic drug loading properties of HA. It was reported by the researchers that the prepared HA-β-CD hydrogels loaded and released more hydrophobic hydrocortisone than pure HA hydrogels [139]. Zhang et al. prepared hydrogels composed of PNIPA and β-CD-grafted polyethylenimine (PEI) via radical polymerization. Propranolol was loaded into the hydrogel to study the release properties. The researchers reported that the formation of inclusion complexes between the drug molecules and CD provided a sustained release of propranolol. The release behavior of propranolol from prepared hydrogels were modulated by a change in the environmental temperature [140]. Rosa dos Santos et al. grafted β-CD to poly(2-hydroxyethyl methacrylate)-co-glycidyl methacrylate (pHEMA-co-GMA) hydrogels in order to improve diclofenac loading. It was concluded by the researchers that the prepared hydrogel system was able to prevent drug leakage and to sustain drug delivery for two weeks [141].

Unlike above mentioned chemically CD-bonded hydrogels, Kanjickal et al. loaded the cyclosporine-β-CD (CyA-β-CD) inclusion complex into the polyethylene glycol (PEG) hydrogels for release. The PEG hydrogels were found to have favorable release characteristics compared with the release from PEG hydrogels [142]. Quaglia et al. complexed nicardipine drug with β-CD and investigated the release properties from PEG based hydrogel. It was concluded by the authors that the nicarpidine delivery significantly improved by the complex formation [143]. Tsao et al. complexed hydrophobic paeonol drug with β-CD to improve its solubility. The direct loading of inclusion complex was examined and the complex release properties from the prepared hydrogels were investigated [144]. Gerola et al. prepared curcumin-β-CD inclusion complexes and investigated the complex release behavior from gum-arabic based hydrogels. Considerable increase of aqueous solubility of curcumin and enhanced drug loading and release values were observed by the researchers [103]. This method was found feasible among methods that increase the loading of hydrophobic drugs in hydrogel network due to its versatile and flexible implementation [144].

5.1. Materials and Methods for Controlled Release

Sodium chloride (NaCl) (>99%, w/w), hydrochloric acid (HCl) (37%, v/v), sodium hydroxide (NaOH) (>97%, w/w), potassium dihydrogen phosphate (KH_2PO_4) (> 98%, w/w) were purchased from Sigma-Aldrich (St. Louis, MO, USA).

5.1.1. Swelling of Hydrogels in Simulated Gastric and Intestinal Media

Swelling behavior of hydrogels were also investigated under the conditions simulating pH, temperature and time likely to be encountered during transit in the gastrointestinal tract. For this purpose, buffer solutions with pH = 1.2 and pH = 6.8 were prepared according to European Pharmacopoeia 8.0 where buffer solution with pH = 1.2 consisted of HCl and NaCl to simulate gastric medium and buffer solution with pH = 6.8 consisted of NaOH and KH_2PO_4 to simulate intestinal medium [145]. The concentrations of buffer solutions were 0.1 M and the pH values of buffer solutions were checked with a pH meter (Mettler-Toledo, SevenEasy model S20, Schwerzenbach, Switzerland).

First, the dried hydrogels were weighed and immersed in 50 ml of buffer solution at a pH of 1.2 for 2 h followed by immersing the hydrogel discs into a buffered solution at a pH of 6.8 for 6 h to simulate gastric and intestinal media, respectively. Swelling experiments were carried out in a shaking water bath (Termal H11960, Istanbul, Turkey) at 37±0.5 °C and a rotational speed of 50 rpm. The hydrogels were removed from the buffer solutions periodically, blotted with a filter paper to remove excess water and weighed. The swelling ratio (SR) and equilibrium swelling ratio (ESR) values were calculated using Equation (5.1) and Equation (5.2), respectively.

$$SR = \frac{W_t - W_d}{W_d} \tag{5.1}$$

$$\mathrm{ESR} = \frac{W_s - W_d}{W_d} \tag{5.2}$$

where W_t is the weight of the hydrogel at time t during swelling, W_s is the weight of the swollen hydrogel and W_d is the weight of the dried hydrogel.

5.1.2. Determination of Cur-β-CD Inclusion Complex Loading and Entrapment Efficiency

Each dried hydrogel disc was immersed in a 50 ml of Cur-β-CD complex solution with a concentration of 0.25 mg ml^{-1} to maintain sink conditions. The loading of the complex into the hydrogels was performed in a shaking water bath (Termal H11960, Istanbul, Turkey) at a rotational speed of 50 rpm and 23 °C for 48 h. The complex loaded hydrogels were taken out from the loading solution, and the concentration of the complex solution was determined spectrophotometrically at 425 nm. The complex loaded hydrogels were freeze-dried at −35 °C under vacuum using a freeze-dryer (Virtis Ultra Super XL, New York, USA). Complex loading (CL) and entrapment efficiency (EE) values of each hydrogel disc were calculated using Equation (5.3) and Equation (5.4), respectively.

$$\mathrm{CL}\ (\%) = \frac{(\mathrm{C_0} - \mathrm{C_1}) \times \mathrm{V}}{\mathrm{W_d}} \times 100 \tag{5.3}$$

$$\mathrm{EE}\ (\%) = \frac{\mathrm{C_0} - \mathrm{C_1}}{\mathrm{C_0}} \times 100 \tag{5.4}$$

where C_0 is the initial concentration of complex solution before loading study (mg ml^{-1}), C_1 is the concentration of complex solution after loading study (mg ml^{-1}), V is the volume of complex solution (ml) and W_d is the weight of the dried hydrogel (mg).

5.1.3. Release of Cur-β-CD Inclusion Complex from Nanocomposite Hydrogels

The release of loaded Cur-β-CD inclusion complex from the prepared hydrogels was studied at the same conditions used in the swelling studies. At specific time intervals, samples of 5 ml from the released medium were taken out and equal volume of fresh buffered solution at 37±0.5 °C was added to the release medium to maintain sink conditions. The amount of released complex was measured spectrophotometrically at 425 nm. The percent cumulative release was calculated according to Equation (5.5).

$$\text{Cumulative release (\%)} = \frac{M_t}{M_\infty} \times 100 \tag{5.5}$$

where M_t is the amount of released complex at time *t* and M_∞ is the total amount of loaded complex in the hydrogels.

5.2. Results and Discussion for Controlled Release

5.2.1. Swelling Study in Simulated Gastric and Intestinal Media

Swelling behavior is an important parameter for the release of the inclusion complex from the hydrogels. The effect of different hydrogel compositions on the swelling ratio of the prepared nanocomposite and conventional hydrogels in the simulating gastrointestinal conditions as a function of time is presented in Figure 5.1. The effect of different NaAlg contents on the swelling of 83/17-20C, 77/23-20C and 71/29-20C hydrogels with the same amount of nanoclay content at pH = 1.2 and pH = 6.8 is given in Figure 5.1a. At pH = 1.2, the nanocomposite hydrogels showed the lowest swelling ratio due to the pH sensitivity of NaAlg. At pK_a values below 4.6, the electrostatic repulsion between the −C(=O)OH groups of NaAlg is suppressed and the electrostatic attraction between the −C(=O)OH of NaAlg and −C(=O)NH groups of PNIPA predominates polymer-water interactions; thus, resulted in low swelling ratios [49]. As the NaAlg content increased swelling ratio decreased. Minimum swelling ratio was obtained for the 71/29-20C hydrogel which has the highest amount of NaAlg because high amount of NaAlg in the hydrogel decreases available free network space which hinders the mobility of polymer chains resulting in lower swelling ratio. The swelling ratio for the nanocomposite hydrogels increased in the order of 71/29-20C < 77/23-20C < 83/17-20C at pH = 1.2. When the nanocomposite hydrogels were transferred from pH = 1.2 to pH = 6.8 medium, a considerable increase in swelling was observed for all the prepared hydrogel formulations. At pH = 6.8, the effect of cross-linking density on swelling ratio was more noticeable than the pH = 1.2. High electrostatic repulsion between $-C(=O)O^-$ groups of NaAlg increased the free volume of the hydrogel matrix; thus, resulted in higher swelling ratios at pH = 6.8.

The effect of different nanoclay contents on the swelling of 83/17-20C, 83/17-30C and 83/17-40C hydrogels with the same amount of NaAlg content at pH = 1.2 and pH = 6.8 is given in Figure 5.1a. The swelling ratio decreased with increasing the nanoclay content. This result can be explained by the fact that more cross-linker content increased the number of cross-linking points and decrease the cross-linking distance between the polymer chains; thus, inhibited the swelling. The swelling ratio of the nanocomposite hydrogels with the same NaAlg content increased in the order of 83/17-40C < 83/17-30C < 83/17-20C.

The effect of different NaAlg contents on the swelling of 83/17-2B, 77/23-2B and 71/29-2B conventional hydrogels with the same amount of BIS at pH = 1.2 and pH = 6.8 is given in Figure 5.1b. At pH = 1.2, no significant difference was observed between the swelling ratios of the conventional hydrogels due to the low swelling ratio (<1). The low swelling ratio at acidic pH can be attributed to the pH sensitivity of NaAlg [146]. When the conventional hydrogels were transferred from pH = 1.2 to pH = 6.8, the swelling ratio increased to an extent, but it is lower than those of nanocomposite hydrogels. At pH = 6.8, the swelling ratio of the conventional hydrogels with the same BIS content increased in the order of 83/17-2B < 77/23-2B < 71/29-2B, which is in reverse order for the nanocomposite hydrogels with the same nanoclay content. Our findings are in good agreement with the results reported by Dumitriu et al. who also observed that the swelling ratio decreased when the ratio of PNIPA increased in the PNIPA based conventional hydrogels [78]. These hydrogels cross-linked with BIS exhibit more denser structure than the PNIPA based nanocomposite hydrogels due to the formation of large number of cross-linking points when BIS is used as the cross-linker. This limits the mobility of the PNIPA chains in the conventional hydrogels; thus, lowering the swelling ratio of the conventional hydrogels [89].

The effect of different BIS contents on the swelling of conventional hydrogels at pH = 1.2 and pH = 6.8 is given in Figure 5.1b. The swelling ratio of conventional hydrogels increased with increasing the BIS content, contrary to the nanocomposite hydrogels. At pH = 1.2, no significant difference was observed between the swelling ratio of the conventional hydrogels with the same NaAlg content. However, at pH = 6.8, the swelling ratio of the conventional hydrogels with the same NaAlg content increased in the order of 83/17-2B < 83/17-4B < 77/23-2B < 77/23-4B < 71/29-2B < 71/29-4B. This result is consistent with the findings of Haraguchi et al. who showed that the PNIPA based nanocomposite and conventional hydrogels exhibited opposite swelling tendencies with respect to the cross-linker content [89].

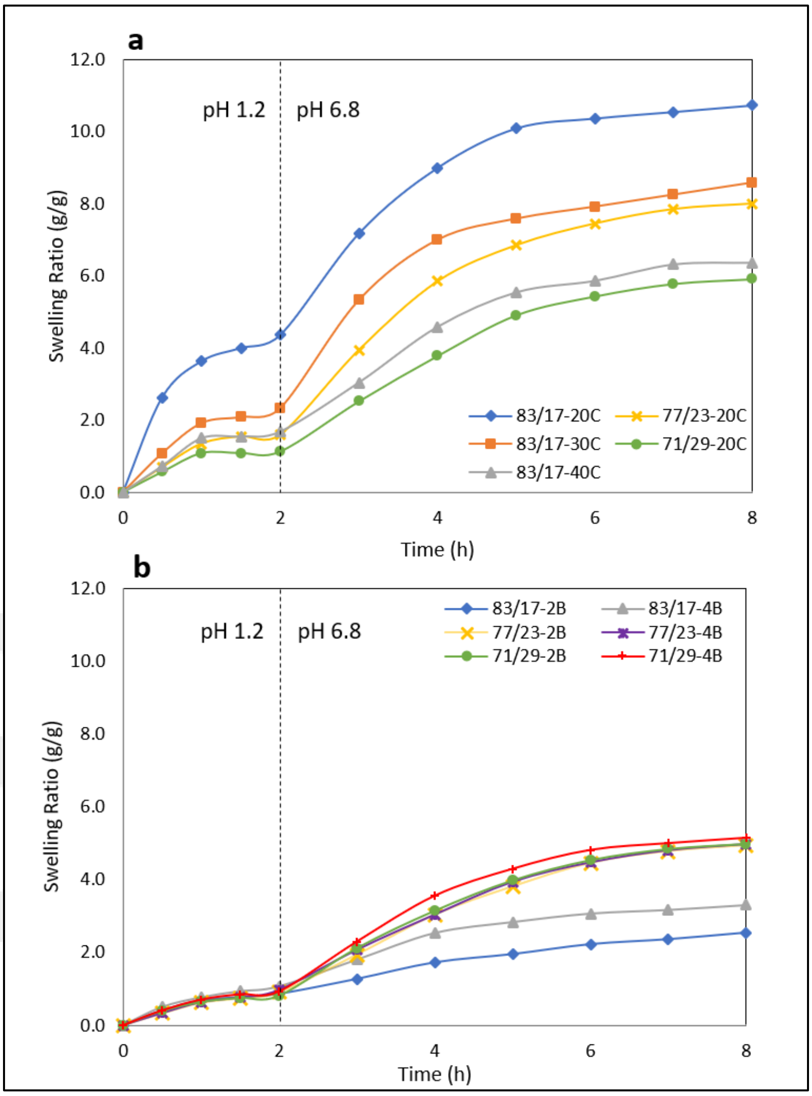

Figure 5.1: Swelling ratios of (a) nanocomposite and (b) conventional hydrogels in simulated gastric (pH = 1.2) and intestinal (pH = 6.8) media at 37 ºC.

5.2.2. Complex Loading and Entrapment Efficiency

The results of CL, EE and ESR of the prepared hydrogels with different compositions are presented in Table 5.1. The CL values range from 7 to 46% while the EE values were in the range of 19 and 81%. Results revealed that CL, EE and ESR values were highly affected by the hydrogel composition. When the nanoclay content increased from 20 to 40%, the CL value decreased from 46.0 to 41.4%, the EE value decreased from 81 to 63% and the ESR value decreased from 15.8 to 13.1. Such decreasing trends in CL, EE and ESR as the nanoclay content increased in the hydrogels were reported to result from the reduction of the free volume within the polymer matrix associated with an increase in cross-linking density [145]. Contrary to the nanocomposite hydrogels, increasing trends were observed when the BIS content increased from 2 to 4% in the conventional hydrogels. This result is consistent with the results of Dumitriu et al. who reported that ESR of PNIPA based conventional hydrogels increased with increasing the BIS content from 2 to 4% [78].

Table 5.1: Complex Loading (CL), Entrapment Efficiency (EE) and Equilibrium Swelling Ratio (ESR) of Prepared Hydrogels at 23 °C.

Hydrogel code	CL (%)	EE (%)	ESR
83/17-20C	46.0	81.0	15.8
83/17-30C	44.0	74.0	13.5
83/17-40C	41.4	63.0	13.1
77/23-20C	42.2	67.5	11.8
71/29-20C	31.3	47.5	10.1
83/17-2B	15.7	39.0	6.5
83/17-4B	15.8	43.0	9.2
77/23-2B	13.8	31.0	5.9
77/23-4B	16.4	38.0	6.9
71/29-2B	7.0	19.0	4.8
71/29-4B	7.6	22.0	6.3

Compared to the conventional hydrogels, nanocomposite hydrogels absorbed more inclusion complex because they had higher ESR values than the conventional hydrogels. In other words, it was possible to load more inclusion complex into the nanocomposite hydrogels due to higher chain flexibility; therefore, they were able to swell more than the conventional hydrogels. Among all the prepared hydrogels, the highest CL, EE and ESR values were obtained for the nanocomposite hydrogel in which NIPA/NaAlg ratio of 83/17 with the nanoclay content of 20% coded as 83/17-20C (Table 5.1). Images of blank and Cur-β-CD inclusion complex loaded hydrogels are shown in Figures 5.2 and 5.3.

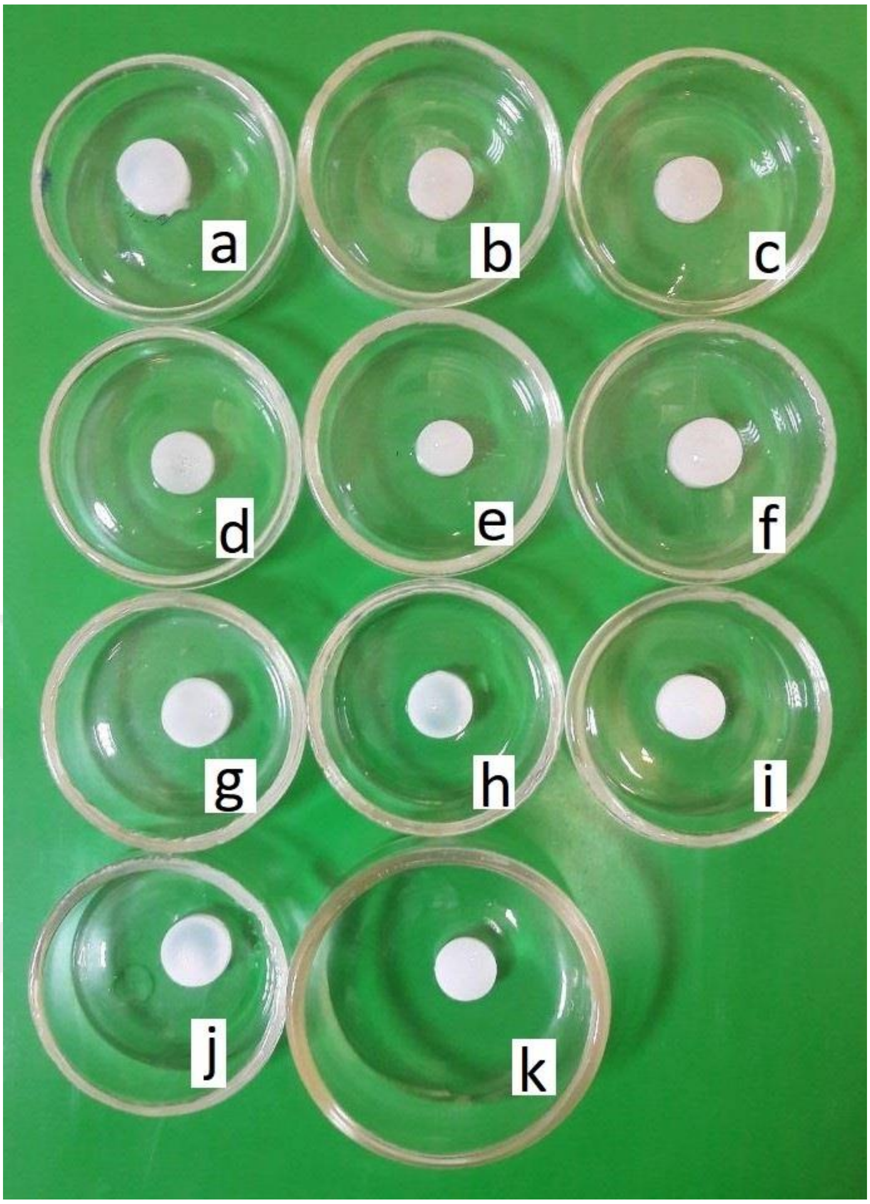

Figure 5.2: Blank hydrogels: (a) 83/17-20C, (b) 83/17-30C, (c) 83/17-40C, (d) 77/23-20C, (e) 71/29-20C, (f) 83/17-2B, (g) 83/17-4B, (h) 77/23-2B, (i) 77/23-4B, (j) 71/29-2B and (k) 71/29-4B.

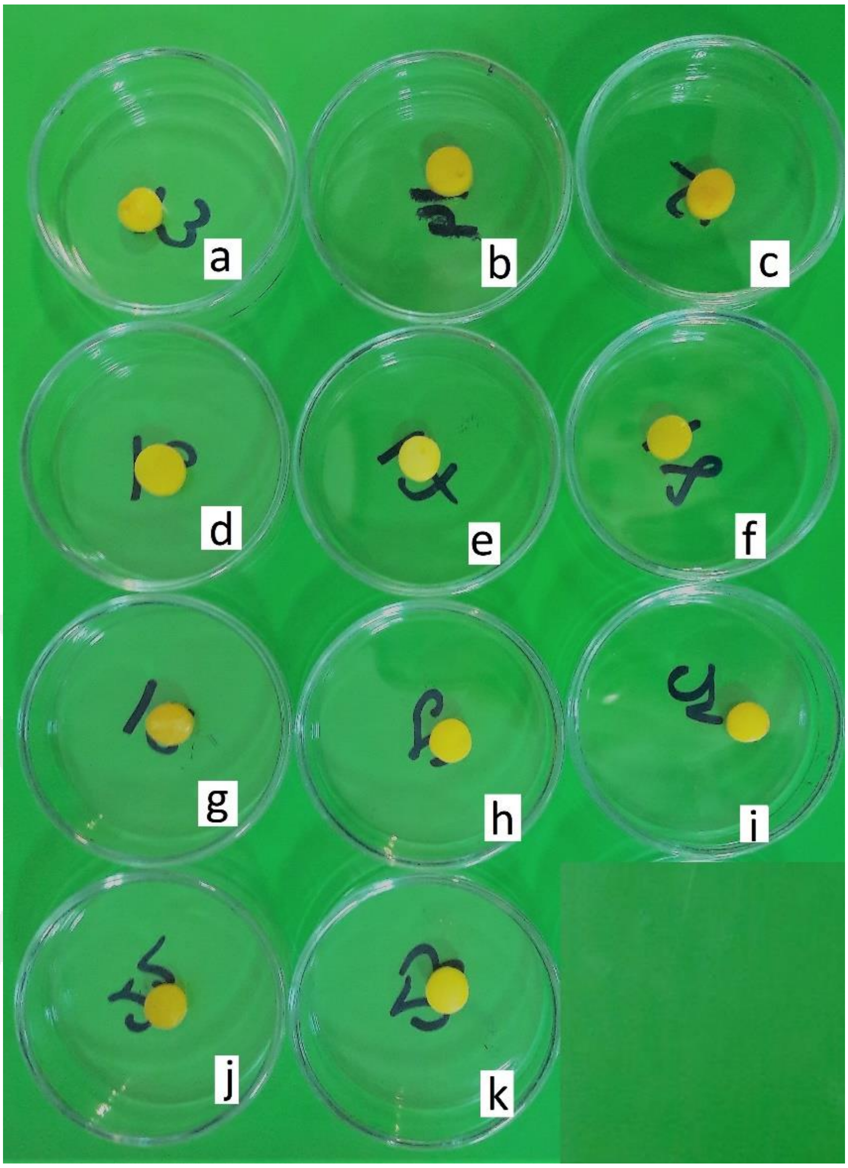

Figure 5.3: Cur-β-CD inclusion complex loaded hydrogels: (a) 83/17-20C, (b) 83/17-30C, (c) 83/17-40C, (d) 77/23-20C, (e) 71/29-20C, (f) 83/17-2B, (g) 83/17-4B, (h) 77/23-2B, (i) 77/23-4B, (j) 71/29-2B and (k) 71/29-4B.

5.2.3. Inclusion Complex Release Study

The effect of different hydrogel compositions on the cumulative inclusion complex release of the prepared nanocomposite and conventional hydrogels in the simulating gastrointestinal conditions as a function of time is presented in Figure 5.4. The effect of different NaAlg contents on the cumulative release of 83/17-20C, 77/23-20C and 71/29-20C nanocomposite hydrogels with the same amount of nanoclay content at pH = 1.2 and pH = 6.8 is given in Figure 5.4a. At pH = 1.2, the nanocomposite hydrogels showed the lowest release. The release of inclusion complex was directly proportional to the swelling ratio. The higher the swelling, the higher the release of the inclusion complex. The cumulative release for nanocomposite hydrogels increased in the order of 71/29-20C < 77/23-20C < 83/17-20C at pH = 1.2. The cumulative release at pH = 6.8 was found to be higher than the cumulative release at pH = 1.2. At the end of 8 h of release, the maximum cumulative release value (52.4%) was obtained for the 83/17-20C hydrogel while the minimum cumulative release (29.5%) took place for the 71/29-20C hydrogel. The cumulative release of the inclusion complex from the nanocomposite hydrogels with the same nanoclay content increased in the order of 71/29-20C < 77/23-20C < 83/17-20C.

The effect of different nanoclay contents on the cumulative release of 83/17-20C, 83/17-30C and 83/17-40C hydrogels with the same amount of NaAlg content at pH = 1.2 and pH = 6.8 is given in Figure 5.4a. It was observed that the cumulative release decreased as the nanoclay content increased. Results of the cumulative release study complies with the results of the swelling study. At the end of 8 h of release, the maximum and minimum cumulative release values were obtained for the 83/17-20C (52.4%) and 83/17-40C (39.2%) hydrogels, respectively. The cumulative release of the inclusion complex from the nanocomposite hydrogels with the same NaAlg content increased in the order of 83/17-40C < 83/17-30C < 83/17-20C.

The effect of different NaAlg contents on the cumulative release of 83/17-2B, 77/23-2B and 71/29-2B conventional hydrogels with the same amount of BIS at pH = 1.2 and pH = 6.8 is given in Figure 5.4b. At pH = 1.2, no significant difference was observed between the cumulative release values of the conventional hydrogels. When the conventional hydrogels were transferred from pH = 1.2 to pH = 6.8, the cumulative release increased, but it was lower than the cumulative release values of the nanocomposite hydrogels. At pH = 6.8, the cumulative release of the inclusion complex from the conventional hydrogels with the same BIS content increased in the order of 83/17-2B < 77/23-2B < 71/29-2B, which is in reverse order for the nanocomposite hydrogels with the same nanoclay content.

The effect of different BIS contents on the cumulative release of conventional hydrogels at pH = 1.2 and pH = 6.8 is given in Figure 5.4b. The complex release values of conventional hydrogels increased with increasing the BIS content, contrary to the nanocomposite hydrogels. The opposite swelling tendencies of nanocomposite and conventional hydrogels with respect to the cross-linker content caused the existence of opposite inclusion complex release profiles. Therefore, higher amounts of BIS must be used as a cross-linker to achieve higher release values for the conventional hydrogels. Although no significant difference was observed between the cumulative release values of conventional hydrogels at pH = 1.2, the cumulative release of the inclusion complex from the conventional hydrogels with the same NaAlg content at pH = 6.8 increased in the order of 83/17-2B < 83/17-4B < 77/23-2B < 77/23-4B < 71/29-2B < 71/29-4B.

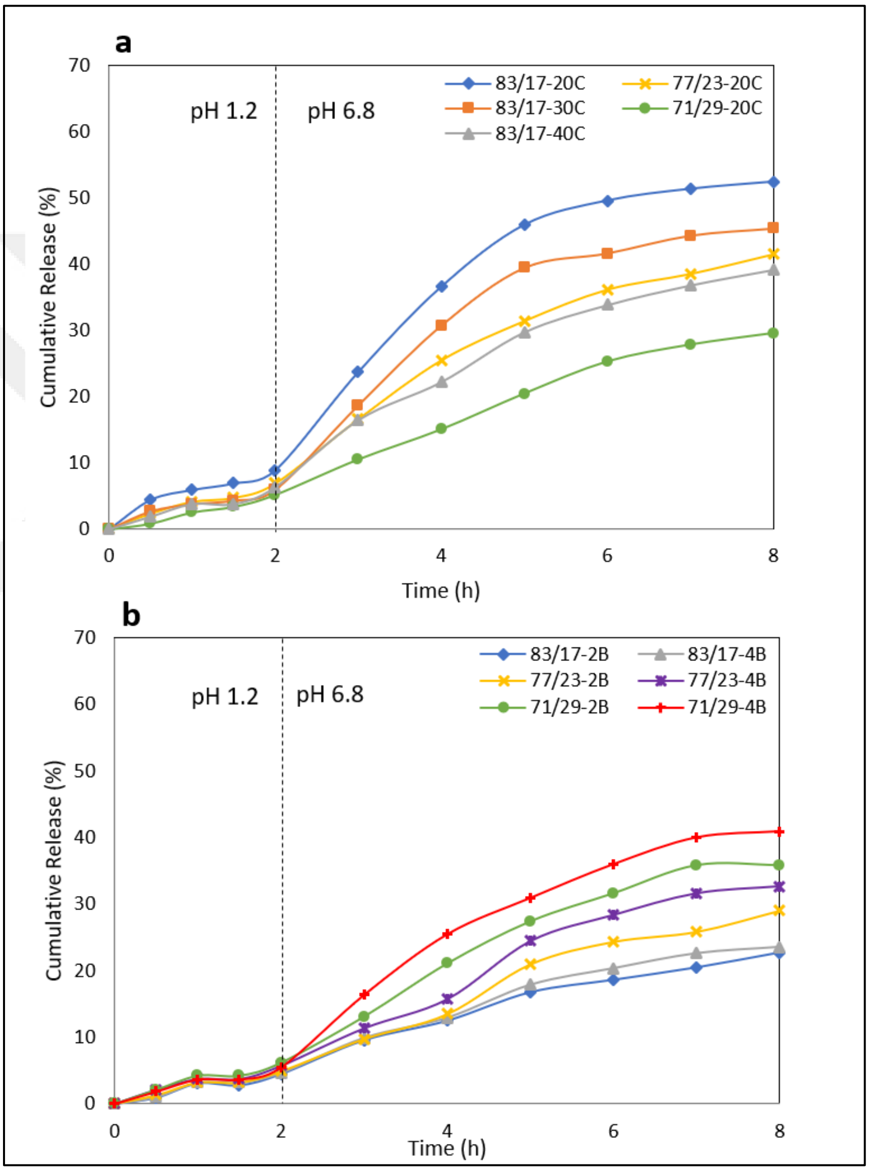

Figure 5.4: Cumulative inclusion complex release profiles of (a) nanocomposite and (b) conventional hydrogels in simulated gastric (pH = 1.2) and intestinal (pH = 6.8) media at 37 °C.

6. CONCLUSIONS

In this study, NaAlg and PNIPA based pH/temperature responsive nanocomposite and conventional hydrogels were prepared by free radical solution polymerization. The bentonite nanoclay acted as a cross-linker instead of organic cross-linkers in the nanocomposite hydrogels. The conventional hydrogels were cross-linked with BIS. All prepared hydrogels were characterized by SEM, DSC, FT-IR and XRD methods. SEM micrographs of the hydrogels revealed highly porous structure. The pore sizes decreased, and the number of pores increased with increasing the cross-linker amount in the hydrogels. The conventional hydrogels were found to have more porous network structures than nanocomposites. It was observed by the DSC thermograms that the LCST value was not dependent on the NaAlg and cross-linker content, since the PNIPA polymer retained its own property. The T_g values of prepared nanocomposite and conventional hydrogels with the same nanoclay content decreased as the NaAlg content increased. The nanocomposite hydrogels with the same NaAlg content have been observed almost the same T_g, irrespective of the amount of nanoclay, close to the linear PNIPA. On the contrary, the T_g value in conventional hydrogels increased as the BIS content increases. The FT-IR spectroscopy results confirmed the successful formation of PNIPA and NaAlg based nanocomposite and conventional hydrogel networks. The XRD profiles of nanocomposite hydrogels revealed that some of the nanoclay sheets are exfoliated in the structure whereas some of exist as clay tactoids in the polymeric matrix. The hydrogel swelling studies confirmed the pH/temperature responsive swelling behavior. The ESR was affected by the pH, temperature, NaAlg and nanoclay content in the hydrogel. The ESR of all prepared nanocomposite hydrogels increased with increasing the pH from 1.2 to 6.8 at the temperature of 5 °C. At temperatures higher than 5 °C, the maximum ESR values obtained at pH = 8. It was observed that the ESR value of nanocomposite hydrogels decreased with increasing the nanoclay content regardless of pH and temperature. The ESR of the nanocomposite hydrogels decreased as the NaAlg content increased from 20 to 40%. Conventional hydrogels showed similar pH dependency as the nanocomposite hydrogels because of containing the same amounts of NaAlg. Although the conventional hydrogels showed similar swelling behavior on pH change of the medium, they showed less dependency on amount of NaAlg and nanoclay change and have lower ESR values than the nanocomposite hydrogels. The results indicated that the synthesized nanocomposite hydrogels have better water holding capacity than the conventional hydrogels which can be adjusted by controlling the amount of nanoclay in the hydrogel.

The feasibility of curcumin loading to β-CD was successfully demonstrated by using the co-precipitation method. Aqueous solubility of curcumin was greatly improved by preparing Cur-β-CD inclusion complex via co-precipitation method. The Benesi-Hildebrand method was used to determine the stoichiometric ratio of the inclusion. The stoichiometric ratio between curcumin and β-CD was found to be 1:2 for the formation of inclusion complex, and the association constant was determined as $3.80 \times 10^{8}\ \mathrm{M}^{-2}$. The inclusion complex formation was confirmed by spectral and thermal studies. CL, EE and ESR values were highly affected by the hydrogel composition. It was shown that nanocomposite hydrogels absorbed more inclusion complex than the conventional hydrogels. Swelling ratio and cumulative release were also dependent on the hydrogel composition and pH. In simulated gastric fluid (pH = 1.2), all prepared hydrogels showed the lowest swelling ratios while in simulated intestinal fluid (pH = 6.8), all the hydrogels revealed higher swelling ratios. As the nanoclay content increased, the swelling ratio and cumulative release decreased in nanocomposite hydrogels. On the contrary, as the ratio of BIS as the cross-linker in the conventional hydrogels increased, the swelling ratio and cumulative release also increased. Higher amounts of BIS must be used as a cross-linker to achieve higher release values for the conventional hydrogels. This study revealed that the nanocomposite hydrogels are the promising carriers for the targeted delivery of curcumin in gastrointestinal tract of humans to increase the solubility and bioavailability of curcumin. Increased solubility and bioavailability of curcumin would be valuable not only in pharmaceutical applications but also in cosmetic, agricultural and food industries. Targeted delivery of the hydrophobic drugs or active agents could be achieved by the use of nanocomposite hydrogels.

REFERENCES

[1] Das D., Ghosh P., Ghosh A., Haldar C., Dhara S., Panda A.B., Pal S., (2015), "Stimulus-responsive, biodegradable, biocompatible, covalently cross-linked hydrogel based on dextrin and poly (N-isopropylacrylamide) for in vitro/in vivo controlled drug release", ACS Applied Materials & Interfaces, 7 (26), 14338-14351.

[2] Ahmed E. M., (2015), "Hydrogel: Preparation, characterization, and applications: A review", Journal of Advanced Research, 6 (2), 105-121.

[3] Elashnikov R., Slepička P., Rimpelova S., Ulbrich P., Švorčík V., Lyutakov O., (2017), "Temperature-responsive PLLA/PNIPAM nanofibers for switchable release", Material Science & Engineering C-Materials for Biological Applications, 72, 293-300.

[4] Wang J., Zhao G., Wang X., Peng X., Li Y., (2015), "Synthesis of magnetic thermosensitive microcontainers for enzyme immobilization", Journal of Nanoparticle Research, 17 (5), 224.

[5] Han L., Zhang Y., Lu X., Wang K., Wang Z., Zhang H., (2016), "Polydopamine nanoparticles modulating stimuli-responsive PNIPAM hydrogels with cell/tissue adhesiveness", ACS Applied Materials & Interfaces, 8 (42), 29088-29100.

[6] Haraguchi K., Farnworth R., Ohbayashi A., Takehisa T., (2003), "Compositional effects on mechanical properties of nanocomposite hydrogels composed of poly (N, N-dimethylacrylamide) and clay", Macromolecules, 36 (15), 5732-5741.

[7] Haraguchi K., (2007), "Nanocomposite hydrogels", Current Opinion in Solid State and Materials Science, 11 (3-4), 47-54.

[8] Haraguchi K., Takehisa T., and Fan S., (2002), "Effects of clay content on the properties of nanocomposite hydrogels composed of poly(N-isopropylacrylamide) and clay", Macromolecules, 35 (27), 10162-10171.

[9] Djonlagic J., Lancuski A., Nikolic M. S., Rogan, J. Ostojic, S., Petrovic Z., (2017), "Hydrogels reinforced with nanoclays with improved response rate", Journal of Applied Polymer Science, 134 (9).

[10] Haraguchi K., Takehisa T., (2002), "Nanocomposite hydrogels: A unique organic-inorganic network structure with extraordinary mechanical, optical, and swelling/de-swelling properties", Advanced Materials, 14 (16), 1120-1124.

[11] Haraguchi K., Li H. J., Matsuda K., Takehisa T., Elliott E., (2005), "Mechanism of forming organic/inorganic network structures during in-situ free-radical polymerization in PNIPA−clay nanocomposite hydrogels", Macromolecules, 38 (8), 3482-3490.

[12] Haraguchi K., Li, H. J., (2006), "Mechanical properties and structure of polymer−clay nanocomposite gels with high clay content", Macromolecules, 39 (5), 1898-1905.

[13] De Sousa Rodrigues L. A., Figueiras A., Veiga F., de Freitas R. M., Nunes L. C. C., da Silva Filho E. C., da Silva Leite C. M., (2013), "The systems containing clays and clay minerals from modified drug release: A review", Colloids and Surfaces B: Biointerfaces, 103, 642-651.

[14] Gao C., Ren J., Zhao C., Kong W., Dai Q., Chen Q., Liu C., Sun R., (2016), "Xylan-based temperature/pH sensitive hydrogels for drug controlled release", Carbohydrate Polymers, 151, 189-197.

[15] Adnadjevic B., Jovanovic J., Drakulic B., (2007), "Isothermal kinetics of (E)-4-(4-metoxyphenyl)-4-oxo-2-butenoic acid release from poly (acrylic acid) hydrogel", Thermochimica Acta, 466 (1-2), 38-48.

[16] Brannon-Peppas L., Peppas, N. A., (1991), "Equilibrium swelling behavior of pH-sensitive hydrogels", Chemical Engineering Science, 46 (3), 715-722.

[17] de Moura M. R., Ahmad Aouada F., Favaro S. L., Radovanovic E., Forti Rubira A., Muniz E. C., (2009), "Release of BSA from porous matrices constituted of alginate–Ca^{2+} and PNIPAAm-interpenetrated networks", Material Science & Engineering C-Materials for Biological Applications, 29 (8), 2319-2325.

[18] Guo B. L., Gao Q. Y., (2007), "Preparation and properties of a pH/temperature-responsive carboxymethyl chitosan/poly(N-isopropylacrylamide) semi-IPN hydrogel for oral delivery of drugs", Carbohydrate Research, 342 (16), 2416-2422.

[19] Shalaby W. S., Blevins W. E., Park K., (1991), “Gastric retention of enzyme-digestible hydrogels in the canine stomach under fasted and fed conditions: Preliminary analysis using new analytical techniques”. In: Dunn, R. L., Ottenbrite, R. M., Editors, “Polymeric Drugs and Drug Delivery Systems”, ACS Symposium Series.

[20] Yang K., Wan S., Chen B., Gao W., Chen J., Liu M., He B., Wu H., (2016), "Dual pH and temperature responsive hydrogels based on β-cyclodextrin derivatives for atorvastatin delivery", Carbohydrate Polymers, 136, 300-306.

[21] Grant G. T., Morris E. R., Rees D. A., Smith P. J., Thom D., (1973), "Biological interactions between polysaccharides and divalent cations: the egg-box model", FEBS Letters, 32 (1), 195-198.

[22] Tønnesen H. H., Karlsen J., (2002), "Alginate in drug delivery systems", Drug Development and Industrial Pharmacy, 28 (6), 621-630.

[23] Ganguly S., Maity P. P., Mondal S., Das P., Bhawal P., Dhara S., Das, N. C., (2018), "Polysaccharide and poly (methacrylic acid) based biodegradable elastomeric biocompatible semi-IPN hydrogel for controlled drug delivery", Materials Science and Engineering: C, 92, 34-51.

[24] Wen C., Lu L., Li X., (2014), "Mechanically Robust Gelatin–Alginate IPN Hydrogels by a Combination of Enzymatic and Ionic Crosslinking Approaches", Macromolecular Materials and Engineering, 299 (4), 504-513.

[25] Kulkarni R. V., Sreedhar V., Mutalik S., Setty C. M., Sa B., (2010), "Interpenetrating network hydrogel membranes of sodium alginate and poly (vinyl alcohol) for controlled release of prazosin hydrochloride through skin", International Journal of Biological Macromolecules, 47 (4), 520-527.

[26] Mangolim C. S., Moriwaki C., Nogueira A. C., Sato F., Baesso M. L., Neto A. M., Matioli G., (2014), "Curcumin–β-cyclodextrin inclusion complex: stability, solubility, characterisation by FT-IR, FT-Raman, X-ray diffraction and photoacoustic spectroscopy, and food application", Food Chemistry, 153, 361-370.

[27] Yallapu M. M., Jaggi M., Chauhan, S. C., (2010), "β-Cyclodextrin-curcumin self-assembly enhances curcumin delivery in prostate cancer cells", Colloids Surfaces B: Biointerfaces, 79 (1), 113-125.

[28] Zheng B., Zhang Z., Chen F., Luo X., McClements D. J., (2017), "Impact of delivery system type on curcumin stability: Comparison of curcumin degradation in aqueous solutions, emulsions, and hydrogel beads", Food Hydrocolloids, 71, 187-197.

[29] Cheng A. L., Hsu C. H., Lin J. K., Hsu M. M., Ho, Y. F., Shen T. S., Ko, J. Y., Lin, J. T., Lin B. R., Ming-Shiang W., Yu H. S., Jee S. H., Chen G. S., Chen T. M., Chen C. A., Lai M. K., Pu Y. S., Pan M. H., Wang Y. J., Tsai C. C., Hsieh C. Y., (2001), "Phase I clinical trial of curcumin, a chemopreventive agent, in patients with high-risk or pre-malignant lesions", Anticancer Research, 21, 2895-2900.

[30] Wang Y., Lu Z., Lv F., Bie, X., (2009), "Study on microencapsulation of curcumin pigments by spray drying", European Food Research and Technology, 229 (3), 391-396.

[31] Guo R., Lan Y., Xue W., Cheng B., Zhang Y., Wang C., Ramakrishna S., (2017), "Collagen-cellulose nanocrystal scaffolds containing curcumin-loaded microspheres on infected full-thickness burns repair", Journal of Tissue Engineering and Regenerative Medicine, 11 (12), 3544-3555.

[32] Paramera E. I., Konteles S. J., Karathanos V. T., (2011), "Stability and release properties of curcumin encapsulated in *Saccharomyces cerevisiae*, β-cyclodextrin and modified starch", Food Chemistry, 125 (3), 913-922.

[33] Hasan M., Belhaj N., Benachour H., Barberi-Heyob M., Kahn C., Jabbari E., Linder M., Arab-Tehrany E., (2014), "Liposome encapsulation of curcumin: physico-chemical characterizations and effects on MCF7 cancer cell proliferation", International Journal of Pharmaceutics, 461 (1-2), 519-528.

[34] Jahed V., Zarrabi A., Bordbar A. K., Hafezi M. S., (2014), "NMR (1 H, ROESY) spectroscopic and molecular modelling investigations of supramolecular complex of β-cyclodextrin and curcumin", Food Chemistry, 165, 241-246.

[35] Yadav V. R., Suresh S., Devi K., Yadav S., (2009), "Effect of cyclodextrin complexation of curcumin on its solubility and antiangiogenic and anti-inflammatory activity in rat colitis model", AAPS Pharmscitech, 10 (3), 752.

[36] Szejtli J., (1996) "Inclusion of Guest molecules, Selectivity and Molecular Recognition by Cyclodextrins". In: J. Szejtli, T. Osa, Editors, "Comprehensive Supramolecular Chemistry: Cyclodextrins", Pergamon.

[37] Szente L. Szejtli J., (2004), "Cyclodextrins as food ingredients", Trends in Food Science & Technology, 15 (3), 137-142.

[38] Tao F., Hill L. E., Peng Y., Gomes C. L., (2014), "Synthesis and characterization of β-cyclodextrin inclusion complexes of thymol and thyme oil for antimicrobial delivery applications", LWT - Food Science and Technology , 59 (1), 247-255.

[39] Okay O., (2009), "General properties of hydrogels, in Hydrogel sensors and actuators". In: G. Gerlach, K.F. Arndt, "Hydrogel Sensors and Actuators: Engineering and Technology", Springer.

[40] Zohuriaan-Mehr M., Omidian H., Doroudiani S., Kabiri K., (2010), "Advances in non-hygienic applications of superabsorbent hydrogel materials", Journal of Materials Science, 45 (21), 5711-5735.

[41] Ferfera-Harrar H., Aiouaz N., Dairi N., (2015), "Synthesis and Properties of Chitosan-Graft Polyacrylamide/Gelatin Superabsorbent Composites for Wastewater Purification", Polymer, 6, 9.

[42] Rakhshaei R., Namazi H., (2017), "A potential bioactive wound dressing based on carboxymethyl cellulose/ZnO impregnated MCM-41 nanocomposite hydrogel", Materials Science and Engineering: C, 73, 456-464.

[43] Capuano N., Logoluso N., Gallazzi E., Drago L., Romanò, C. L., (2018), "One-stage exchange with antibacterial hydrogel coated implants provides similar results to two-stage revision, without the coating, for the treatment of peri-prosthetic infection", Knee Surgery, Sports Traumatology, Arthroscopy, 1-6.

[44] Thombare N., Mishra S., Siddiqui M., Jha U., Singh D., Mahajan G. R., (2018), "Design and development of guar gum based novel, superabsorbent and moisture retaining hydrogels for agricultural applications", Carbohydrate Polymers, 185, 169-178.

[45] Treenate P., Monvisade P., (2017), "In vitro drug release profiles of pH-sensitive hydroxyethylacryl chitosan/sodium alginate hydrogels using paracetamol as a soluble model drug", International Journal of Biological Macromolecules, 99, 71-78.

[46] Miyata T., Uragami T., Nakamae K., (2002), "Biomolecule-sensitive hydrogels", Advanced Drug Delivery Reviews, 54 (1), 79-98.

[47] Stuart M. A. C., Huck W. T., Genzer J., Müller M., Ober C., Stamm M., Sukhorukov G. B., Szleifer I., Tsukruk V. V., Urban M., (2010), "Emerging applications of stimuli-responsive polymer materials", Nature Materials, 9 (2), 101.

[48] Tanaka T., Nishio I., Sun S.T., Ueno-Nishio S., (1982), "Collapse of gels in an electric field", Science, 218 (4571), 467-469.

[49] Kasapoglu-Calik M., Ozdemir M., (2016), "Synthesis, characterization and, swelling behavior of semi-IPN nanocomposite hydrogels of alginate with poly (N-isopropylacrylamide) crosslinked by nanoclay", Journal of Applied Polymer Science, 133 (12), 43222.

[50] Culin J., Smit I., Andreis M., Veksli Z., Anzlovar A., Zigon M., (2005), "Motional heterogeneity and phase separation of semi-interpenetrating networks and mixtures based on functionalised polyurethane and polymethacrylate prepolymers", Polymer, 46 (1), 89-99.

[51] Zhang J. and Peppas N. A., (2000), "Synthesis and characterization of pH- and temperature-sensitive poly(methacrylic acid)/poly(N-isopropylacrylamide) interpenetrating polymeric networks", Macromolecules, 33 (1), 102-107.

[52] Ma J. H., Fan B., Liang B. R., Xu J., (2010), "Synthesis and characterization of Poly(N-isopropylacrylamide)/Poly(acrylic acid) semi-IPN nanocomposite microgels", Journal of Colloid and Interface Science, 341 (1), 88-93.

[53] Song L. Y., Zhu M. F., Chen Y. M., Haraguchi K., (2008), "Temperature- and pH-sensitive nanocomposite gels with semi-interpenetrating organic/inorganic networks", Macromolecular Chemistry and Physics, 209 (15), 1564-1575.

[54] Dhara D., Nisha C., Chatterji P. R., (2001), "Interpenetrating Networks of Poly (N-isopropyl-acrylamide) with Anionic and Cationic Polymers", Macromolecular Chemistry and Physics, 202 (18), 3617-3623.

[55] Liu Y.Y., Shao Y. H., Lü J., (2006), "Preparation, properties and controlled release behaviors of pH-induced thermosensitive amphiphilic gels", Biomaterials, 27 (21), 4016-4024.

[56] Brazel C. S. Peppas N. A., (1995), "Synthesis and Characterization of Thermo- and Chemomechanically Responsive Poly (N-isopropylacrylamide-co-methacrylic acid) Hydrogels", Macromolecules, 28 (24), 8016-8020.

[57] Diez-Pena E., Quijada-Garrido I., Barrales-Rienda J., (2002), "On the water swelling behaviour of poly (N-isopropylacrylamide)[P (N-iPAAm)], poly (methacrylic acid)[P (MAA)], their random copolymers and sequential interpenetrating polymer networks (IPNs)", Polymer, 43 (16), 4341-4348.

[58] Zhang X., Li C., Hu Y., Liu R., He L., Fang S., (2014), "A novel temperature and pH dual-responsive hybrid hydrogel with polyhedral oligomeric silsesquioxane as crosslinker: synthesis, characterization and drug release properties", Polymer International, 63 (12), 2030-2041.

[59] Xiang Y., Peng Z., Chen D., (2006), "A new polymer/clay nano-composite hydrogel with improved response rate and tensile mechanical properties", European Polymer Journal, 42 (9), 2125-2132.

[60] Shen J., Li N., Ye M., (2015), "Preparation and characterization of dual-sensitive double network hydrogels with clay as a physical crosslinker", Applied Clay Science, 103, 40-45.

[61] Haraguchi K., Takada T., (2005), "Characteristic Sliding Frictional Behavior on the Surface of Nanocomposite Hydrogels Consisting of Organic-Inorganic Network Structure", Macromolecular Chemistry and Physics, 206 (15), 1530-1540.

[62] Zhang J., Wang A., (2007), "Study on superabsorbent composites. IX: Synthesis, characterization and swelling behaviors of polyacrylamide/clay composites based on various clays", Reactive and Functional Polymers, 67 (8), 737-745.

[63] Ma J., Zhang L., Fan B., Xu Y., Liang B., (2008), "A novel sodium carboxymethylcellulose/poly (N-isopropylacrylamide)/Clay semi-IPN nanocomposite hydrogel with improved response rate and mechanical properties", Journal of Polymer Science Part B: Polymer Physics, 46 (15), 1546-1555.

[64] Lee W. F., Fu Y. T., (2003), "Effect of montmorillonite on the swelling behavior and drug-release behavior of nanocomposite hydrogels", Journal of Applied Polymer Science, 89 (13), 3652-3660.

[65] Otake K., Inomata H., Konno M., Saito S., (1990), "Thermal-Analysis of the Volume Phase-Transition with N-Isopropylacrylamide Gels", Macromolecules, 23 (1), 283-289.

[66] Li B., Jiang Y., Liu Y., Wu Y., Yu H., Zhu M., (2009), "Novel poly (N-isopropylacrylamide)/clay/poly (acrylamide) IPN hydrogels with the response rate and drug release controlled by clay content", Journal of Polymer Science Part B: Polymer Physics, 47 (1), 96-106.

[67] Zhang X. Z., Wu D. Q., Chu C. C., (2003), "Effect of the crosslinking level on the properties of temperature-sensitive poly (N-isopropylacrylamide) hydrogels", Journal of Polymer Science Part B: Polymer Physics, 41 (6), 582-593.

[68] Schild H. G., (1992), "Poly(N-isopropylacrylamide) - experiment, theory and application", Progress in Polymer Science, 17 (2), 163-249.

[69] Zhang G. Q., Zha L. S., Zhou M. H., Ma J. H., Liang B. R., (2005), "Preparation and characterization of pH-and temperature-responsive semi–interpenetrating polymer network hydrogels based on linear sodium alginate and crosslinked poly (N-isopropylacrylamide)", Journal of Applied Polymer Science, 97 (5), 1931-1940.

[70] Zhang G.Q., Zha L. S., Zhou M. H., Ma J. H., Liang B. R., (2005), "Rapid deswelling of sodium alginate/poly (N-isopropylacrylamide) semi-interpenetrating polymer network hydrogels in response to temperature and pH changes", Colloid and Polymer Science, 283 (4), 431-438.

[71] Shi J., Alves N. M., Mano J. F., (2006), "Drug release of pH/temperature-responsive calcium alginate/poly (N-isopropylacrylamide) semi-IPN beads", Macromolecular Bioscience, 6 (5), 358-363.

[72] Gao G., Du G., Sun Y., Fu J., (2015), "Self-healable, tough, and ultrastretchable nanocomposite hydrogels based on reversible polyacrylamide/montmorillonite adsorption", ACS Applied Materials & Interfaces, 7 (8), 5029-5037.

[73] Zawrah M., Khattab R., Saad E., Gado R., (2014), "Effect of surfactant types and their concentration on the structural characteristics of nanoclay", Spectrochimica Acta Part A: Molecular and Biomolecular Spectroscopy, 122, 616-623.

[74] Shah K. J., Mishra M. K., Shukla A. D., Imae T., Shah D. O., (2013), "Controlling wettability and hydrophobicity of organoclays modified with quaternary ammonium surfactants", Journal of Colloid and Interface Science, 407, 493-499.

[75] Onoshima D., Imae T., (2006), "Dendritic nano-and microhydrogels fabricated by triethoxysilyl focal dendrons", Soft Matter, 2 (2), 141-148.

[76] Madejova J., (2003), "FTIR techniques in clay mineral studies", Vibrational Spectroscopy, 31 (1), 1-10.

[77] Tomic Z. P., Asanin D., Antic-Mladenovic S., Poharc-Logar V., Makreski P., (2012), "NIR and MIR spectroscopic characteristics of hydrophilic and hydrophobic bentonite treated with sulphuric acid", Vibrational Spectroscopy, 58, 95-103.

[78] Dumitriu R. P., Mitchell G. R., Vasile C., (2011), "Multi-responsive hydrogels based on N-isopropylacrylamide and sodium alginate", Polymer International, 60 (2), 222-233.

[79] Lawrie G., Keen I., Drew B., Chandler-Temple A., Rintoul L., Fredericks P., Grøndahl, L., (2007), "Interactions between alginate and chitosan biopolymers characterized using FTIR and XPS", Biomacromolecules, 8 (8), 2533-2541.

[80] Futscher M. H., Philipp M., Müller-Buschbaum P., Schulte A., (2017), "The Role of Backbone Hydration of Poly (N-isopropyl acrylamide) Across the Volume Phase Transition Compared to its Monomer", Scientific Reports, 7 (1), 17012.

[81] Erbil C., Topuz D., Gökçeören A., Şenkal, B., (2011), "Network parameters of poly (N-isopropylacrylamide)/montmorillonite hydrogels: effects of accelerator and clay content", Polymers for Advanced Technologies, 22 (12), 1696-1704.

[82] Wang X., Yang L., Zhang J., Wang C., Li Q., (2014), "Preparation and characterization of chitosan–poly (vinyl alcohol)/bentonite nanocomposites for adsorption of Hg (II) ions", Chemical Engineering Journal, 251, 404-412.

[83] Zhang G. Q., Zha L. S., Zhou M. H., Ma J. H., Liang, B. R., (2005), "Rapid deswelling of sodium alginate/poly(N-isopropylacrylamide) semi-interpenetrating polymer network hydrogels in response to temperature and pH changes", Colloid and Polymer Science, 283 (4), 431-438.

[84] Cao Y., Shen X., Chen Y., Guo J., Chen Q., Jiang X., (2005), "pH-induced self-assembly and capsules of sodium alginate", Biomacromolecules, 6 (4), 2189-2196.

[85] Ma J., Xu Y., Fan B., Liang B., (2007), "Preparation and characterization of sodium carboxymethylcellulose/poly (N-isopropylacrylamide)/clay semi-IPN nanocomposite hydrogels", European Polymer Journal, 43 (6), 2221-2228.

[86] Pourjavadi A., Ghasemzadeh H., Soleyman R., (2007), "Synthesis, characterization, and swelling behavior of alginate-g-poly(sodium acrylate)/kaolin superabsorbent hydrogel composites", Journal of Applied Polymer Science, 105 (5), 2631-2639.

[87] Mahdavinia G. R., Marandi G. B., Pourjavadi A., Kiani G., (2010), "Semi-IPN Carrageenan-Based Nanocomposite Hydrogels: Synthesis and Swelling Behavior", Journal of Applied Polymer Science, 118 (5), 2989-2997.

[88] Li Z., Shen J., Ma H., Lu X., Shi M., Li N., Ye M., (2012), "Preparation and characterization of sodium alginate/poly (N-isopropylacrylamide)/clay semi-IPN magnetic hydrogels", Polymer Bulletin, 68 (4), 1153-1169.

[89] Haraguchi K., (2011), "Synthesis and properties of soft nanocomposite materials with novel organic/inorganic network structures", Polymer Journal, 43 (3), 223.

[90] Ak T., Gülçin, İ., (2008), "Antioxidant and radical scavenging properties of curcumin", Chemico-Biological Interactions, 174 (1), 27-37.

[91] Sandur S. K., Pandey M. K., Sung B., Ahn K. S., Murakami A., Sethi G., Limtrakul P., Badmaev V., Aggarwal B.B., (2007), "Curcumin, demethoxycurcumin, bisdemethoxycurcumin, tetrahydrocurcumin and turmerones differentially regulate anti-inflammatory and anti-proliferative responses through a ROS-independent mechanism", Carcinogenesis, 28 (8), 1765-1773.

[92] Mun S. H., Joung D. K., Kim Y. S., Kang O. H., Kim S. B., Seo, Y. S., Kim Y. C., Lee D. S., Shin D. W., Kweon K. T., (2013), "Synergistic antibacterial effect of curcumin against methicillin-resistant Staphylococcus aureus", Phytomedicine, 20 (8-9), 714-718.

[93] Ghoneum M., Gollapudi S., (2011), "Synergistic apoptotic effect of arabinoxylan rice bran (MGN-3/Biobran) and curcumin (turmeric) on human multiple myeloma cell line U266 in vitro", Neoplasma, 58 (2), 118.

[94] Wilken R., Veena M. S., Wang M. B., Srivatsan E. S., (2011), "Curcumin: A review of anti-cancer properties and therapeutic activity in head and neck squamous cell carcinoma", Molecular Cancer, 10 (1), 12.

[95] Aggarwal B. B., (2008), "Prostate cancer and curcumin: Add spice to your life", Cancer Biology & Therapy, 7 (9), 1436-1440.

[96] Gupta V., Aseh A., Ríos C. N., Aggarwal B. B., Mathur A. B., (2009), "Fabrication and characterization of silk fibroin-derived curcumin nanoparticles for cancer therapy", International Journal of Nanomedicine, 4, 115.

[97] Tønnesen H. H., Másson M., Loftsson T., (2002), "Studies of curcumin and curcuminoids. XXVII. Cyclodextrin complexation: solubility, chemical and photochemical stability", International Journal of Pharmaceutics, 244 (1), 127-135.

[98] Siviero A., Gallo E., Maggini V., Gori L., Mugelli A., Firenzuoli F., Vannacci A., (2015), "Curcumin, a golden spice with a low bioavailability", Journal of Herbal Medicine, 5 (2), 57-70.

[99] Merrell J. G., McLaughlin S. W., Tie L., Laurencin C. T., Chen A. F., Nair L. S., (2009), "Curcumin-loaded poly (ε-caprolactone) nanofibres: Diabetic wound dressing with anti-oxidant and anti-inflammatory properties", Clinical and Experimental Pharmacology and Physiology, 36 (12), 1149-1156.

[100] Harada T., Pham D. T., Leung M. H., Ngo H. T., Lincoln S. F., Easton C. J., Kee T. W., (2010), "Cooperative binding and stabilization of the medicinal pigment curcumin by diamide linked γ-cyclodextrin dimers: a spectroscopic characterization", The Journal of Physical Chemistry B, 115 (5), 1268-1274.

[101] Hegge A., Schüller R., Kristensen S., Tønnesen H., (2008), "In vitro release of curcumin from vehicles containing alginate and cyclodextrin Studies of curcumin and curcuminoides. XXXIII", Die Pharmazie-An International Journal of Pharmaceutical Sciences, 63 (8), 585-592.

[102] Dandawate P. R., Vyas A., Ahmad A., Banerjee S., Deshpande J., Swamy K. V., Jamadar A., Dumhe-Klaire A. C., Padhye S., Sarkar F. H., (2012), "Inclusion complex of novel curcumin analogue CDF and β-cyclodextrin (1: 2) and its enhanced in vivo anticancer activity against pancreatic cancer", Pharmaceutical Research, 29 (7), 1775-1786.

[103] Gerola A. P., Silva D. C., Jesus S., Carvalho R. A., Rubira A. F., Muniz E. C., Borges O., Valente A. J., (2015), "Synthesis and controlled curcumin supramolecular complex release from pH-sensitive modified gum-arabic-based hydrogels", RSC Advances, 5 (115), 94519-94533.

[104] López-Tobar E., Blanch G. P., del Castillo M. R., Sánchez-Cortés, S., (2012), "Encapsulation and isomerization of curcumin with cyclodextrins characterized by electronic and vibrational spectroscopy", Vibrational Spectroscopy, 62, 292-298.

[105] Marcolino V. A., Zanin G. M., Durrant L. R., Benassi M. D. T., Matioli G., (2011), "Interaction of curcumin and bixin with β-cyclodextrin: complexation methods, stability, and applications in food", Journal of Agricultural and Food Chemistry, 59 (7), 3348-3357.

[106] Medronho B., Valente A. J., Costa P., Romano A., (2014), "Inclusion complexes of rosmarinic acid and cyclodextrins: stoichiometry, association constants, and antioxidant potential", Colloid and Polymer Science, 292 (4), 885-894.

[107] Wang X., Luo Z., Xiao Z., (2014), "Preparation, characterization, and thermal stability of β-cyclodextrin/soybean lecithin inclusion complex", Carbohydrate Polymers, 101, 1027-1032.

[108] Wang J., Cao Y., Sun B., Wang C., (2011), "Physicochemical and release characterisation of garlic oil-β-cyclodextrin inclusion complexes", Food Chemistry, 127 (4), 1680-1685.

[109] Patro N. M., Sultana A., Terao K., Nakata D., Jo A., Urano A., Ishida Y., Gorantla R. N., Pandit V., Devi K., (2014), "Comparison and correlation of in vitro, in vivo and in silico evaluations of alpha, beta and gamma cyclodextrin complexes of curcumin", Journal of Inclusion Phenomena and Macrocyclic Chemistry, 78 (1-4), 471-483.

[110] Mohan P. R. K., Sreelakshmi G., Muraleedharan C. V., Joseph R., (2012), "Water soluble complexes of curcumin with cyclodextrins: Characterization by FT-Raman spectroscopy", Vibrational Spectroscopy, 62 (Supplement C), 77-84.

[111] Cabral-Marques H., Almeida R., (2009), "Optimisation of spray-drying process variables for dry powder inhalation (DPI) formulations of corticosteroid/cyclodextrin inclusion complexes", European Journal of Pharmaceutics and Biopharmaceutics, 73 (1), 121-129.

[112] Marques H. M. C., (2010), "A review on cyclodextrin encapsulation of essential oils and volatiles", Flavour and Fragrance Journal, 25 (5), 313-326.

[113] Liu L., Zhu S., (2006), "Preparation and characterization of inclusion complexes of prazosin hydrochloride with β-cyclodextrin and hydroxypropyl-β-cyclodextrin", Journal of Pharmaceutical and Biomedical Analysis, 40 (1), 122-127.

[114] Nieddu M., Rassu G., Boatto G., Bosi P., Trevisi P., Giunchedi P., Carta A., Gavini E., (2014), "Improvement of thymol properties by complexation with cyclodextrins: In vitro and in vivo studies", Carbohydrate Polymers, 102, 393-399.

[115] Junco S., Casimiro T., Ribeiro N., Da Ponte M. N., Marques H. C., (2002), "A comparative study of naproxen–beta cyclodextrin complexes prepared by conventional methods and using supercritical carbon dioxide", Journal of Inclusion Phenomena and Macrocyclic Chemistry, 44 (1-4), 117-121.

[116] Zhang W., Li X., Yu T., Yuan L., Rao G., Li D., Mu C., (2015), "Preparation, physicochemical characterization and release behavior of the inclusion complex of trans-anethole and β-cyclodextrin", Food Research International, 74, 55-62.

[117] Abarca R. L., Rodriguez F. J., Guarda A., Galotto M. J., Bruna J. E., (2016), "Characterization of beta-cyclodextrin inclusion complexes containing an essential oil component", Food Chemistry, 196, 968-975.

[118] Tang B., Ma L., Wang H. Y., Zhang, G. Y., (2002), "Study on the supramolecular interaction of curcumin and β-cyclodextrin by spectrophotometry and its analytical application", Journal of Agricultural and Food Chemistry, 50 (6), 1355-1361.

[119] Benesi H. A., Hildebrand, J., (1949), "A spectrophotometric investigation of the interaction of iodine with aromatic hydrocarbons", Journal of the American Chemical Society, 71 (8), 2703-2707.

[120] Valente A. J., Söderman O., (2014), "The formation of host–guest complexes between surfactants and cyclodextrins", Advances in Colloid and Interface Science, 205, 156-176.

[121] Chalumot G., Yao C., Pino V., Anderson, J. L., (2009), "Determining the stoichiometry and binding constants of inclusion complexes formed between aromatic compounds and β-cyclodextrin by solid-phase microextraction coupled to high-performance liquid chromatography", Journal of Chromatography A, 1216 (27), 5242-5248.

[122] Rachmawati H., Edityaningrum C. A., Mauludin R., (2013), "Molecular inclusion complex of curcumin–β-cyclodextrin nanoparticle to enhance curcumin skin permeability from hydrophilic matrix gel", AAPS Pharmscitech, 14 (4), 1303-1312.

[123] Tablet C., Matei, I., Hillebrand M., (2012), "The determination of the stoichiometry of cyclodextrin inclusion complexes by spectral methods: possibilities and limitations". In: A. Innocenti, Editor, "Stoichiometry and Research-The Importance of Quantity in Biomedicine", InTech.

[124] Baglole K. N., Boland P. G., Wagner, B. D., (2005), "Fluorescence enhancement of curcumin upon inclusion into parent and modified cyclodextrins", Journal of Photochemistry and Photobiology A: Chemistry, 173 (3), 230-237.

[125] Hedges A. R., Shieh W. J., Sikorski, C. T., (1995), "Use of Cyclodextrins for Encapsulation in the Use and Treatment of Food Products, In: S.J. Risch, G. A. Reineccius, Editors, "Encapsulation and Controlled Release of Food Ingredients", ACS Symposium Series.

[126] Kolev T. M., Velcheva E. A., Stamboliyska B. A., Spiteller M., (2005), "DFT and experimental studies of the structure and vibrational spectra of curcumin", International Journal of Quantum Chemistry, 102 (6), 1069-1079.

[127] Friend D. R., (1991), "Colon-specific drug delivery", Advanced Drug Delivery Reviews, 7 (1), 149-199.

[128] Nguyen D. N., Raghavan S. S., Tashima L. M., Lin E. C., Fredette S. J., Langer R. S., Wang C., (2008), "Enhancement of poly (orthoester) microspheres for DNA vaccine delivery by blending with poly (ethylenimine)", Biomaterials, 29 (18), 2783-2793.

[129] Lai W. F., Shum H. C., (2015), "Hypromellose-graft-chitosan and its polyelectrolyte complex as novel systems for sustained drug delivery", ACS Applied Materials & Interfaces, 7 (19), 10501-10510.

[130] Watanabe M., Kawano K., Toma K., Hattori Y., Maitani Y., (2008), "In vivo antitumor activity of camptothecin incorporated in liposomes formulated with an artificial lipid and human serum albumin", Journal of Controlled Release, 127 (3), 231-238.

[131] Tamilvanan S., Venkateshan N., Ludwig A., (2008), "The potential of lipid- and polymer-based drug delivery carriers for eradicating biofilm consortia on device-related nosocomial infections", Journal of Controlled Release, 128 (1), 2-22.

[132] Gupta P., Vermani K., Garg S., (2002), "Hydrogels: from controlled release to pH-responsive drug delivery", Drug Discovery Today, 7 (10), 569-579.

[133] Fu G., Soboyejo W. O., (2011), "Investigation of swellable poly (N-isopropylacrylamide) based hydrogels for drug delivery", Materials Science and Engineering: C, 31 (5), 1084-1090.

[134] Bilia A., Carelli V., Di Colo G., Nannipieri E., (1996), "In vitro evaluation of a pH-sensitive hydrogel for control of GI drug delivery from silicone-based matrices", International Journal of Pharmaceutics, 130 (1), 83-92.

[135] Zhang X. Z., Zhuo R. X., Cui J. Z., Zhang J. T., (2002), "A novel thermo-responsive drug delivery system with positive controlled release", International Journal of Pharmaceutics, 235 (1-2), 43-50.

[136] Hua S., Ma H., Li X., Yang H., Wang A., (2010), "pH-sensitive sodium alginate/poly (vinyl alcohol) hydrogel beads prepared by combined Ca^{2+} crosslinking and freeze-thawing cycles for controlled release of diclofenac sodium", International Journal of Biological Macromolecules, 46 (5), 517-523.

[137] Işıklan N., Küçükbalcı G., (2016), "Synthesis and characterization of pH-and temperature-sensitive materials based on alginate and poly (N-isopropylacrylamide/acrylic acid) for drug delivery", Polymer Bulletin, 73 (5), 1321-1342.

[138] Shim W. S., Yoo J. S., Bae Y. H., Lee D. S., (2005), "Novel injectable pH and temperature sensitive block copolymer hydrogel", Biomacromolecules, 6 (6), 2930-2934.

[139] Zawko S. A., Truong Q., Schmidt C. E., (2008), "Drug-binding hydrogels of hyaluronic acid functionalized with β-cyclodextrin", Journal of Biomedical Materials Research Part A: An Official Journal of The Society for Biomaterials, The Japanese Society for Biomaterials, and The Australian Society for Biomaterials and the Korean Society for Biomaterials, 87 (4), 1044-1052.

[140] Zhang J. T., Xue Y. N., Gao F. Z., Huang S. W., Zhuo R. X., (2008), "Preparation of temperature-sensitive poly (N-isopropylacrylamide)/β-cyclodextrin-grafted polyethylenimine hydrogels for drug delivery", Journal of Applied Polymer Science, 108 (5), 3031-3037.

[141] Dos Santos J. F. R., Alvarez-Lorenzo C., Silva M., Balsa L., Couceiro J., Torres-Labandeira J. J., Concheiro A., (2009), "Soft contact lenses functionalized with pendant cyclodextrins for controlled drug delivery", Biomaterials, 30 (7), 1348-1355.

[142] Kanjickal D., Lopina S., Evancho-Chapman M. M., Schmidt S., Donovan D., (2005), "Improving delivery of hydrophobic drugs from hydrogels through cyclodextrins", Journal of Biomedical Materials Research Part A: An Official Journal of The Society for Biomaterials, The Japanese Society for Biomaterials, and The Australian Society for Biomaterials and the Korean Society for Biomaterials, 74 (3), 454-460.

[143] Quaglia F., Varricchio G., Miro A., La Rotonda M. I., Larobina D., Mensitieri G., (2001), "Modulation of drug release from hydrogels by using cyclodextrins: the case of nicardipine/β-cyclodextrin system in crosslinked polyethylenglycol", Journal of Controlled Release, 71 (3), 329-337.

[144] Tsao J. Y., Tsai H. H., Wu C. P., Lin P. Y., Su S. Y., Chen L. D., Tsai F. J., Tsai Y., (2010), "Release of paeonol-β-CD complex from thermo-sensitive poly (N-isopropylacrylamide) hydrogels", International Journal of Pharmaceutics, 402 (1-2), 123-128.

[145] European Pharmacopoeia 8th edition, (2010), “Recommendations on methods for dosage forms testing”, In: European Pharmacopoeia Commission & Council of Europe, Strasbourg.

[146] Xie L., Jiang M., Dong X., Bai X., Tong J., Zhou J., (2012), "Controlled mechanical and swelling properties of poly (vinyl alcohol)/sodium alginate blend hydrogels prepared by freeze–thaw followed by Ca^+ crosslinking", Journal of Applied Polymer Science, 124 (1), 823-831.

BIOGRAPHY

Meltem Kasapoğlu Çalık was born in 1986, Edirne. She received his B.Sc. degree from Department of Chemical Engineering, Marmara University in 2009. In 2010, she started her M.Sc. study at the Department of Chemical Engineering, Gebze Institute of Technology under the supervision of Prof. Dr. Murat Özdemir. Between 2013 and 2018, being as a research assistant, she pursued her Ph.D. study under the supervision of Prof. Dr. Murat Özdemir at the Department of Chemical Engineering, Institute of Natural and Applied Sciences, Gebze Technical University. Since 2018, she has been working as a lecturer at the Department of Chemical Technology, Gedik Vocational School, Istanbul Gedik University.

APPENDICES

Appendix A: Time Dependent Swelling Ratio Plots of Nanocomposite and Conventional Hydrogels at Different pH and Temperature Media

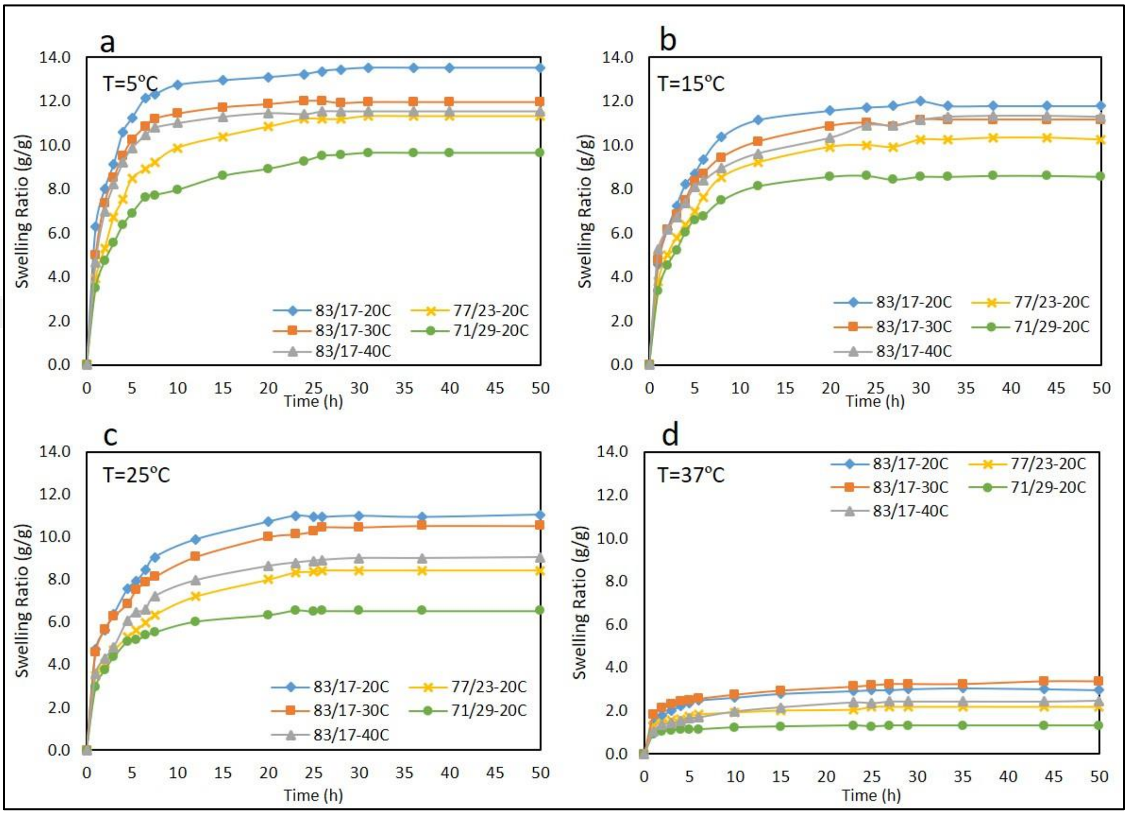

Figure A1.1: Swelling ratio of nanocomposite hydrogels at 5°C (a), 15°C (b), 25 °C (c) and 37°C (d) in pH = 1.2.

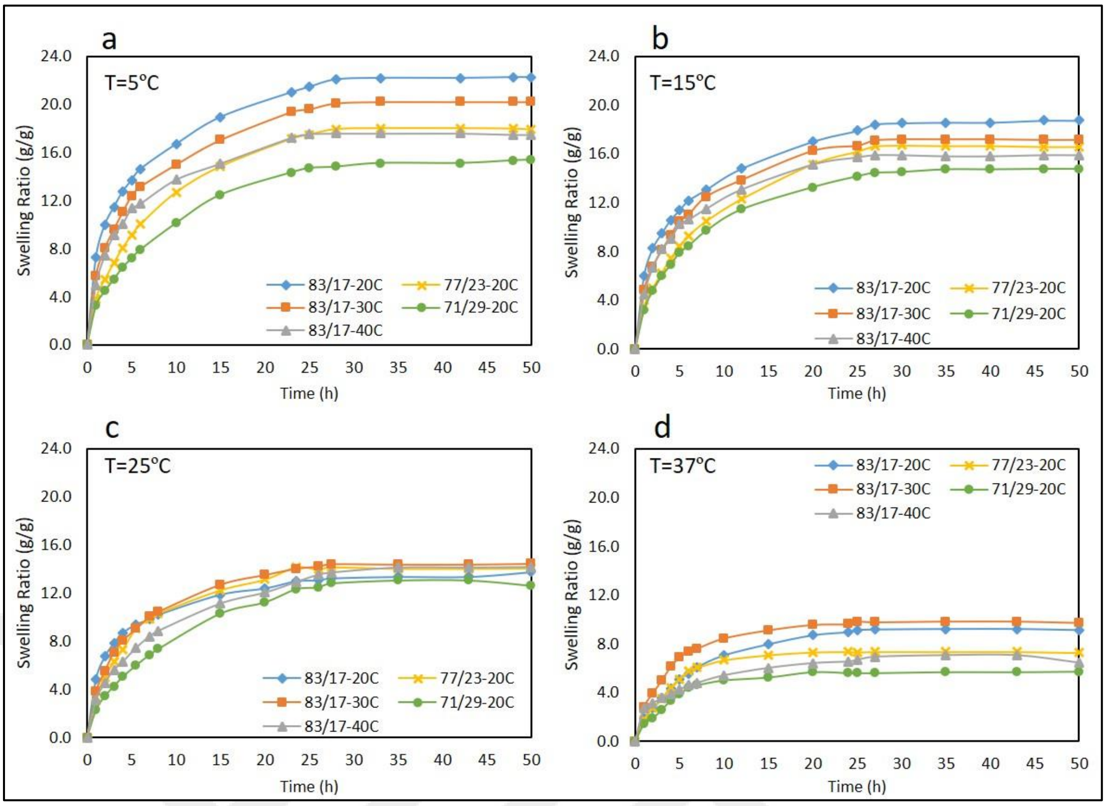

Figure A1.2: Swelling ratio of nanocomposite hydrogels at 5°C (a), 15°C (b), 25 °C (c) and 37°C (d) in pH = 3.0.

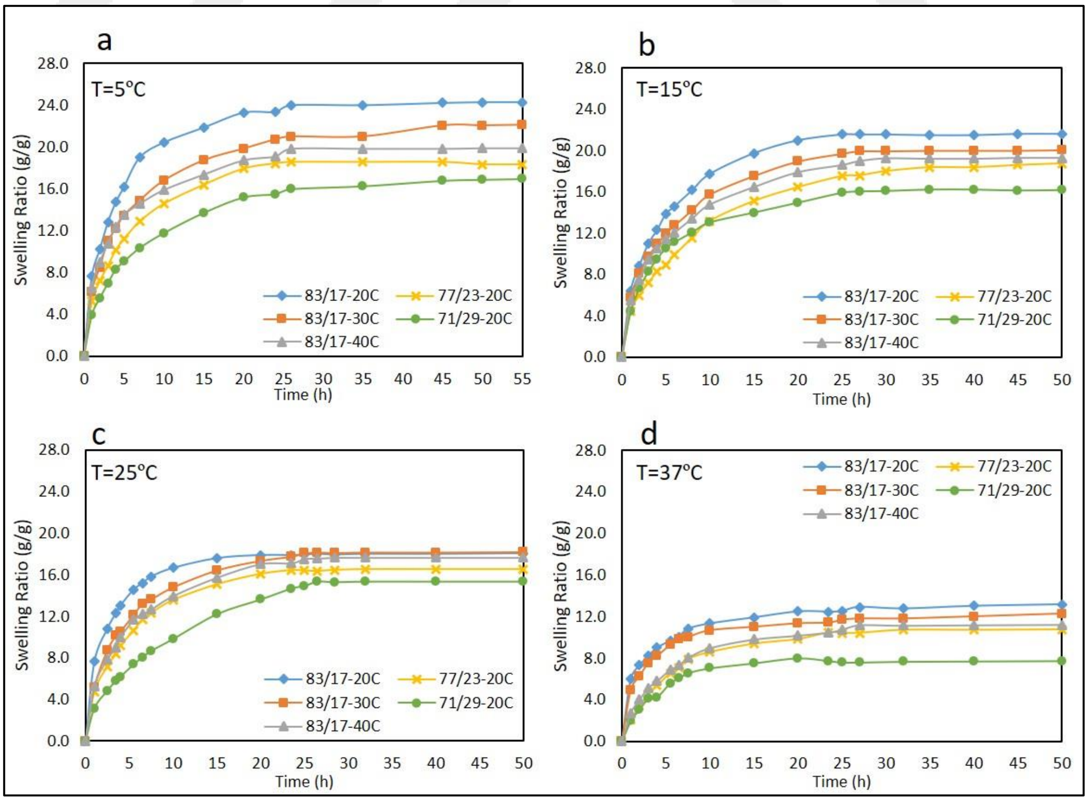

Figure A1.3: Swelling ratio of nanocomposite hydrogels at 5°C (a), 15°C (b), 25 °C (c) and 37°C (d) in pH = 5.0.

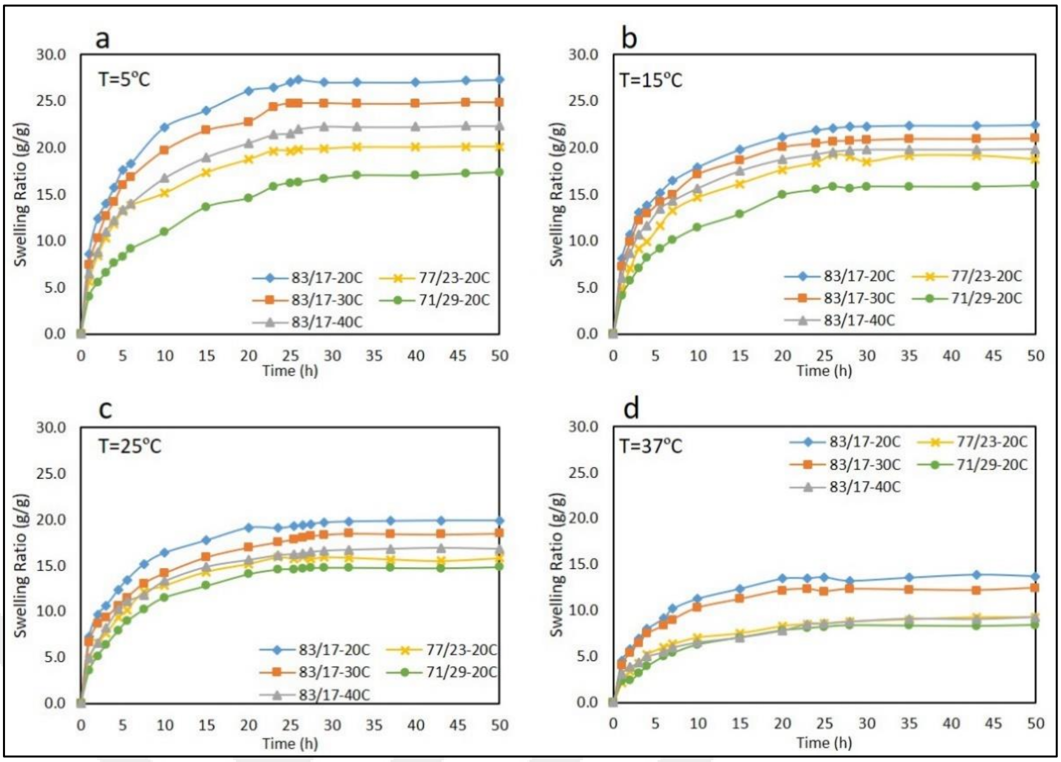

Figure A1.4: Swelling ratio of nanocomposite hydrogels at 5°C (a), 15°C (b), 25 °C (c) and 37°C (d) in pH = 6.8.

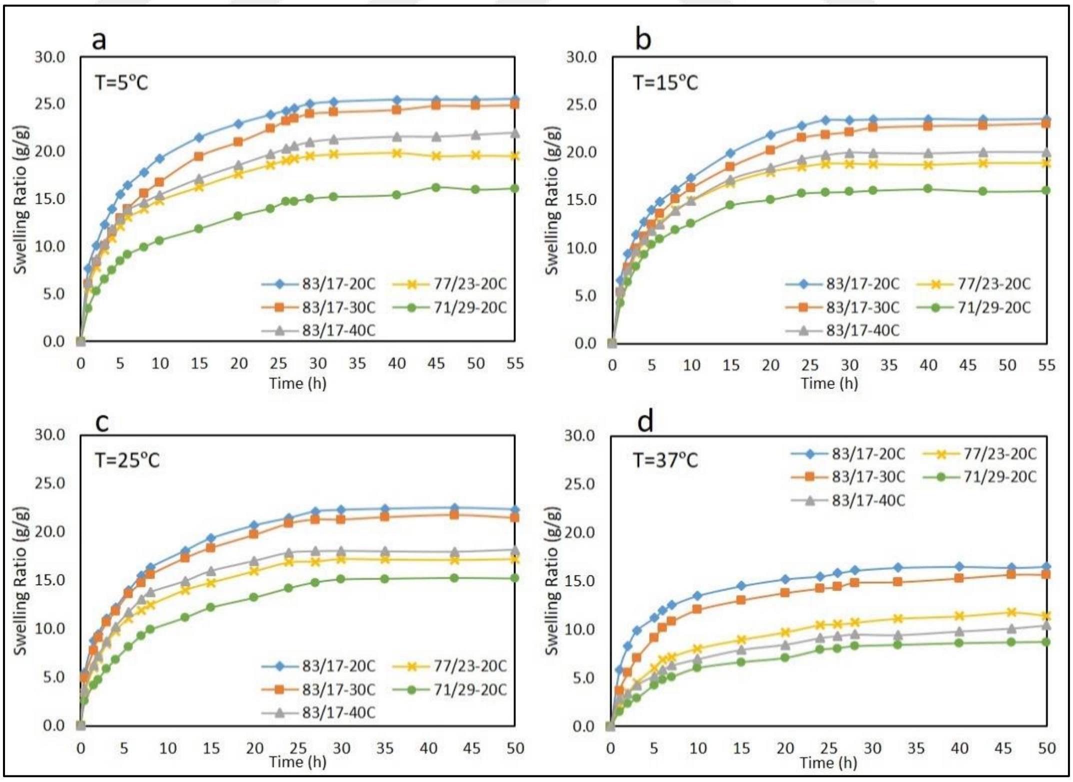

Figure A1.5: Swelling ratio of nanocomposite hydrogels at 5°C (a), 15°C (b), 25 °C (c) and 37°C (d) in pH = 8.0.

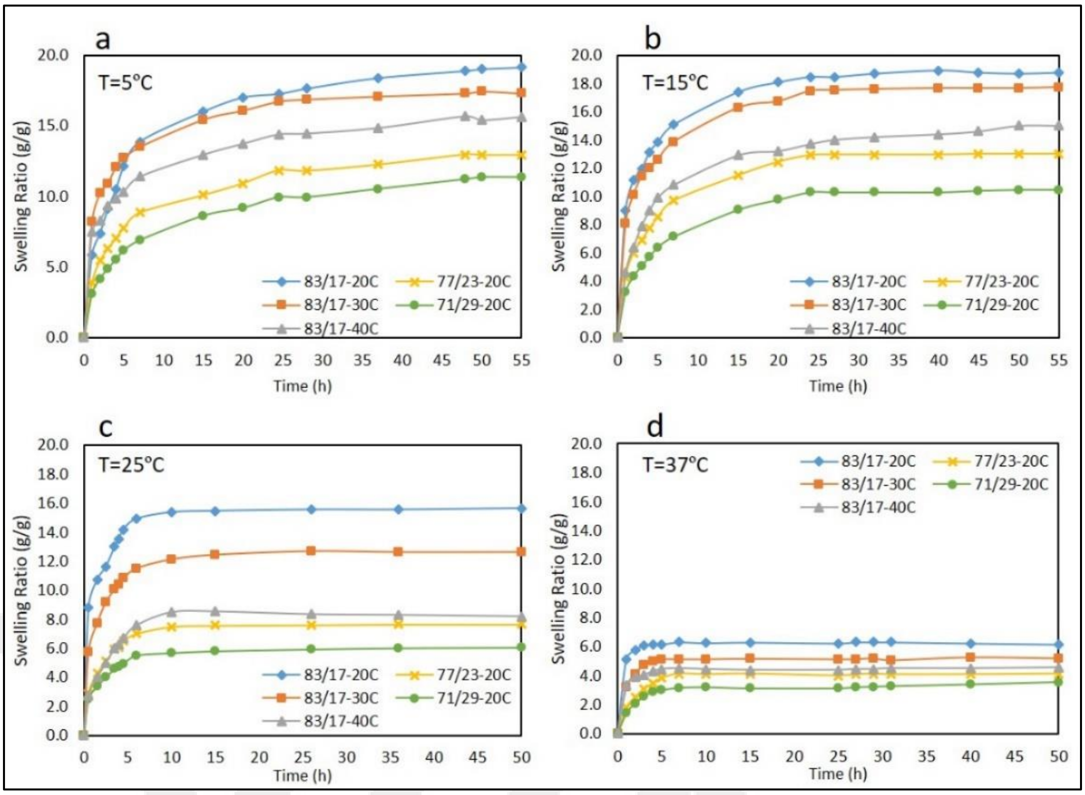

Figure A1.6: Swelling ratio of nanocomposite hydrogels at 5°C (a), 15°C (b), 25 °C (c) and 37°C (d) in pH = 10.0.

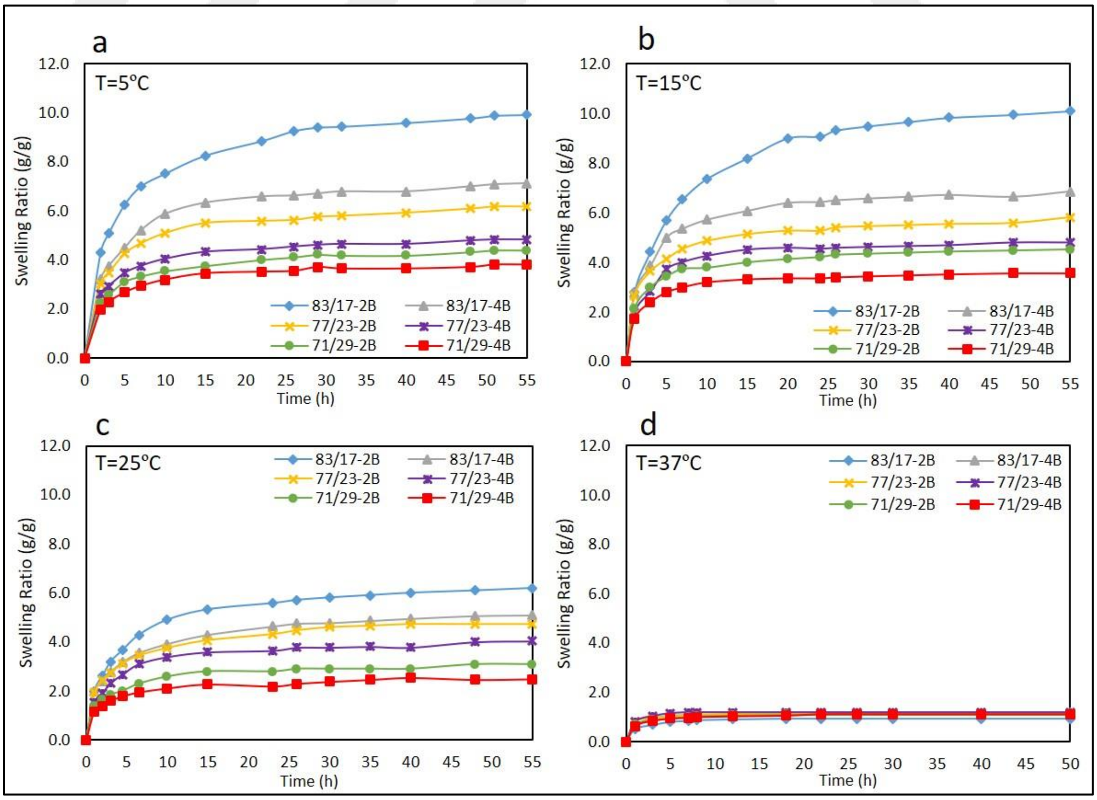

Figure A1.7: Swelling ratio of conventional hydrogels at 5°C (a), 15°C (b), 25 °C (c) and 37°C (d) in pH = 1.2.

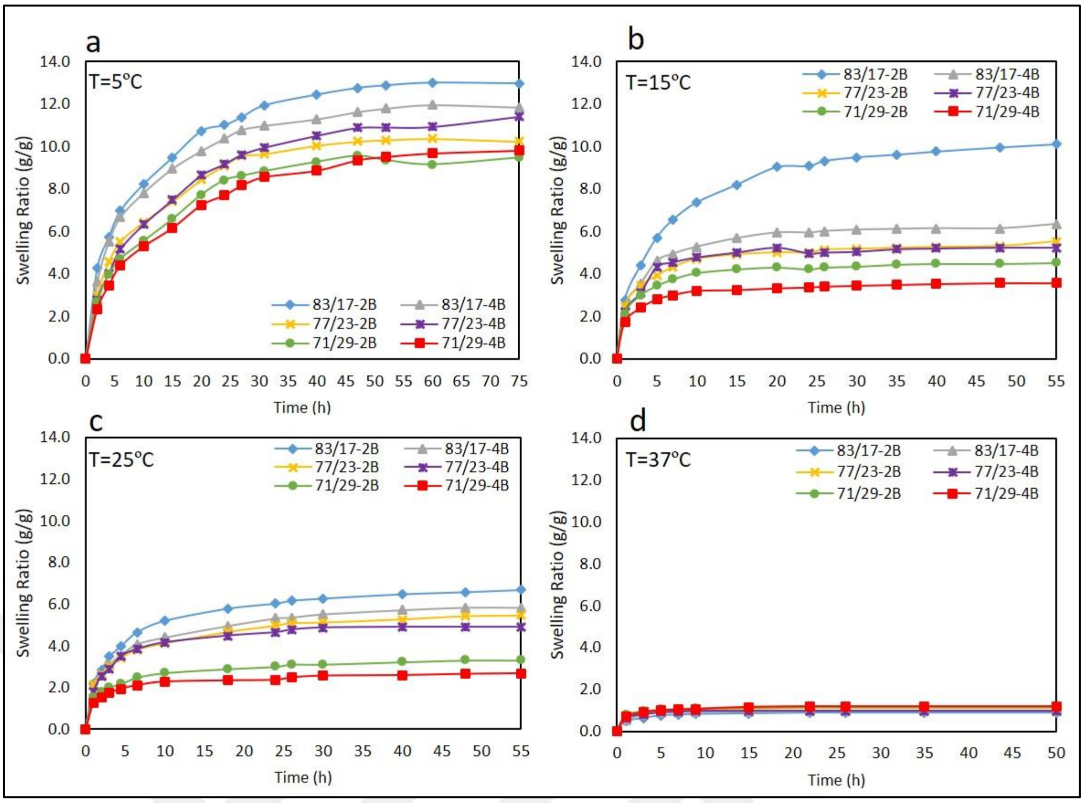

Figure A1.8: Swelling ratio of conventional hydrogels at 5°C (a), 15°C (b), 25 °C (c) and 37°C (d) in pH = 3.0.

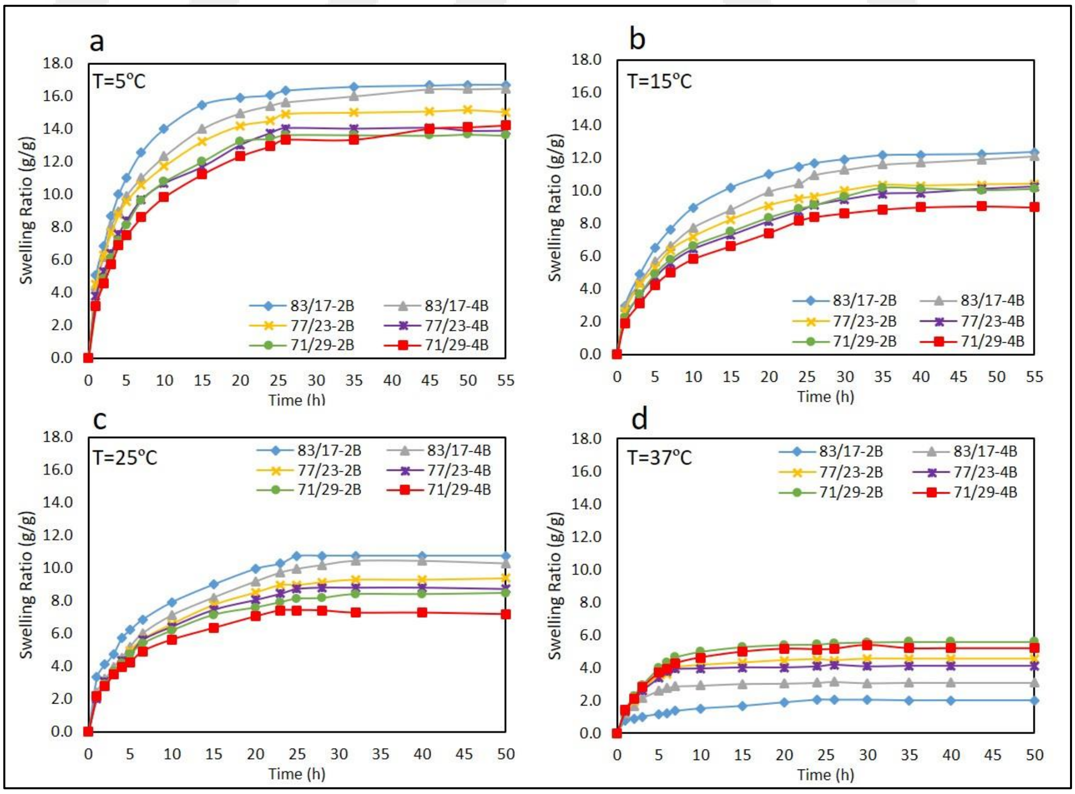

Figure A1.9: Swelling ratio of conventional hydrogels at 5°C (a), 15°C (b), 25 °C (c) and 37°C (d) in pH = 5.0.

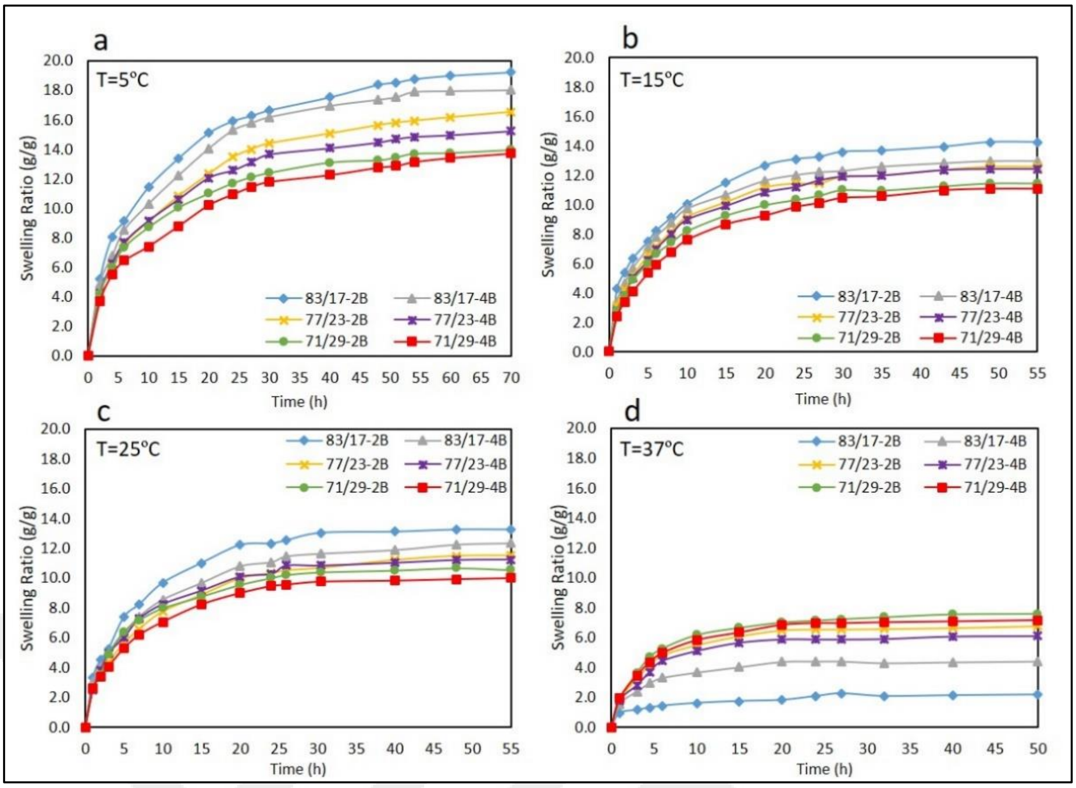

Figure A1.10: Swelling ratio of conventional hydrogels at 5°C (a), 15°C (b), 25 °C (c) and 37°C (d) in pH = 6.8.

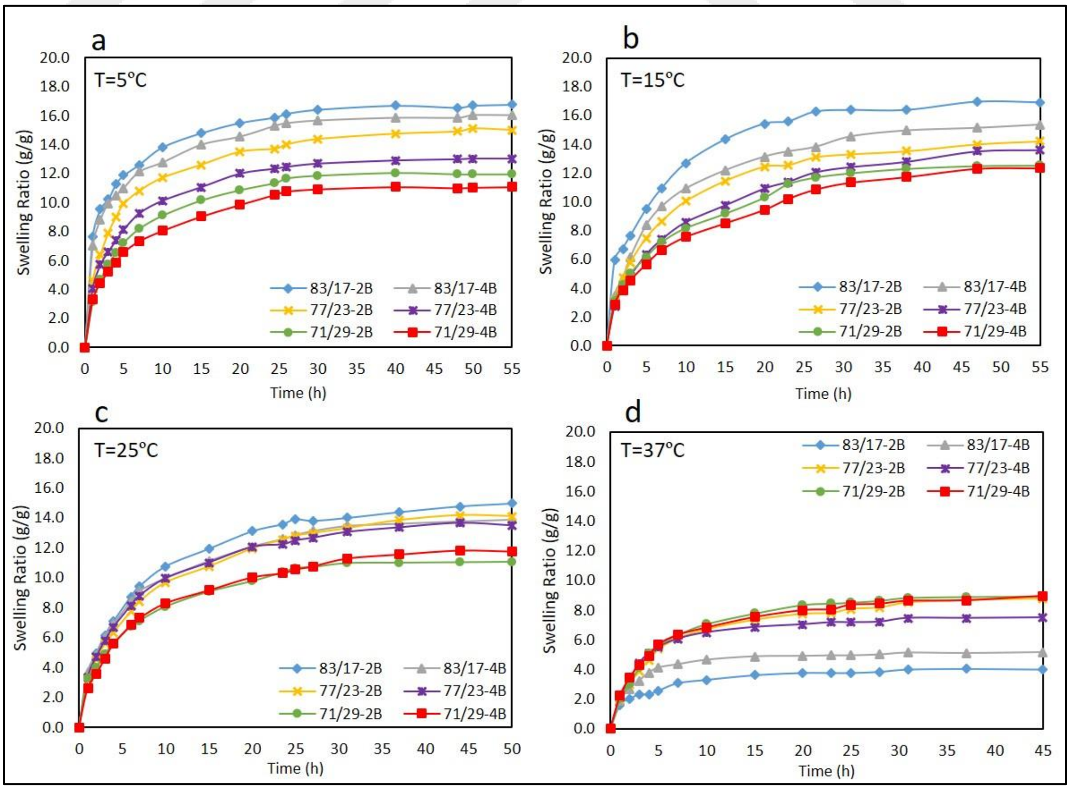

Figure A1.11: Swelling ratio of conventional hydrogels at 5°C (a), 15°C (b), 25 °C (c) and 37°C (d) in pH = 8.0.

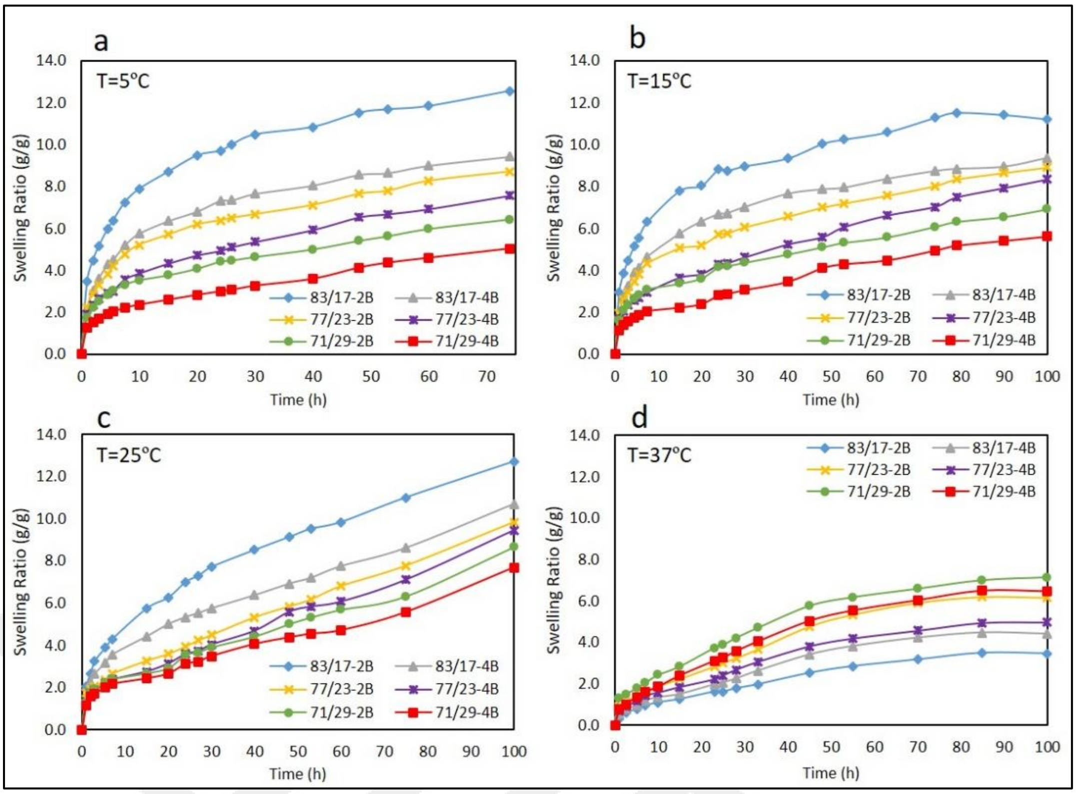

Figure A1.12: Swelling ratio of conventional hydrogels at 5°C (a), 15°C (b), 25 °C (c) and 37°C (d) in pH = 10.0.

Appendix B: UV calibration curve.

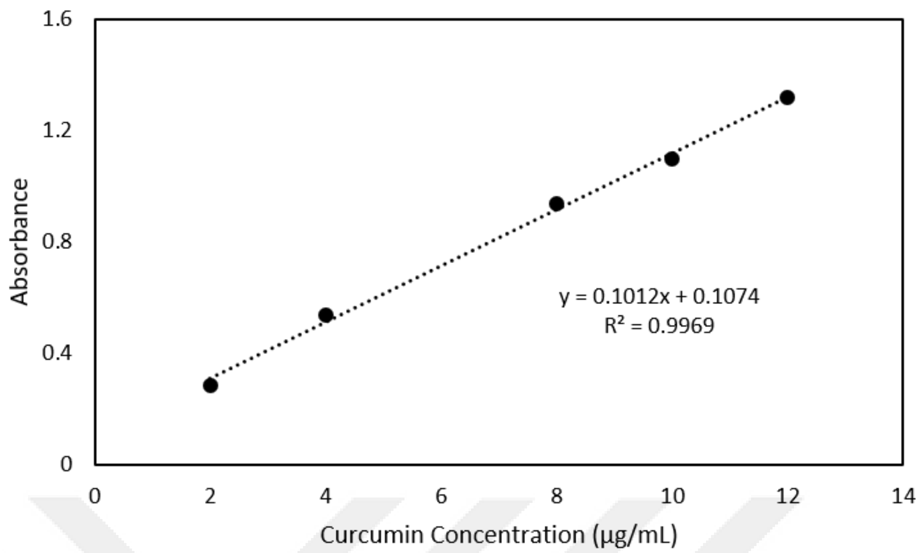

Figure B1.1: UV calibration curve of curcumin at 425 nm.